To the Graduate Council:

I am submitting herewith a thesis written by Von Carlos Huffstetler entitled "The Polarization Behavior of Selected Cathodic Reactions Used in Corrosion Testing of Stainless Steels and Nickel Base Alloys." I recommend that it be accepted in partial fulfillment of the requirements for the degree of Master of Science, with a major in Chemical Engineering.

E. E. Stansbury

E. E. Stansbury, Major Professor

We have read this thesis
and recommend its acceptance:

Joseph J. Perona

Edward L. Clark

Accepted for the Council:

L. Evans Pate

Vice Chancellor
Graduate Studies and Research

Thesis
T1
.H84
cop. 2

THE POLARIZATION BEHAVIOR OF SELECTED CATHODIC REACTIONS USED IN CORROSION TESTING OF STAINLESS STEELS AND NICKEL BASE ALLOYS

A Thesis

Presented for the

Master of Science

Degree

The University of Tennessee, Knoxville

Von Carlos Huffstetler

December 1977

134569

ACKNOWLEDGMENTS

The author wishes to express his gratitude to both Dr. E. E. Stansbury of the Chemical and Metallurgical Engineering Department of The University of Tennessee for his assistance, guidance, and patience, and Mrs. M. B. Canterbury for her generous contribution in typing and editing this report.

ABSTRACT

The purpose of this study was to examine the electrochemical nature of three different acid solutions and to evaluate factors affecting the shape of the polarization curves. Potentiodynamic polarization curves were obtained for 10% hydrochloric acid, 50% sulfuric acid-0.1 M ferric sulfate, and 10% chromic acid on a platinized platinum surface and on various nickel rich alloys. The polarization measurements were generally conducted at room temperature in hydrogen saturated solutions. However, several polarization curves were also measured in aerated solutions in order to determine the influence of oxygen on the electrochemical characteristics of each acid. Conclusions from this investigation are given below.

The equilibrium potentials on Pt in the hydrogen saturated solutions are 0.02 V vs. S.H.E. for HCl, 0.82 V for sulfuric acid-ferric sulfate, and 1.17 V for CrO_3 acid.

In the case of each solution, $i_{L,c}$ is significantly larger than $i_{L,a}$ due to the greater concentration of reducible species present.

The oxidation of hydrogen in hydrogen saturated 10% HCl on Pt exhibits diffusion control with a constant limiting current density; however, at sufficiently positive potentials, a decreasing current density region exists that is independent of stirring.

In aerated 10% HCl solution on Pt, the oxygen electrode is complicated and is difficult to reproduce. Anodically, an oxide film is continuously forming on the metal surface which yields irreproducible results until the entire metal surface becomes covered with the oxide film. Cathodically, a stable intermediate of peroxide is formed whenever oxygen is reduced to water. Increasing peroxide concentrations cause decreasing rest potential values until an equilibrium level of peroxide is formed.

Anodic polarization of selected Ni-Cr-Mo alloys in hydrogen saturated 10% HCl revealed active-passive behavior for each alloy with E_{corr} in each case close to the reversible hydrogen electrode. As the Cr content of an alloy was increased, a decrease of E_{pp} occurred which tended to expand the passive region.

Although the actual Fe^{2+} activity was not known for the sulfuric acid-ferric sulfate solution, it was calculated to be five times smaller than the Fe^{3+} activity for $E_o = 0.82$ V.

The reduction of ferric ions occurs at a limiting current density of $i_{L,c} = 10^{-2}$ a/cm^2, which is about a hundred times larger than the limiting current densities for either chromic acid or oxygen reduction. Thus, the nickel base alloys will tend to spontaneously passivate easiest in the sulfuric acid-ferric sulfate.

The 10% chromic acid solution is such a powerful oxidant at this concentration that the presence of oxygen has no

effect on the polarization curves. However, the relatively low limiting current density of $i_{L,c} = 3 \times 10^{-5}$ a/cm^2 will not spontaneously passivate the nickel base alloy unless the i_{crit} for the alloy is less than $i_{L,c}$.

TABLE OF CONTENTS

CHAPTER		PAGE
I.	INTRODUCTION	1
II.	REVIEW OF THE LITERATURE	3
	Corrosion Characteristics	3
	Potentiostatic Polarization Behavior	9
	Standard Anodic Polarization Curve	17
III.	CORROSION THEORY	25
	Definition of Terms	25
	Polarization	27
	Charge transfer polarization	28
	Diffusion polarization	31
	Combined polarization effects	36
	Passivation	38
	Methods for Applied Current-Potential Curve Determination	46
	Galvanostatic method	46
	Potentiostatic method	50
IV.	EXPERIMENTAL PROCEDURE	55
	Electrolytic Solutions	55
	Specimen Materials	55
	Polarization Test Cell	56
	Experimental Technique	60
V.	RESULTS AND DISCUSSION	63
	Experimental Standardization	63
	10% Hydrochloric Acid Solution	67
	50% Sulfuric Acid-0.1 M Ferric Sulfate Solution	80
	10% Chromic Acid Solution	89
VI.	CONCLUSIONS AND RECOMMENDATIONS	98
	Conclusions	98
	Recommendations	100
LIST OF REFERENCES		102
VITA		107

LIST OF TABLES

TABLE		PAGE
I.	Analyses of Hastelloy C Alloys	4
II.	Electrode Potential Measurements in Boiling Solutions	7
III.	Nominal Compositions of the Nickel Base Alloys	57
IV.	Anodic Polarization Parameters for Normal Sulfuric Acid on Type 430 Stainless Steel	66
V.	Anodic Polarization Parameters for 10% Hydrochloric Acid on Nickel Base Alloys	79

LIST OF FIGURES

FIGURE		PAGE
1.	Cross Sections of Oxalic Acid Etch Structures . . .	5
2.	Schematic Summary of Relationship of Heat Treatment, Etch Structures and Corrosion of Wrought Ni-Cr-Mo Alloys	8
3.	Relationship Between Overvoltage and Current for the Anodic and Cathodic Reactions of a Single Electrode System	11
4.	Relationship Between Overvoltage and Applied Cathodic Current for a Single Electrode System	12
5.	Relationship Between Overvoltage and Current for a Corroding Electrode System Consisting of Two Coexisting Electrochemical Reactions . . .	13
6.	Relationship Between Overvoltage and Applied Cathodic Current for a Corroding Electrode System	15
7.	Actual vs. Measured Anodic Dissolution Behavior of an Active-Passive Metal. Active State Stable (Schematic)	16
8.	Actual vs. Measured Anodic Dissolution Behavior of an Active-Passive Metal. Active and Passive States Stable (Schematic) . .	18
9.	Actual vs. Measured Anodic Dissolution Behavior of an Active-Passive Metal. Passive State Stable (Spontaneous Passivation) Schematic	19
10.	Standard 430 Stainless Steel Curve	21
11.	Laboratory Repeatability with a Single 430 Stainless Steel Sample	22
12.	Laboratory Reproducibility Attainable from Two Different 430 Stainless Steel Samples	23
13.	Major Variations Affecting Anodic Polarization Curve of 430 Stainless Steel	24

FIGURE PAGE

14. Simplified Hydrogen-Reduction Under Charge Transfer Control 29

15. Charge Transfer Polarization Curve for a Reversible Electrode 32

16. Effect of Limiting Current Density on Cathodic Overvoltage 34

17. Velocity Effects on Corrosion Rate of Cathodic Reaction Under Diffusion Control . . . 35

18. Effect of Resistance Polarization on the Relationship Between Overvoltage and Applied Cathodic Current for a Single Electrode System 37

19. Effect of Diffusion Polarization on the Relationship Between Overvoltage and Applied Cathodic Current for a Single Electrode System 39

20. Schematic Anodic Dissolution Behavior of a Metal Exhibiting an Active-Passive Transition 40

21. The Corrosion Behavior of Metals Exhibiting Active-Passive Transitions 42

22. Effect of Primary Passive Potential on Active-Passive System Under Charge Transfer Control 44

23. Effect of Critical Anodic Current Density on Active-Passive System Under Diffusion Control 45

24. Typical Galvanostatic Circuit Diagram 47

25. Anodic Polarization Curve Obtained by Varying Current 49

26. Potentiometric Circuit for Maintaining Desired Potential 51

27. Potentiometric Equivalent Series Circuit 52

28. Effect of Total Series Resistance on the Measured Anodic Polarization Curve 54

FIGURE		PAGE
29.	Upper Part of Electrode Assembly System	58
30.	Electrode Assembly	59
31.	Schematic Circuit for Automatic Potentiodynamic Polarization Apparatus	62
32.	Polarization Curves on 430 S.S. in a Hydrogen Saturated N H_2SO_4 Solution Exhibiting Increasing Crevice Effects	65
33.	Polarization Curves on Platinum in a Hydrogen Saturated 10% HCl Solution	72
34.	Polarization Curves on Platinum in an Air Saturated 10% HCl Solution	73
35.	Polarization Curves on Various Nickel Base Alloys in a Hydrogen Saturated 10% HCl Solution	78
36.	Polarization Curves on Platinum in a Hydrogen Saturated 50% H_2SO_4-0.1 M $Fe_2(SO_4)_3$ Solution	81
37.	Polarization Curves on Platinum in an Air Saturated 50% H_2SO_4-0.1 M $Fe_2(SO_4)_3$ Solution	82
38.	Polarization Curves on Platinum in a Hydrogen Saturated 10% Chromic Acid Solution	92
39.	Polarization Curves on Platinum in an Air Saturated 10% Chromic Acid Solution	94
40.	Polarization Curves on Nickel Base Alloy 2 in a Hydrogen Saturated 10% Chromic Acid Solution	95
41.	Polarization Curves on Nickel Base Alloy 2 in an Air Saturated 10% Chromic Acid Solution	96

CHAPTER I

INTRODUCTION

Commercial grade nickel-rich alloys containing nominally 58% nickel, 15% chromium, 17% molybdenum, 5% iron, and 5% tungsten are often selected for severely corrosive environments in which austenitic stainless steels would be inadequate. Because corrosion resistance of nickel-chromium-molybdenum alloys may be adversely affected by improper heat treatments, a rapid method of detecting adverse corrosion response has been reported which utilizes acid solutions providing a wide range of electrochemical potentials. In solutions of sulfuric acid-ferric sulfate, chromic acid, or hydrochloric acid, nickel-rich alloys exhibited varying though reproducible patterns of corrosion as a function of heat treatment temperature and alloy microstructure. In relatively short test periods, it was possible to distinguish between samples properly heat-treated and those improperly heat-treated on the basis of the corrosion rates in these solutions. This testing method determined procedures necessary for optimizing corrosion resistance of these nickel-rich alloys.

The above acidic solutions were not characterized electrochemically other than by a single potential measurement. To understand the electrochemical nature of these corrosion systems, the experimental work of this thesis

utilized potentiodynamic polarization techniques to obtain cathodic and anodic polarization curves for selected nickel-based alloys. The polarization curves were conducted in each of the above solutions against an inert platinum auxiliary electrode; factors affecting the shape of the polarization curves are examined.

CHAPTER II

REVIEW OF THE LITERATURE

This chapter provides a brief summary of the significant literature pertaining to this research.

I. CORROSION CHARACTERISTICS

The effect of heat treatment on the corrosion resistance of wrought nickel-based alloys has been investigated in detail by Streicher[37]. Seven heats of Hastelloy C, a commercial grade nickel-chromium-molybdenum alloy, were heated in the range of 800° to 2375°F and were subsequently subjected to both reducing and oxidizing media. The composition limits of this alloy are nominally 58% nickel, 15% chromium, 17% molybdenum, and 5% iron. The actual analyses of the seven heats tested are given in Table I. By deliberately etching samples in oxalic acid, Streicher obtained etch structures that were classified as step, groove, or ditch. Schematic cross sections of the three structures are given in Figure 1.

The solutions used in the corrosion testing included a hydrogen evolving acid, e.g., hydrochloric acid, and acids in which the cathodic process consists of the reduction of metallic cations, e.g., ferric ions in sulfuric acid-ferric sulfate solution and hexavalent chromium ions in chromic acid solution. To obtain data on the corrosion mechanism

TABLE I

ANALYSES OF HASTELLOY C ALLOYS[a]

Heat	Content, Percent Weight											
	Cr	Mo	W	Fe	V	Co	Mn	C[b]	Si[b]	P	S	Ni
A	15.56	15.88	3.47	5.10	0.22	1.12	0.56	0.060	0.55	0.010	0.011	57.46
B	16.36	15.52	4.14	5.08	0.31	0.85	0.59	0.065	0.74	0.007	0.006	56.33
C	15.81	15.73	3.69	5.55	0.24	0.90	0.57	0.045	0.70	0.007	0.008	56.45
D	15.85	16.17	3.91	5.32	0.24	0.96	0.53	0.050	0.74	0.009	0.009	56.20
E	14.88	15.80	3.88	5.68	0.25	1.55	0.80	0.045	0.53	0.010	0.007	56.57
F	15.83	15.98	3.69	5.22	0.22	0.88	0.54	0.053	0.61	0.006	0.006	56.93
H	15.44	15.77	3.79	5.83	0.26	1.27	0.58	0.055	0.80	0.009	0.006	56.19

[a]Hastelloy C samples supplied in form of 1/8-inch sheet.

[b]Separate determinations of C and Si were made on corrosion test specimens.

Source: M. A. Streicher. (1963) *Corrosion*, *19*, 273t.

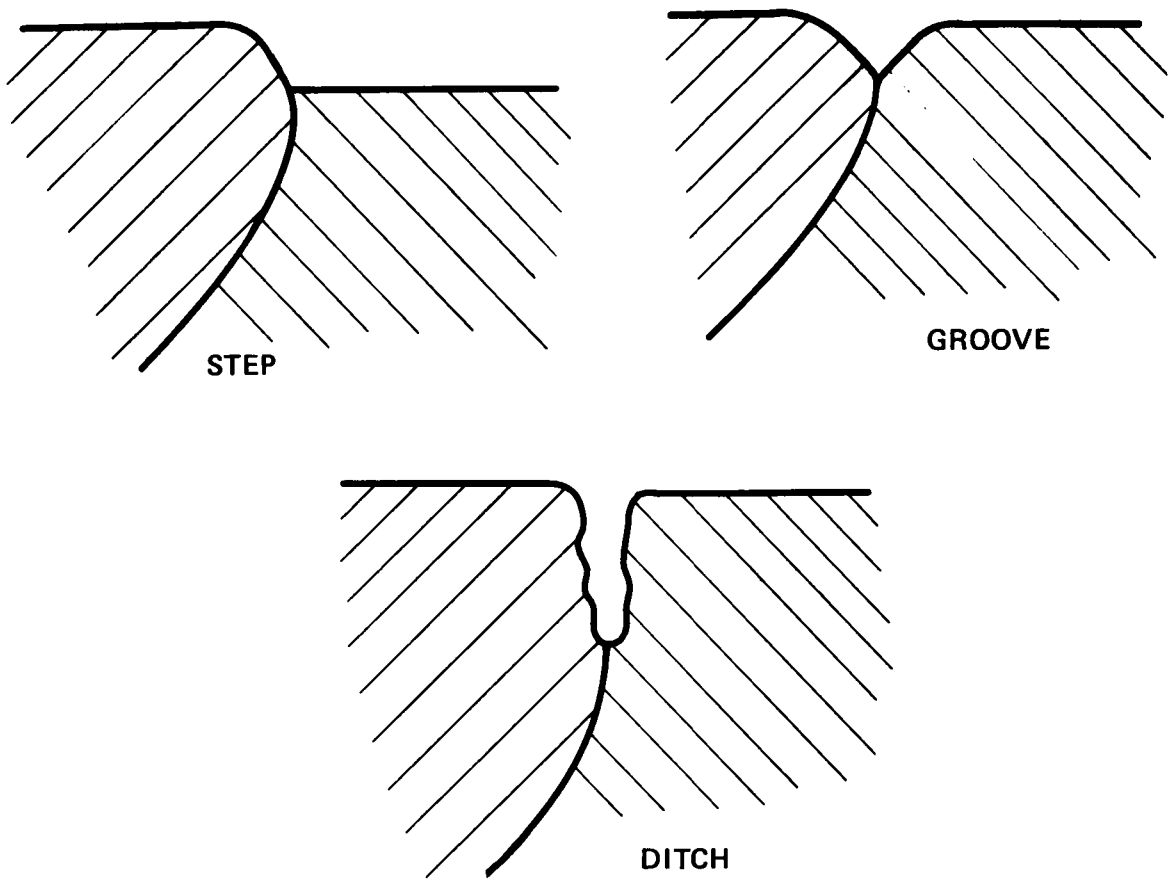


Figure 1. Cross Sections of Oxalic Acid Etch Structures.[37]

in these different acid environments, Streicher made electrode-potential measurements against both a platinized platinum electrode to determine the solution's oxidation-reduction potential and various heat-treated alloy specimens to determine the steady-state corrosion potential, E_{corr}. A summary of these measurements is contained in Table II. From Table II, the effect of heat treatment on steady-state corrosion potential is shown to be negligible. The corrosion potential for hydrochloric acid is near that of a hydrogen electrode, indicating that the dissolution process is governed by the cathodic reaction of hydrogen gas evolution. For sulfuric acid-ferric sulfate and chromic acid, the corrosion potentials are very close to the potentials for the Fe^{+3}/Fe^{+2} and Cr^{+6}/Cr^{+3} reactions on the platinum electrode. With no hydrogen evolution in either media, the corrosion process is controlled by polarization of the anodic areas, such that the alloy surfaces are passivated.

Corrosion tests over a range of heat treatments for a given Hastelloy C alloy in these acidic solutions revealed corrosion rate maxima at 1400°F and at 1900°F. By plotting corrosion rate in each solution as a function of heat treatment, Streicher established a correlation among corrosion rate, heat treatment, and etch structure. Typical effects of heat treatments on Hastelloy C alloys are summarized in the schematic diagram of Figure 2. In hydrochloric acid, only the maximum at 1400°F is revealed, while in chromic acid, only the 1900°F maximum is detected. Both maxima,

TABLE II

ELECTRODE POTENTIAL MEASUREMENTS IN BOILING SOLUTIONS

Solution	Potential Vs Standard Hydrogen Electrode, V				Corrosion Maxima	
		Heat H[a]				
	Pt (Platinized)	Annealed	1 Hr at 1400°F	1 Hr at 1900°F	1400°F	1900°F
Hydrochloric Acid (10%)	+ 0.56[d]	+ 0.04	+ 0.04	+ 0.04	Yes	No
Ferric Sulfate-Sulfuric Acid[b]	+ 0.82	+ 0.80	+ 0.80	+ 0.80	Yes	Yes
Chromic Acid[c] (10% CrO_3)	+ 1.26	+ 1.08	+ 1.09	+ 1.09	No	No

[a]Analysis in Table I.

[b]50% sulfuric acid containing 5.5 g/l Fe^{+3} + 1.15 g/l Fe^{+2}.

[c]Potentials were unaffected by addition of 5 g/600 ml of $Cr(OH)_3$.

[d]These potentials indicate the presence of some oxygen.

Source: M. A. Streicher. (1963) *Corrosion*, *19*, 281t.

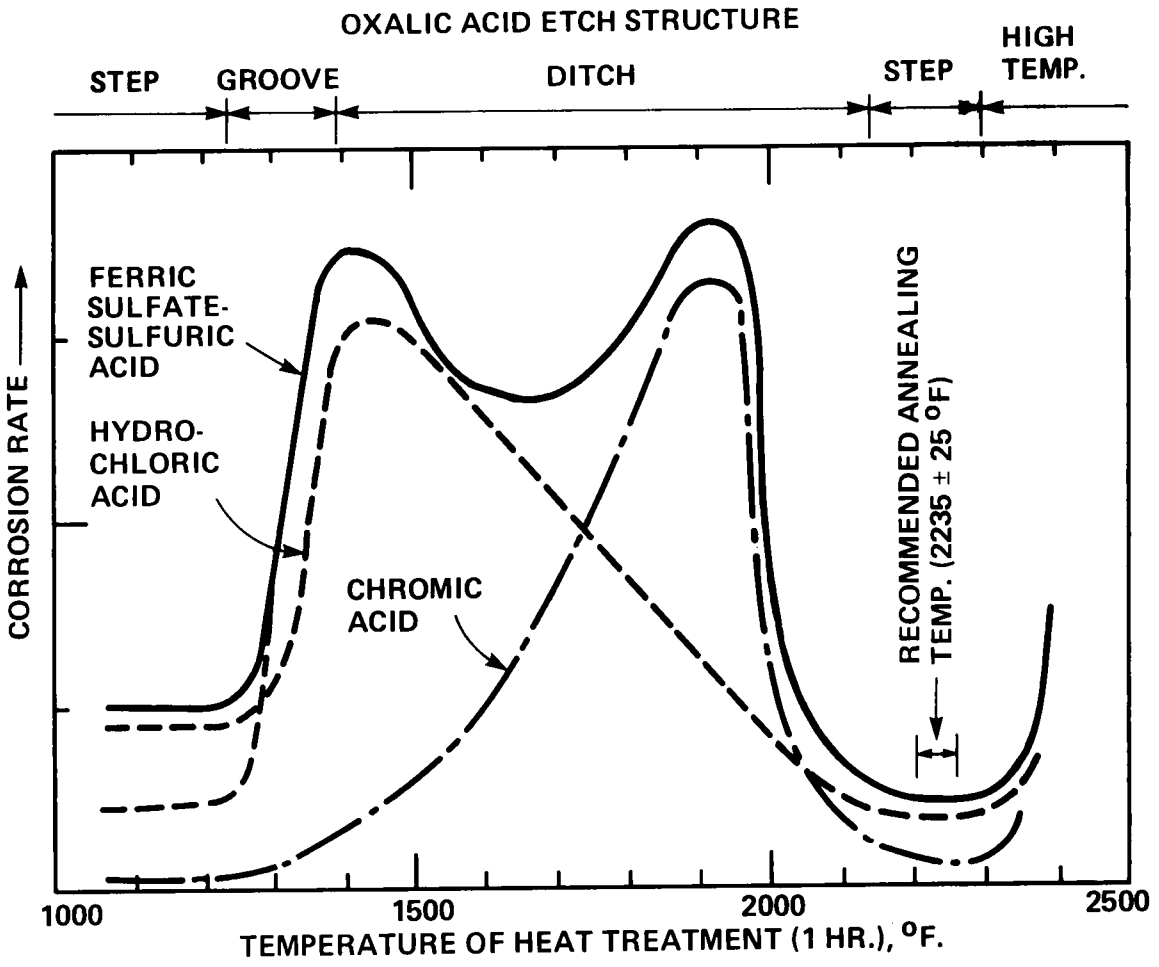


Figure 2. Schematic Summary of Relationship of Heat Treatment, Etch Structures and Corrosion of Wrought Ni-Cr-Mo Alloys.[37]

however, are revealed by exposure to sulfuric acid-ferric sulfate. Examination of Table II in conjunction with Figure 2 indicates that neither the corrosion potential of the alloy nor the oxidation-reduction potential of the solution will reflect whether a single peak or both corrosion maxima are revealed by a given solution. Although the corrosion potential in sulfuric acid (- 0.16 volt) is very near that of hydrochloric acid (- 0.20 volt), both maxima are revealed in sulfuric acid, yet only the peak at 1400°F is seen in hydrochloric acid. Thus, the anion of the acid, rather than the corrosion potential, determines which maximum is revealed.

II. POTENTIOSTATIC POLARIZATION BEHAVIOR

In the case of a single electrode reaction, i.e., a noncorroding electrode system, where substance Z is in equilibrium with its ions Z^+, the rate of oxidation of Z is equal to the rate of reduction of Z^+. The electrode equilibrium may be expressed as

$$\vec{i}_Z = \overleftarrow{i}_Z = i_{0,Z} \, , \qquad (1)$$

where $\vec{i}_Z$ is the current in the forward reduction reaction ($Z^+ + e \rightarrow Z$), $\overleftarrow{i}_Z$ is the current in the reverse oxidation reaction ($Z \rightarrow Z^+ + e$), and $i_{0,Z}$ is referred to as the exchange current for the reaction $Z^+ + e \rightleftarrows Z$. If the reaction rate is controlled by a charge transfer step, there will be

a dependence of current on overvoltage. An illustration of this dependence based on a theoretical model by Stern and Geary[35] is seen in Figure 3. Stern and Geary showed that this dependence cannot be perfectly reproduced experimentally, as shown in Figure 4. When the electrode equilibrium is disturbed by external polarization, the external current used is actually a measure of the difference between the oxidation rate and the reduction rate at that potential:

$$\vec{i}_X = \vec{i}_Z - \overleftarrow{i}_Z \qquad (2)$$

or

$$\overleftarrow{i}_X = \overleftarrow{i}_Z - \vec{i}_Z , \qquad (3)$$

where $\vec{i}_X$ and $\overleftarrow{i}_X$ are the external cathodic and anodic currents, respectively, at some overvoltage, η. As can be seen from Figure 4, as the overvoltage becomes sufficiently removed from the reversible electrode potential, $\vec{i}_X$ approaches the actual reduction current, $\vec{i}_Z$, of the system. However, for overvoltages of 50 mv or less, the competing oxidation current, $\overleftarrow{i}_Z$, becomes more and more significant. As η approaches the reversible potential, Equations (2) and (3) indicate that the experimentally measured external current approaches zero.

In the corroding electrode system, illustrated in Figure 5, at least two co-existing electrochemical reactions must be considered. If the previous system, $Z^+ + e \rightleftarrows Z$,

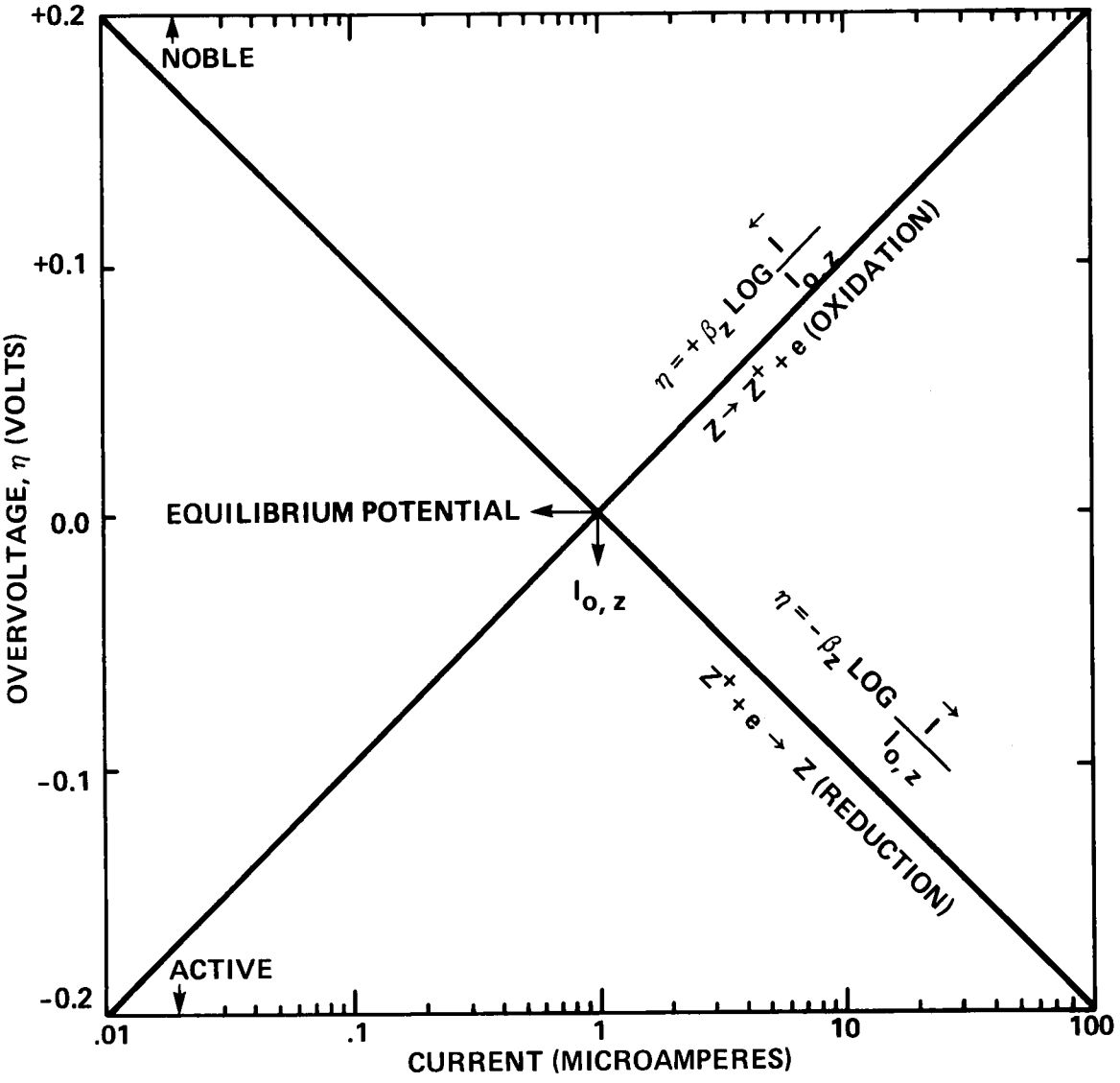


Figure 3. Relationship Between Overvoltage and Current for the Anodic and Cathodic Reactions of a Single Electrode System.[35]

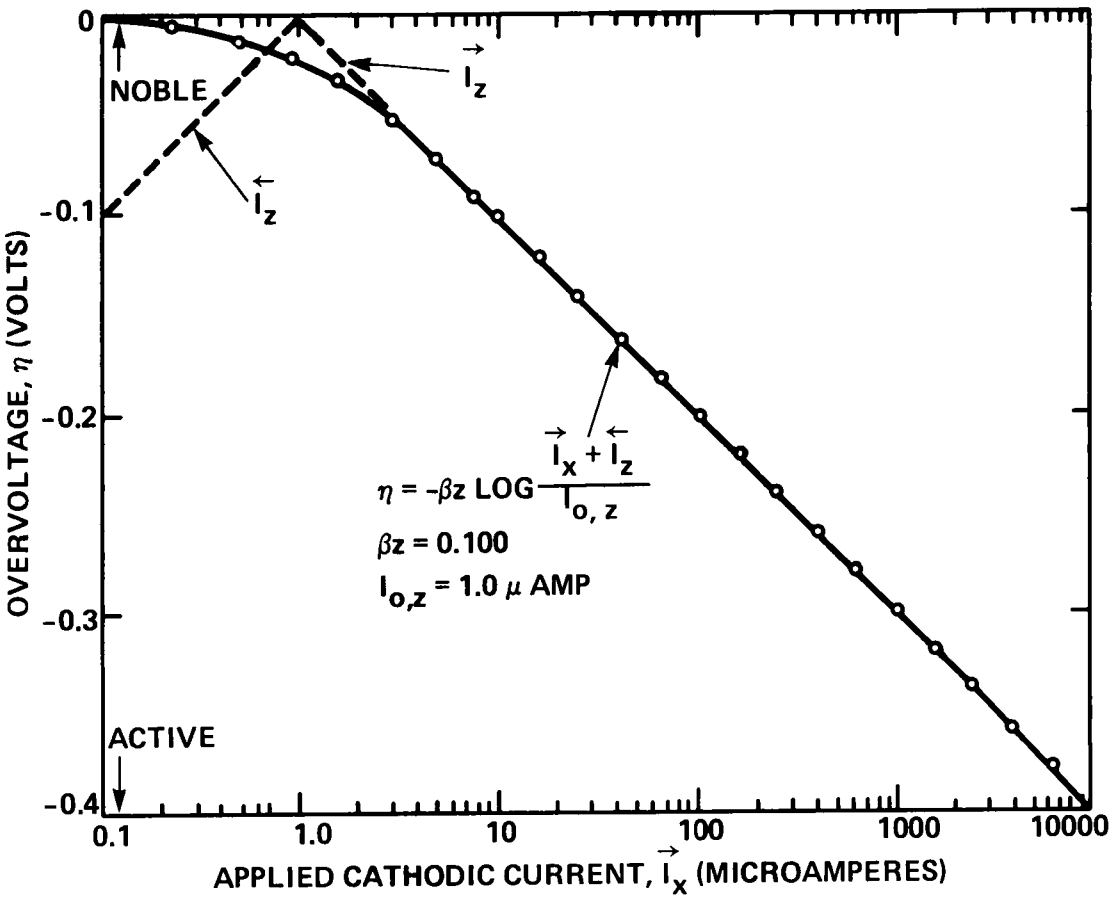


Figure 4. Relationship Between Overvoltage and Applied Cathodic Current for a Single Electrode System.[35]

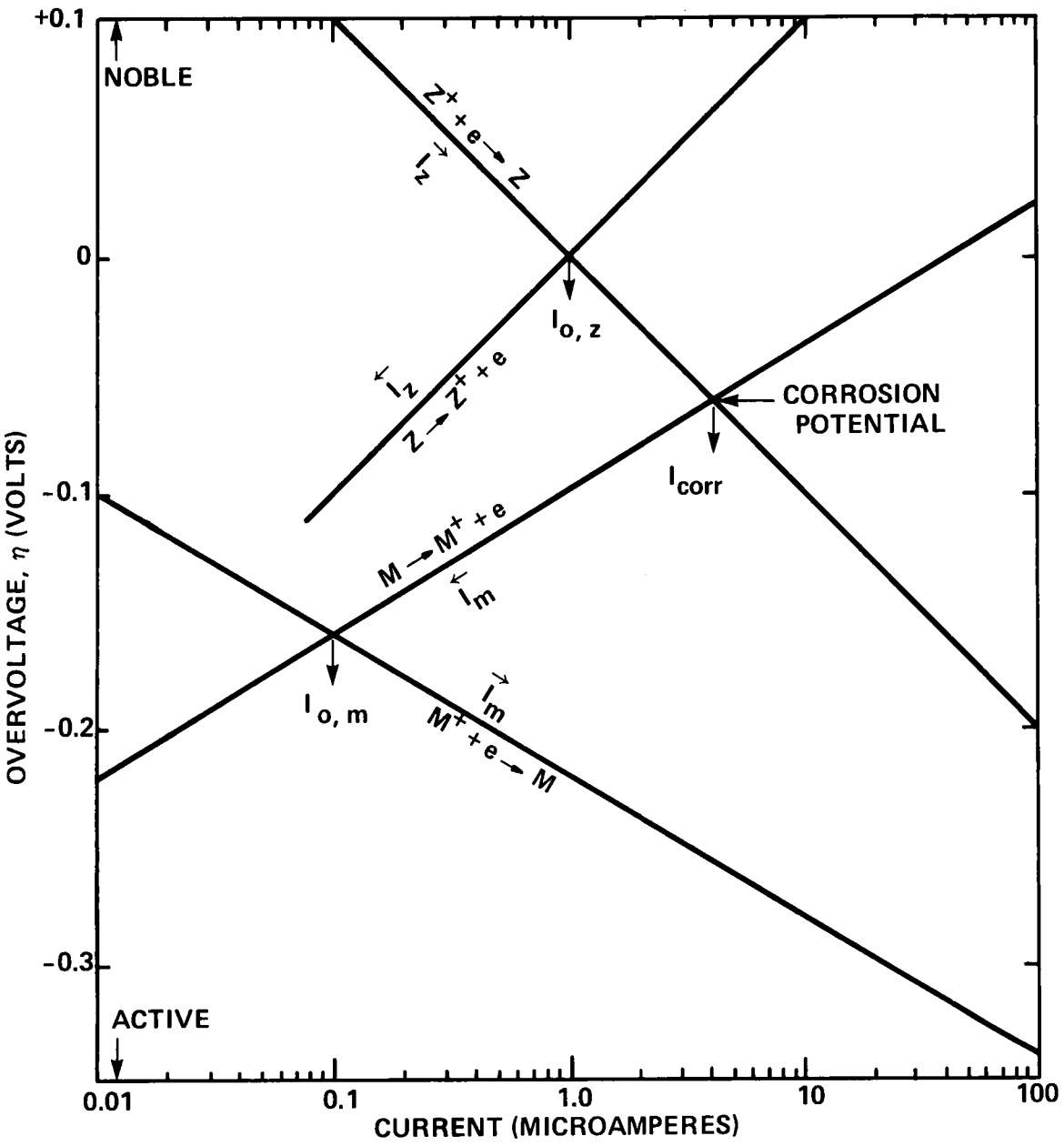


Figure 5. Relationship Between Overvoltage and Current for a Corroding Electrode System Consisting of Two Coexisting Electrochemical Reactions.[35]

is coupled with the oxidation-reduction system of a metal, $M^+ + e \rightleftarrows M$, each system will exhibit its own exchange current and Tafel slope. At the overall system steady-state corrosion potential, E_{corr}, conservation of electron flow requires that the total oxidation rate equals the total reduction rate[35].

$$\vec{i}_Z + \vec{i}_M = \overleftarrow{i}_Z + \overleftarrow{i}_M \qquad (4)$$

Since the corrosion rate is $\overleftarrow{i}_M - \vec{i}_M$, then from Equation (4) it can also be expressed as $\vec{i}_Z - \overleftarrow{i}_Z$. When the corrosion potential is sufficiently removed from the reaction's equilibrium potential, Stern and Geary reason that $\overleftarrow{i}_Z$ and $\vec{i}_M$ become insignificant in comparison to $\vec{i}_Z$ and $\overleftarrow{i}_M$. Therefore, the corrosion rate is equal to $\vec{i}_Z$ or $\overleftarrow{i}_M$. As illustrated in Figure 6, the relationship between η and $\vec{i}_X$ for a corroding system would indicate that to experimentally determine the corrosion potential, E_{corr}, the same considerations encountered near the equilibrium potential of the noncorroding system shown in Figure 3 would also apply here.

In comparing measured polarization curves to actual polarization curves, Greene schematically illustrated three possible cases[7]. Figure 7 shows curves for a metal with an active corrosion potential. The measured curve is distorted in the vicinity of the corrosion potential because of the nearly equal magnitudes of oxidation and reduction rates in this region. The unusual results seen in the measured

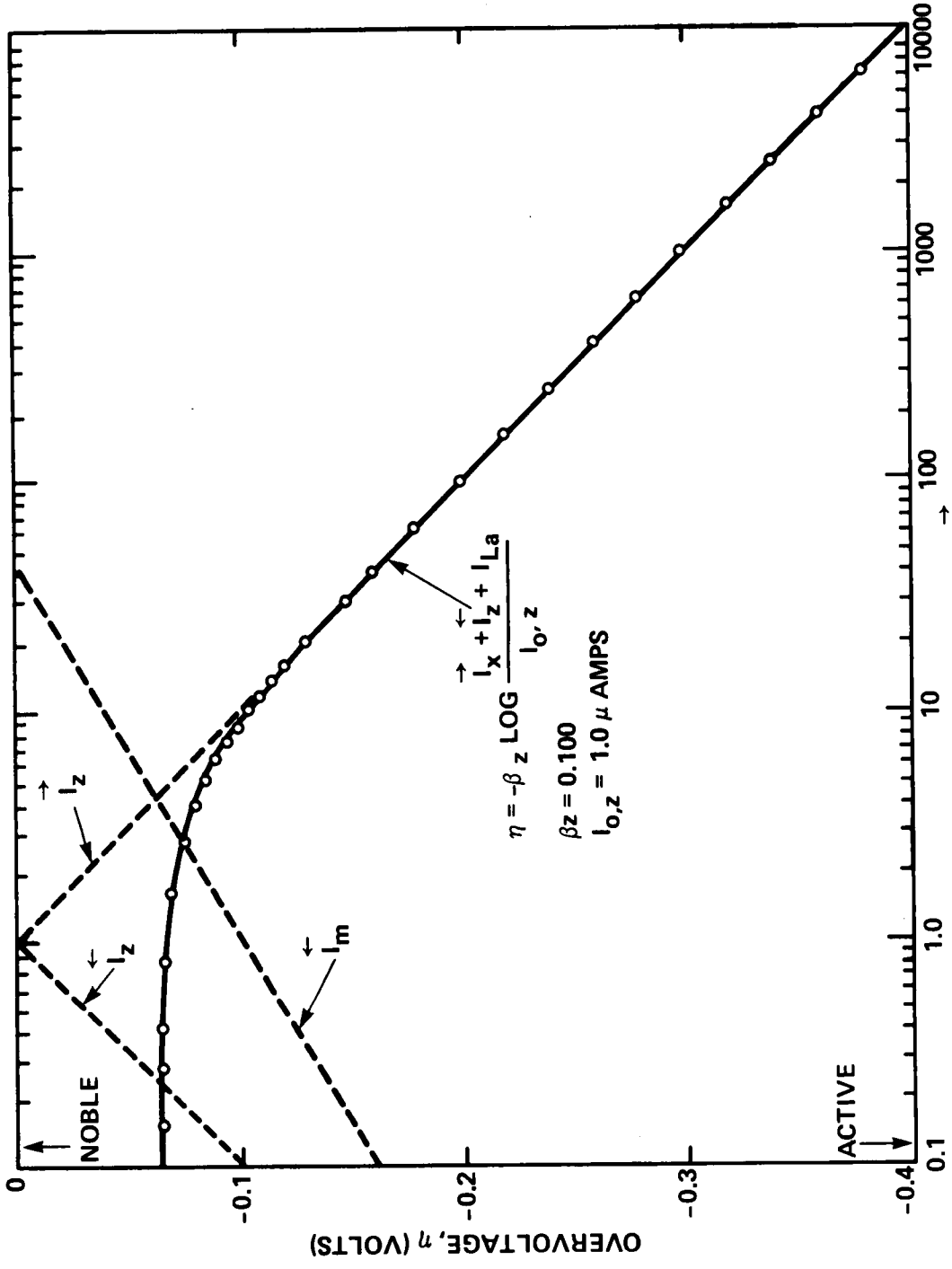


Figure 6. Relationship Between Overvoltage and Applied Cathodic Current For A Corroding Electrode System.[35]

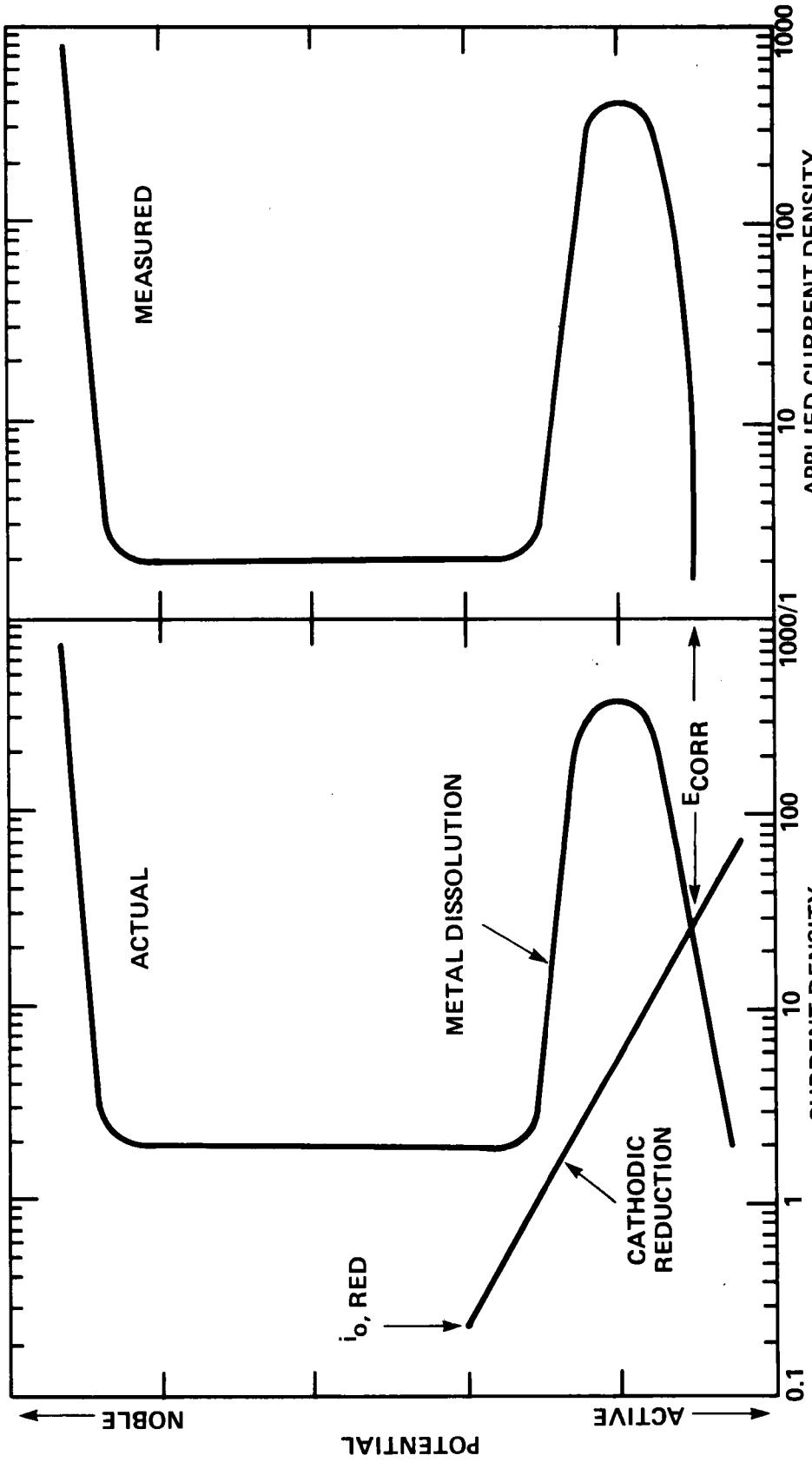


Figure 7. Actual vs. Measured Anodic Dissolution Behavior of An Active-Passive Metal. Active State Stable (Schematic).[7]

curve of Figure 8 are due to cathodic currents present during anodic polarization of the system. This cathodic section is shown as dashes since the logarithmic scale has no zero point. Often referred to as "negative loop," this situation is normally observed in systems possessing stable active and passive states. Figure 9 shows a metal which spontaneously passivates in its environment. The measured curve shows the distortion near E_{corr} and covers only the anodic polarization curve at potentials more noble than E_{corr}. In all of these measured curves, distortion commonly occurs in the vicinity of the corrosion potential and at all other points where the actual anodic and cathodic polarization curves approach each other.

III. STANDARD ANODIC POLARIZATION CURVE

The increasing use of the potentiostat for corrosion measurements throughout the early 1960's emphasized the necessity for experimental reproducibility. An ASTM task group was formed to determine if several different laboratories could reproduce potentiostatic and potentiodynamic anodic polarization curves utilizing a standard experimental procedure[39]. Samples from a single heat of 430 stainless steel were sent to twenty laboratories. Each participant conducted an anodic potentiometric polarization measurement on the sample in a hydrogen-saturated 1.0 $\underline{N}$ H_2SO_4 solution at 30°C. All results were returned to the task group for evaluation and compilation. From this work, a standard

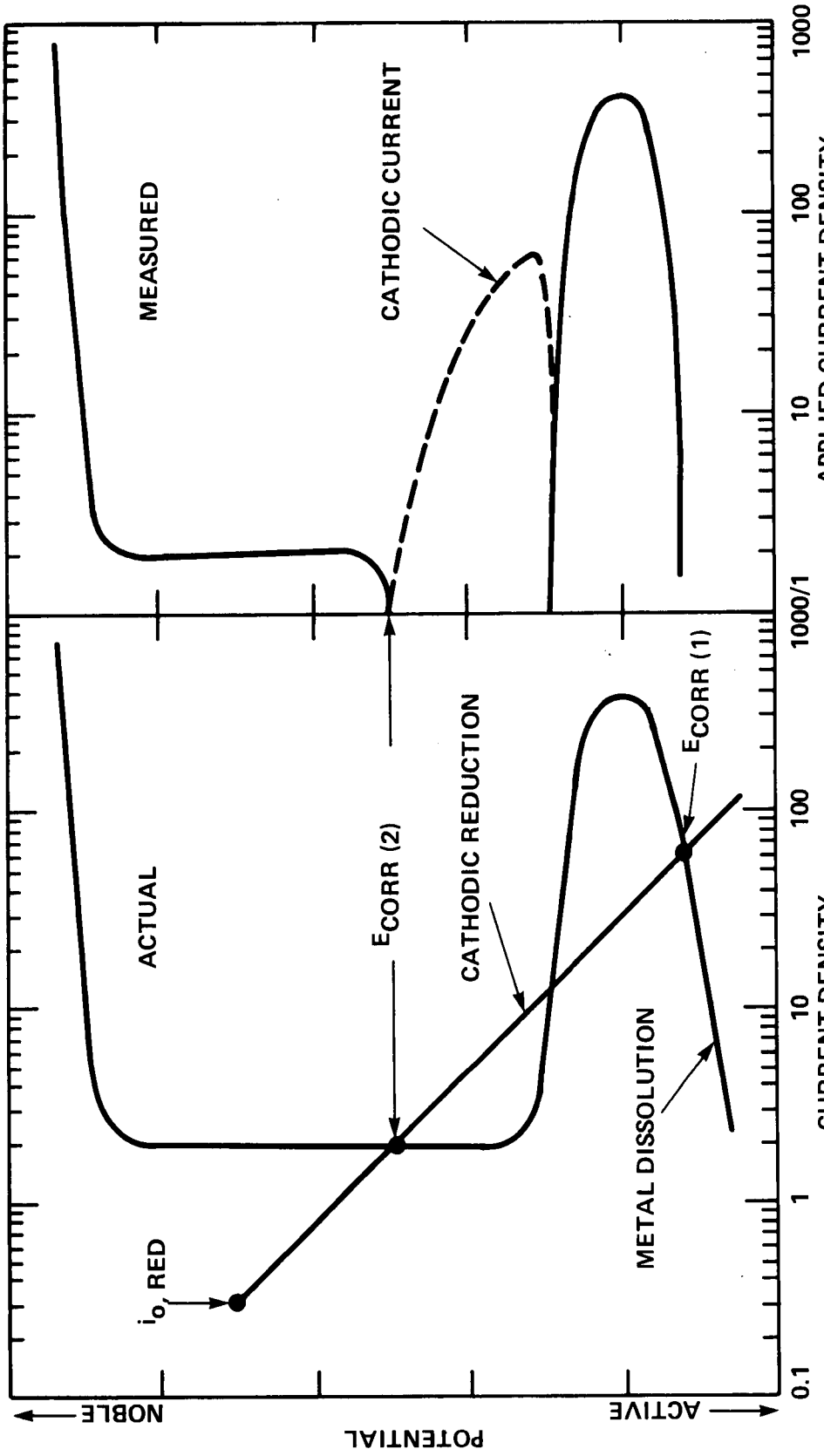


Figure 8. Actual vs. Measured Anodic Dissolution Behavior of An Active-Passive Metal. Active and Passive States Stable (Schematic).[7]

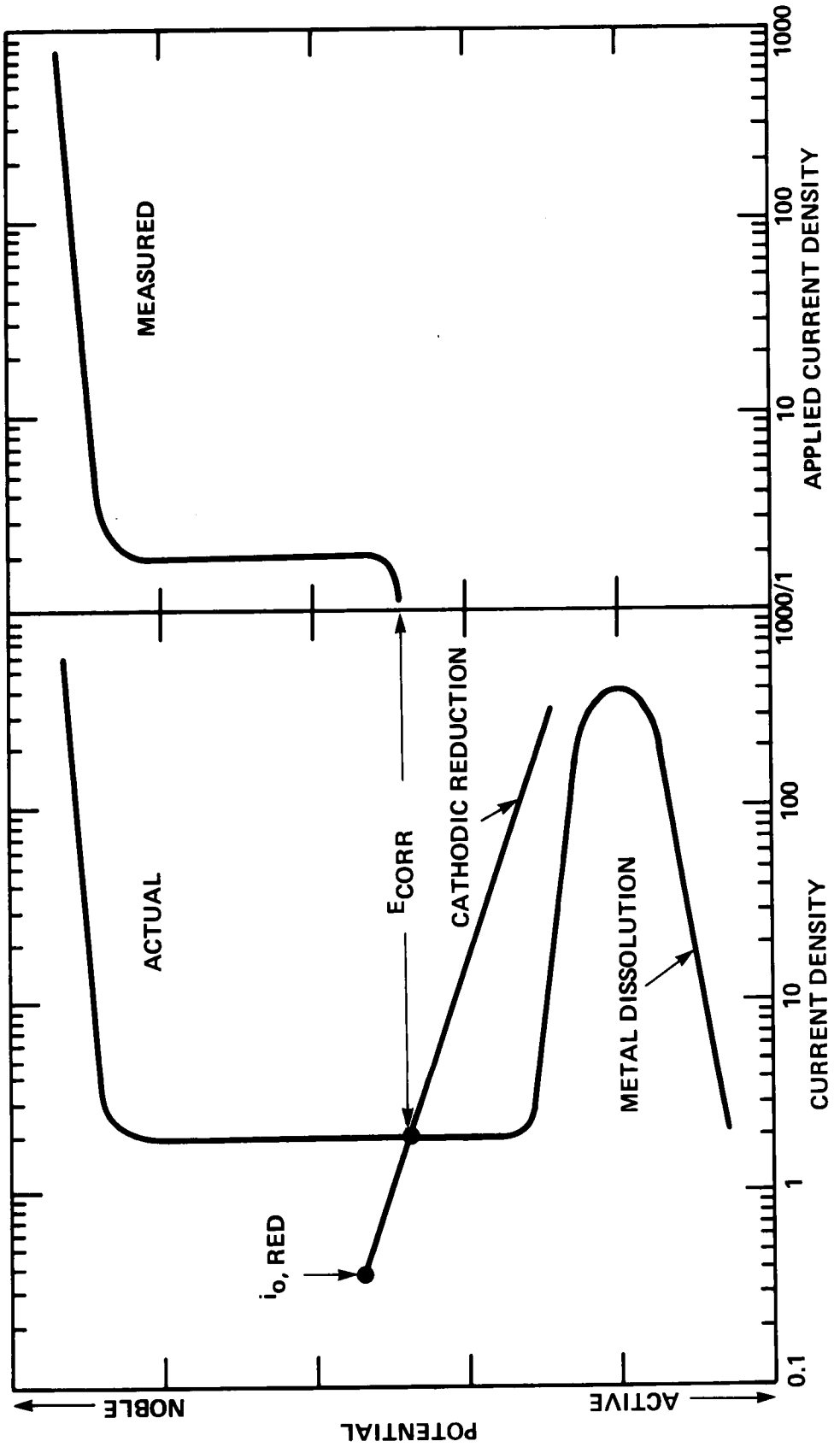


Figure 9. Actual vs. Measured Anodic Dissolution Behavior of An Active-Passive Metal. Passive State Stable (Spontaneous Passivation) Schematic.[7]

curve for 430 stainless steel evolved, as shown in Figure 10, which is today often used as an experimental calibration tool. The shaded area of the curve represents the data spread.

The capability to accurately reproduce potentiostatic and potentiodynamic anodic polarization curves conducted under standardized experimental conditions was demonstrated. The work also showed that proper laboratory procedures would yield repeatable results from a single sample, as illustrated in Figure 11. Figure 12 shows the reproducibility attainable from two different samples taken from the same heat of metal. Runs 1 and 2 represent samples from opposite ends of the 430 stainless steel rod, yet the anodic polarization curves are identical. This indicates that the chemical or metallurgical differences along the rod did not affect the overall results. The influence of some factors which can cause major variations in the results, however, is illustrated in Figure 13. The oxidizing effect of oxygen on the anodic polarization curve of 430 stainless steel was studied earlier by Greene[5]. Greene concluded that the "negative loop" effect of oxygen is typical of any strong oxidizer which, if capable of producing a mixed potential within the passive potential region, can produce stable passivity.

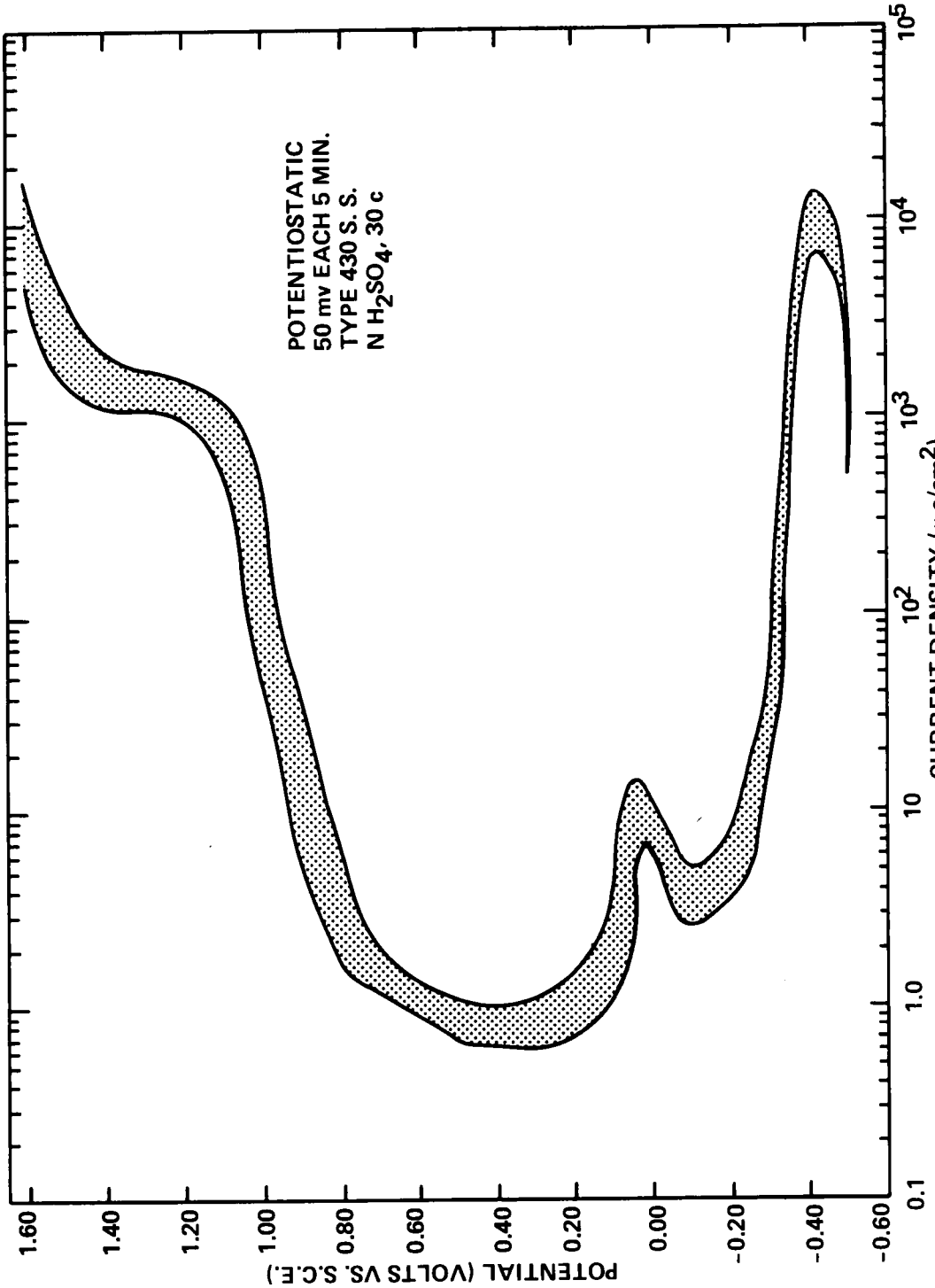


Figure 10. Standard 430 Stainless Steel Curve.[39]

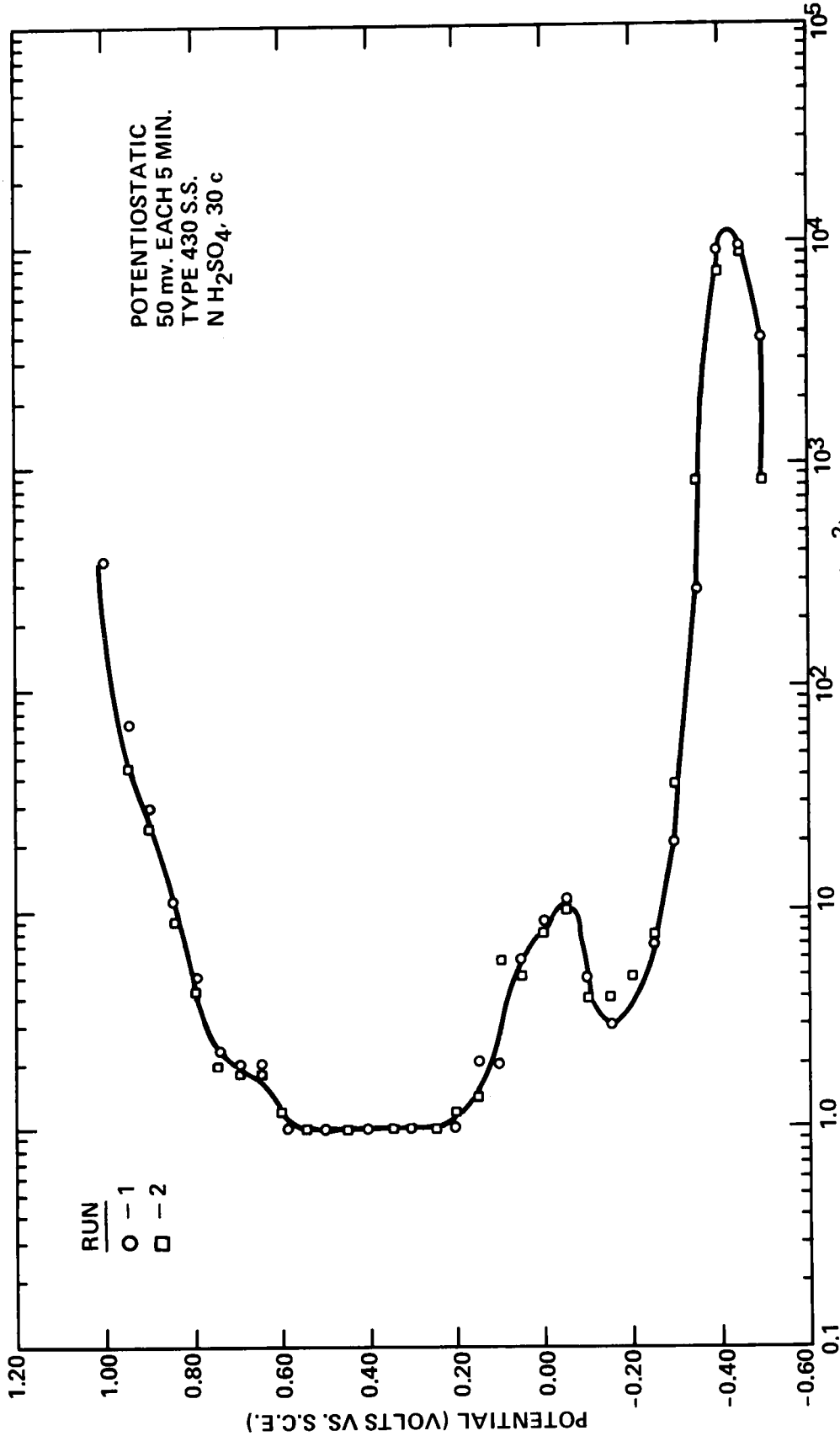


Figure 11. Laboratory Repeatability With A Single 430 Stainless Steel Sample.[39]

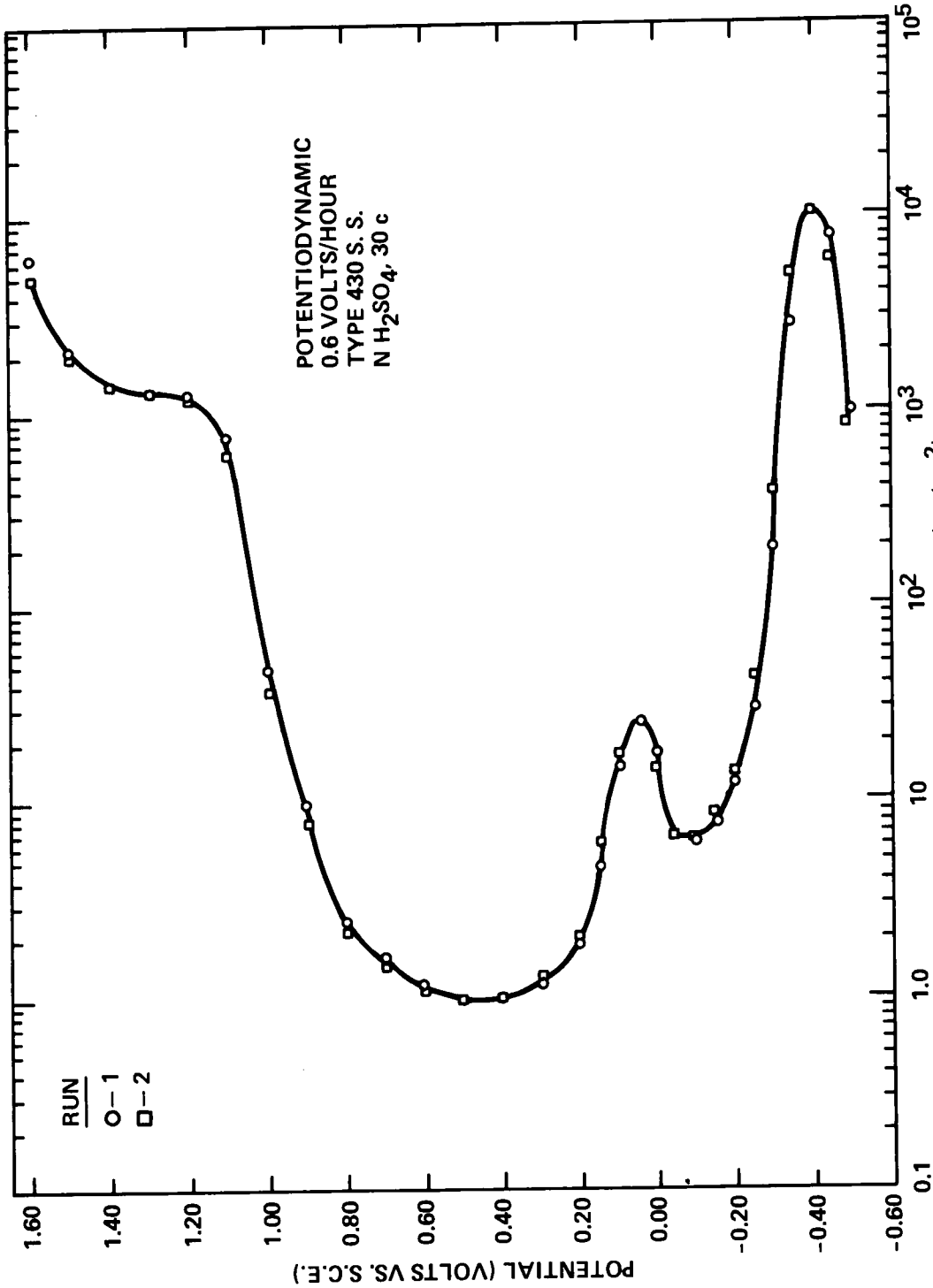


Figure 12. Laboratory Reproducibility Attainable from Two Different 430 Stainless Steel Samples. [39]

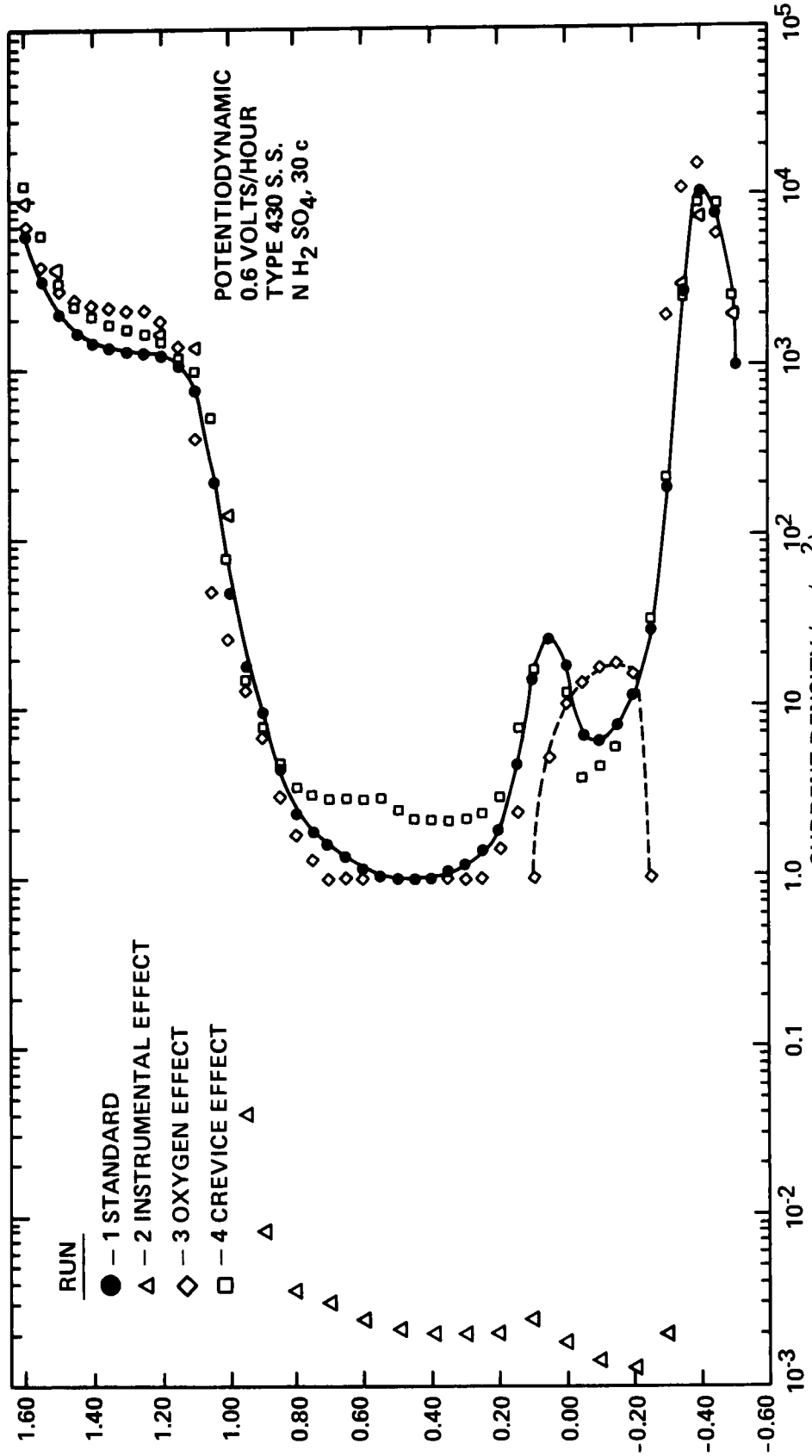


Figure 13. Major Variations Affecting Anodic Polarization Curve of 430 Stainless Steel. [39]

CHAPTER III

CORROSION THEORY

Presented in this chapter is a brief summary of some modern aqueous corrosion concepts. The treatment of basic electrochemical principles is somewhat simplified for clarity; however, all essential simplifying assumptions are stated. The usefulness of the classical potentiostat for predicting corrosion behavior is reviewed along with a discussion concerning the various aspects of anodic and cathodic polarization curve interpretation.

I. DEFINITION OF TERMS

Metallic corrosion is the result of a combination of basic electrochemical reactions: oxidation and reduction. The first of these, oxidation, is the loss of electrons by a constituent of a chemical reaction[40]. The site or electrode at which the oxidation reaction occurs is called the anode, and it exhibits the greater tendency to go into solution[21]. A typical example of an anodic process is the reaction of iron to produce ferrous ions:

$$Fe \rightleftarrows Fe^{+2} + 2e$$

In order to have charge conservation, for every oxidation reaction there must be a corresponding reaction involving

the gain of electrons. These are reduction reactions which take place at cathodic sites which may be areas that are not attacked[21]. Cathodic reactions most often encountered are illustrated as follows[3]:

$2H^+ + 2e \rightleftarrows H_2$	Hydrogen Reduction
$O_2 + 4H^+ + 4e \rightleftarrows 2H_2O$	Oxygen Reduction in Acids
$Fe^{+3} + e \rightleftarrows Fe^{+2}$	Metal Ion Reduction
$Cr_2O_7^{=} + 14H^+ + 6e \rightleftarrows 2Cr^{+3} + 7H_2O$	Metal Ion Reduction

The overall reaction describing a corrosion system would combine the oxidation and reduction half-cell reactions, and the indication of electron transfer would disappear from the equation. An example would be

$$Fe + 2H^+ \rightarrow Fe^{+2} + H_2 .$$

When a metal that is thermodynamically stable with respect to water is in a solution containing its ions, the system is in equilibrium when the rate of oxidation is equal to the rate of reduction. This movement of ions is often expressed in terms of charges transported per unit area per unit time and is called current density[24]. The rate at which cations move into solution from the anode constitutes the anodic current density, $\overleftarrow{i}_M$; whereas, the ions passing

from solution constitute the cathodic current density, $\vec{i}_M$. For an electrochemical reaction, the equilibrium exchange rate is called the exchange current density, i_o. Hence, at equilibrium,

$$i_o = \vec{i}_M = \overleftarrow{i}_M, \tag{5}$$

this current density depends on the metal ion concentration[42]. If this metal-metal ion system considered above is attached to an external electron current source capable of supplying or removing electrons, then the anodic and cathodic current densities are no longer equal and a net oxidation or reduction reaction occurs. Associated with this current flow is a change of potential and the metal electrode is said to be polarized. If a metal is in an aqueous environment where it will be thermodynamically unstable, there will be a net anodic or cathodic reaction. If in the unstable case two metal-metal ion half-cells are electrically joined or coupled, the cells will polarize each other such that the anodic reaction of one will polarize the cathodic reaction of the other and vice versa.

II. POLARIZATION

Polarization is the displacement of electrode potential resulting from the effects of current flow, measured with respect to either reversible equilibrium or steady-state corrosion potentials[21]. The amount by which the potential

changes from its equilibrium value as a result of this current flow is the overvoltage which is defined as

$$\eta = E_L - E \ , \qquad (6)$$

where η is overvoltage, E is the equilibrium corrosion potential, and E_L is the polarized potential. Polarization can essentially be divided into two main types: charge transfer polarization and diffusion polarization.

Charge Transfer Polarization

Charge transfer polarization refers to an electrochemical process which is controlled by the reaction sequence at the metal-electrolyte interface. A simplified illustration of this is the hydrogen-evolution reaction on metal in an acid solution[3]. As shown schematically in Figure 14, the first step is the adsorption or attachment of the hydrogen ion to a hydrogen atom (step 2). Two hydrogen atoms now combine to form a hydrogen molecule (step 3). As more and more hydrogen molecules are formed, they combine to form a bubble of hydrogen gas (step 4). The speed with which hydrogen ions will be reduced will be controlled by the slowest of these steps. As might be apparent from the sequence described above, charge transfer polarization is a type of activation polarization since the critical step in the process involves surmounting an energy barrier.

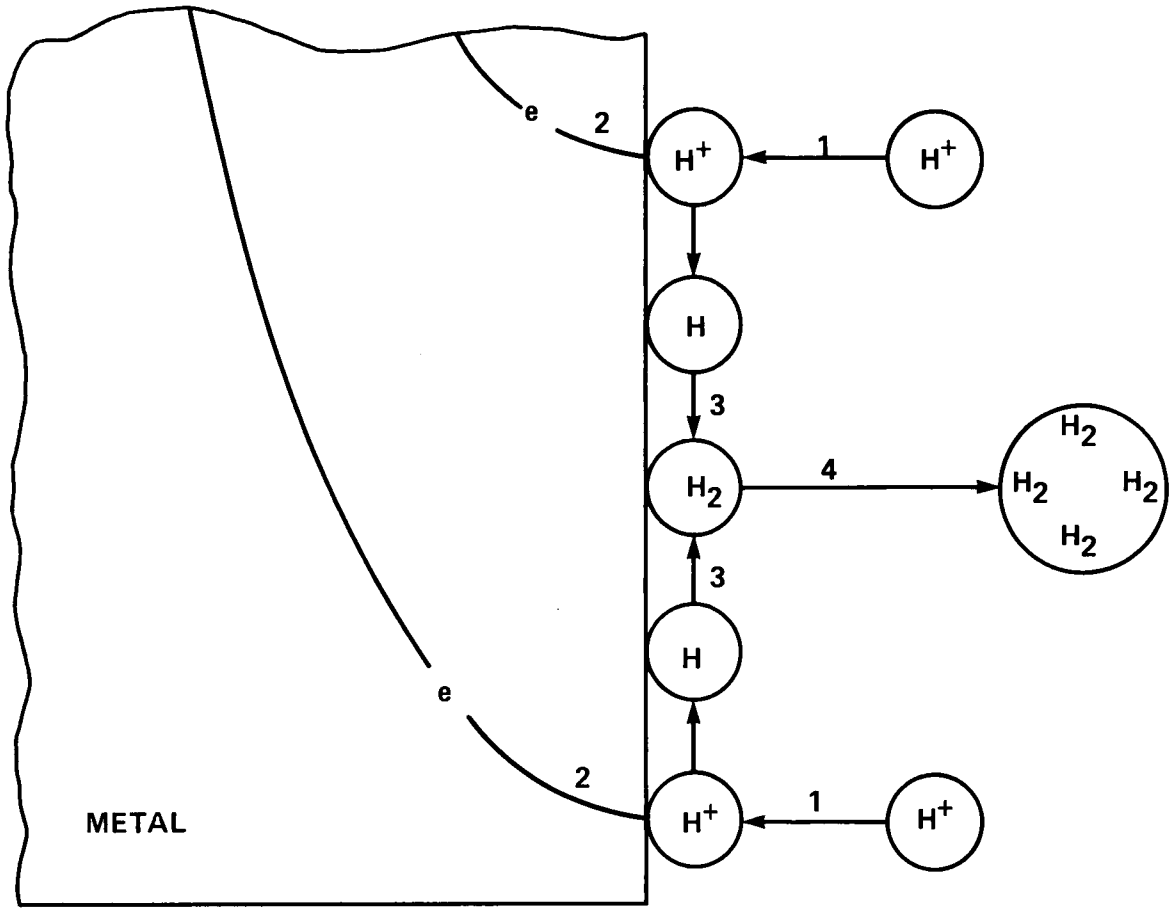


Figure 14. Simplified Hydrogen-Reduction Under Charge Transfer Control.[3]

The relationships between η and I_a and I_c are given by[18]

$$I_a = i_o A_a \left[\exp\frac{(\beta_a)(\eta_a)nF}{RT} - \exp\frac{-(1-\beta_a)(\eta_a)nF}{RT}\right] \quad (7)$$

and

$$I_c = i_o A_c \left[\exp\frac{-(1-\beta_c)(\eta_c)nF}{RT} - \exp\frac{(\beta_c)(\eta_c)nF}{RT}\right], \quad (8)$$

where A_a is the anodic area, A_c is the cathodic area, i_o is exchange current density, β_a and β_c are the anodic and cathodic transfer coefficients, η_a and η_c are the activation overpotentials, n is charge transferred, F is Faraday's constant, R is the ideal gas constant, and T is absolute temperature. When the rate of reduction is much greater than the rate of oxidation, Equation (8) reduces to

$$I_c = i_o A_c \exp[(-\beta_c)\eta_c \frac{nF}{RT}]. \quad (9)$$

When the rate of oxidation is much greater than the rate of reduction, Equation (7) reduces to

$$I_a = i_o A_a \exp[(1-\beta_a)(\eta_a) \frac{nF}{RT}]. \quad (10)$$

Simplified and written in logarithmic form, Equations (9) and (10) can be written in the generalized form

$$\eta_{CT} = \pm \beta \log \frac{i}{i_o} , \qquad (11)$$

where i is the rate of oxidation or reduction in terms of current density and β is the Tafel constant. This is the familiar Tafel equation. The relationship between the actual polarization curves and the experimentally determined polarization curves for a corroding mixed electrode system, each half-cell reaction under charge transfer control, is illustrated in Figure 15. The actual polarization curves are shown in solid lines, while measured curves are shown by dashed lines.

Diffusion Polarization

Diffusion polarization refers to electrochemical reactions which are controlled by the diffusion of the reactive species through the electrolyte. This occurs when the charge transfer reaction rate is of such magnitude that the species being oxidized or reduced cannot reach the surface of the electrode fast enough. The solution adjacent to the surface becomes depleted of the reactive species so that the reaction rate is controlled by the diffusion rate at the interface. The limiting diffusion rate is expressed as the limiting diffusion current density, i_L. The limiting diffusion current density is

$$i_L = \frac{DmF\ C_B}{x} , \qquad (12)$$

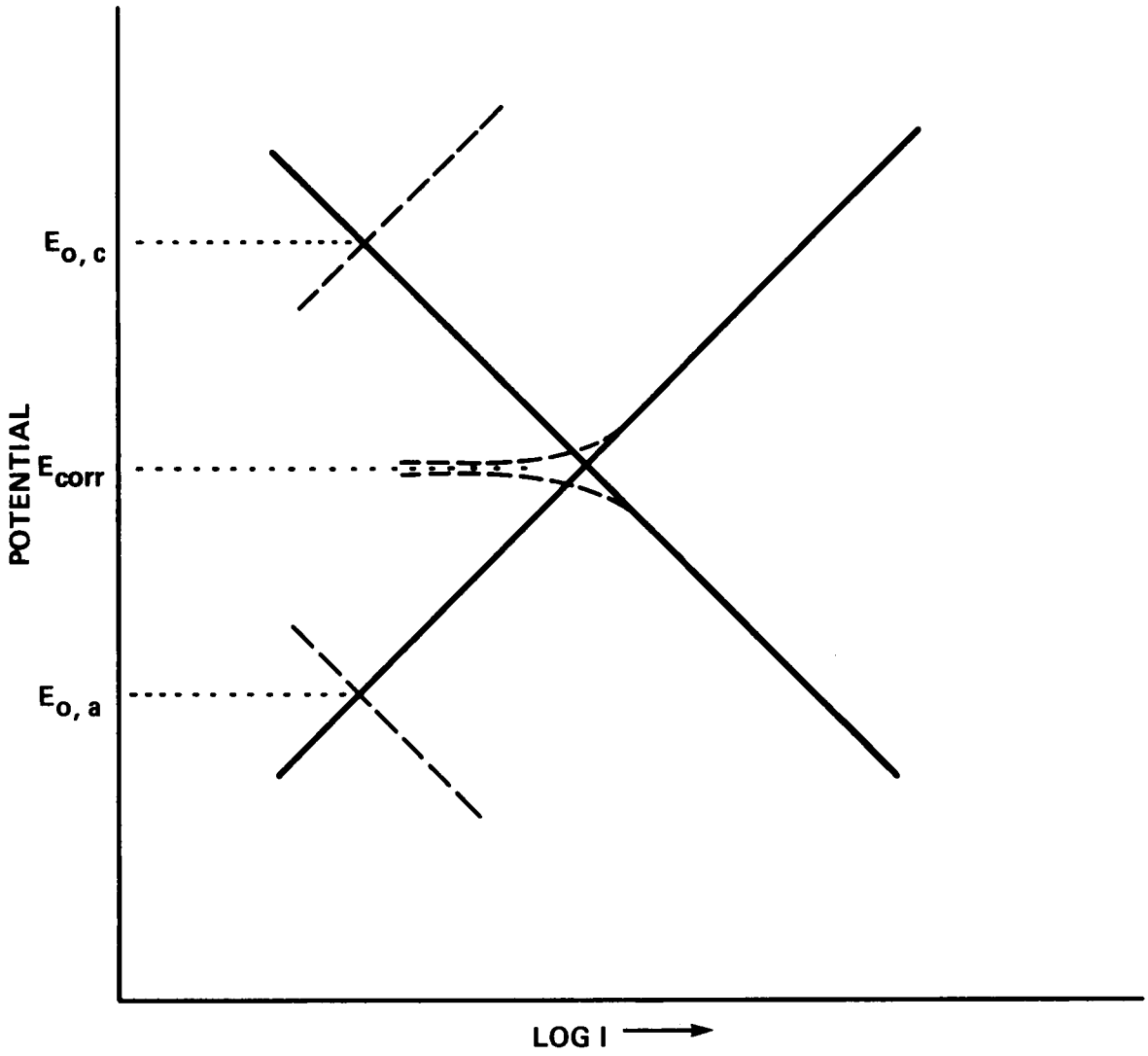


Figure 15. Charge Transfer Polarization Curve for a Reversible Electrode.[2]

where D is the diffusion coefficient of the reacting species, m is the charge on the ion, F is Faraday's constant, C_B is the bulk solution concentration of the reacting species, and x is the thickness of the diffusion layer. The relationship of limiting diffusion current density to diffusion polarization is given by

$$\eta_D = \pm 2.3 \frac{RT}{mF} \log \frac{i_L}{i_L - i} \qquad (13)$$

such that the sign is positive for anodic polarization and negative during cathodic polarization. The limiting diffusion current density for cathodic polarization corresponds to the rate of reduction of ions at the surface which essentially reduces the interface concentration to zero. As can be deduced from Equation (13), as i approaches i_L, the cathodic overvoltage goes to $-\infty$. This is shown schematically in Figure 16. As the limiting diffusion current density is a function of the interface thickness, the diffusion layer thickness is dependent on the velocity of the solution past the electrode surface. As velocity increases, x decreases, and the limiting diffusion current density increases. The effect of solution velocity on corrosion rate for a system in which the cathodic reaction is under diffusion control is shown in Figure 17. Increasing the velocity of the solution can further affect corrosion rates by eroding protective surface films.

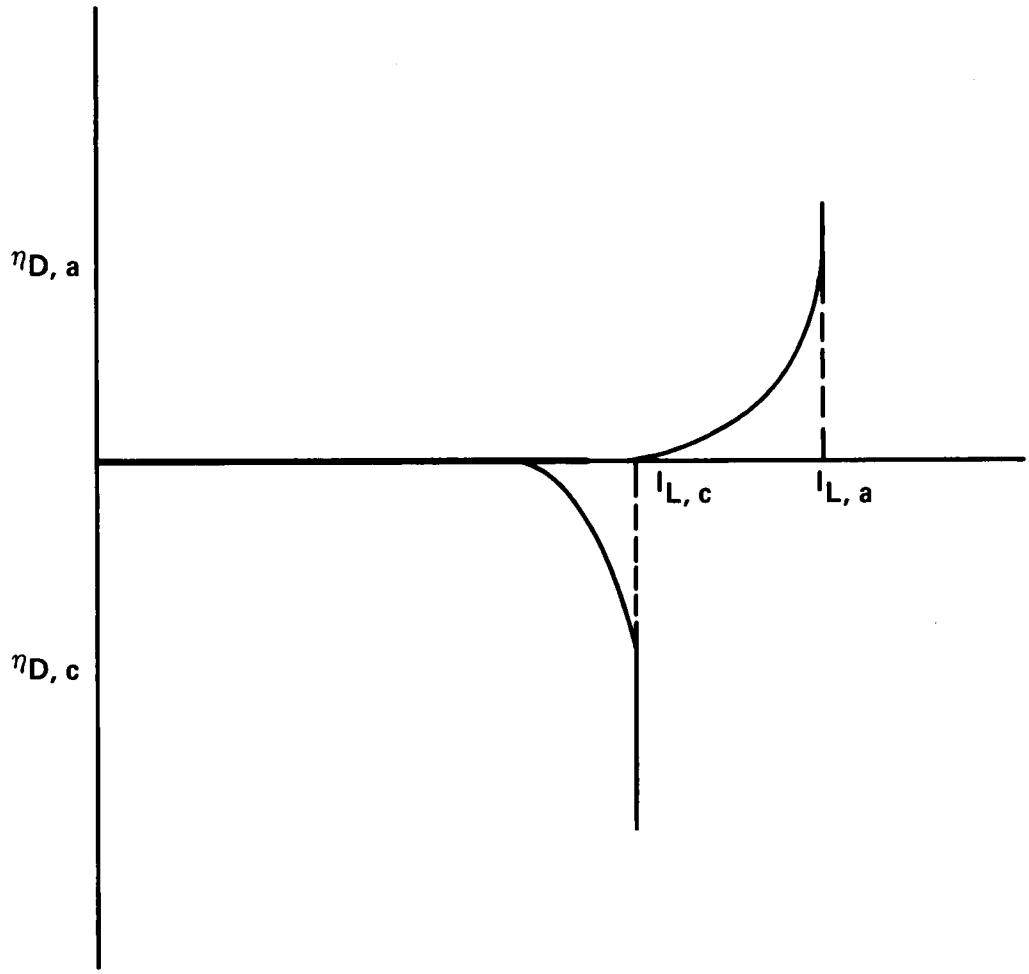


Figure 16. Effect of Limiting Current Density on Cathodic Overvoltage.[30]

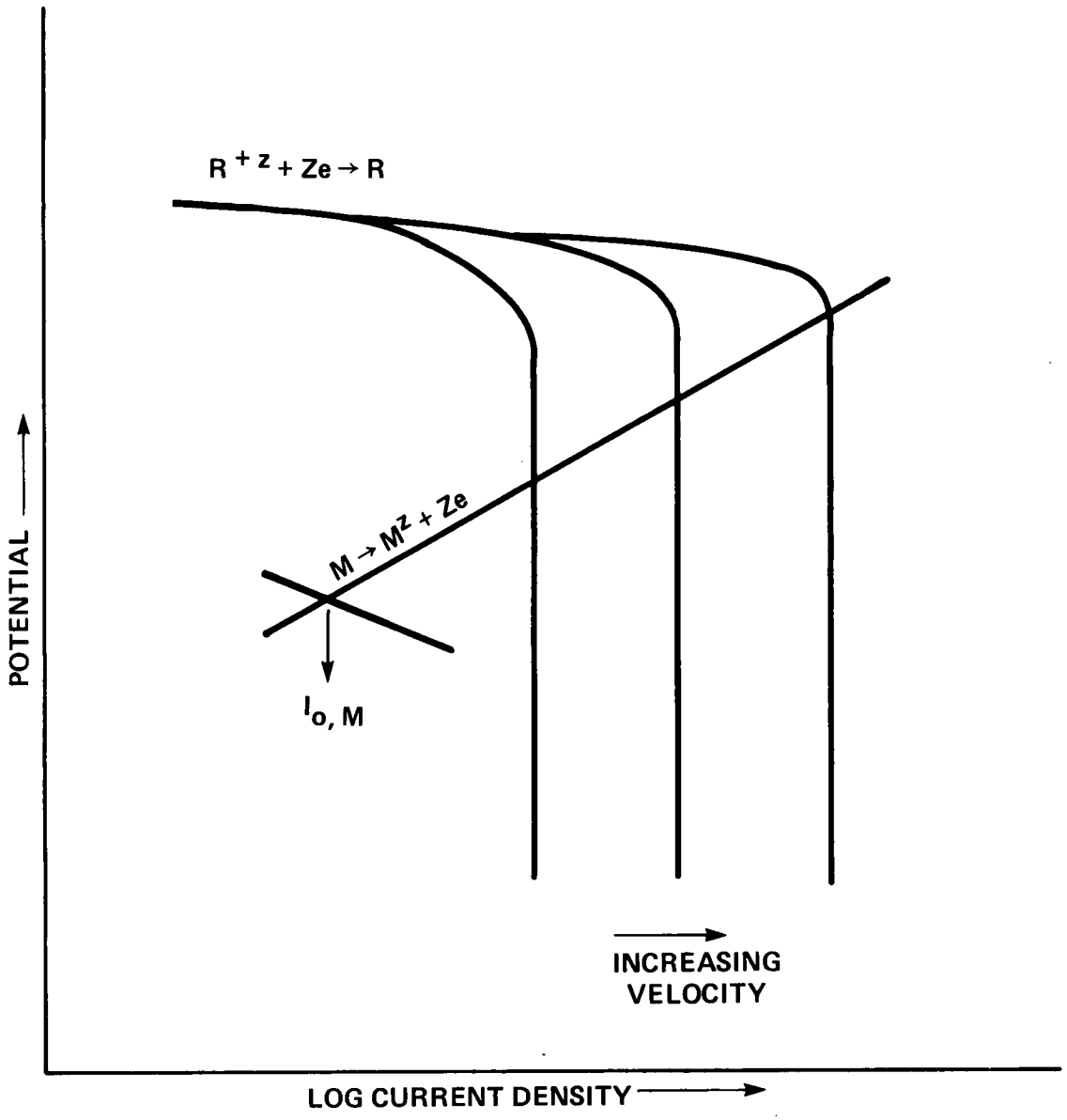


Figure 17. Velocity Effects on Corrosion Rate of Cathodic Reaction Under Diffusion Control.[31]

Combined Polarization Effects

The polarization current is for the most part determined by the magnitude of charge transfer and diffusion polarization. In electrochemical systems, the measured overvoltage is usually considered to be the sum of the charge transfer and diffusion overvoltages characteristic of that current flow; i.e.,

$$\eta = \eta_{CT} + \eta_D + \eta_R \ . \tag{14}$$

The term η_R is the resistance polarization which is a potential drop resulting from current flow through the solution resistance between the reference electrode and the polarized electrode. A function of solution conductivity, distance between the specimen and reference electrode, and system geometry, the expression for resistance polarization is

$$\eta_R = \vec{i}_x \, K_R \tag{15}$$

where K_R is the resistance term. The deviation from Tafel behavior when K_R = 10 ohms[35] is shown in Figure 18.

The combined effects of charge transfer polarization and diffusion polarization for the cathodic polarization of an electrode can be written

$$\eta = - \beta_c \log \frac{\overleftarrow{i}_z + \vec{i}_x}{i_{o,z}} - 2.3 \frac{RT}{mF} \log \frac{i_L}{i_L - i} \tag{16}$$

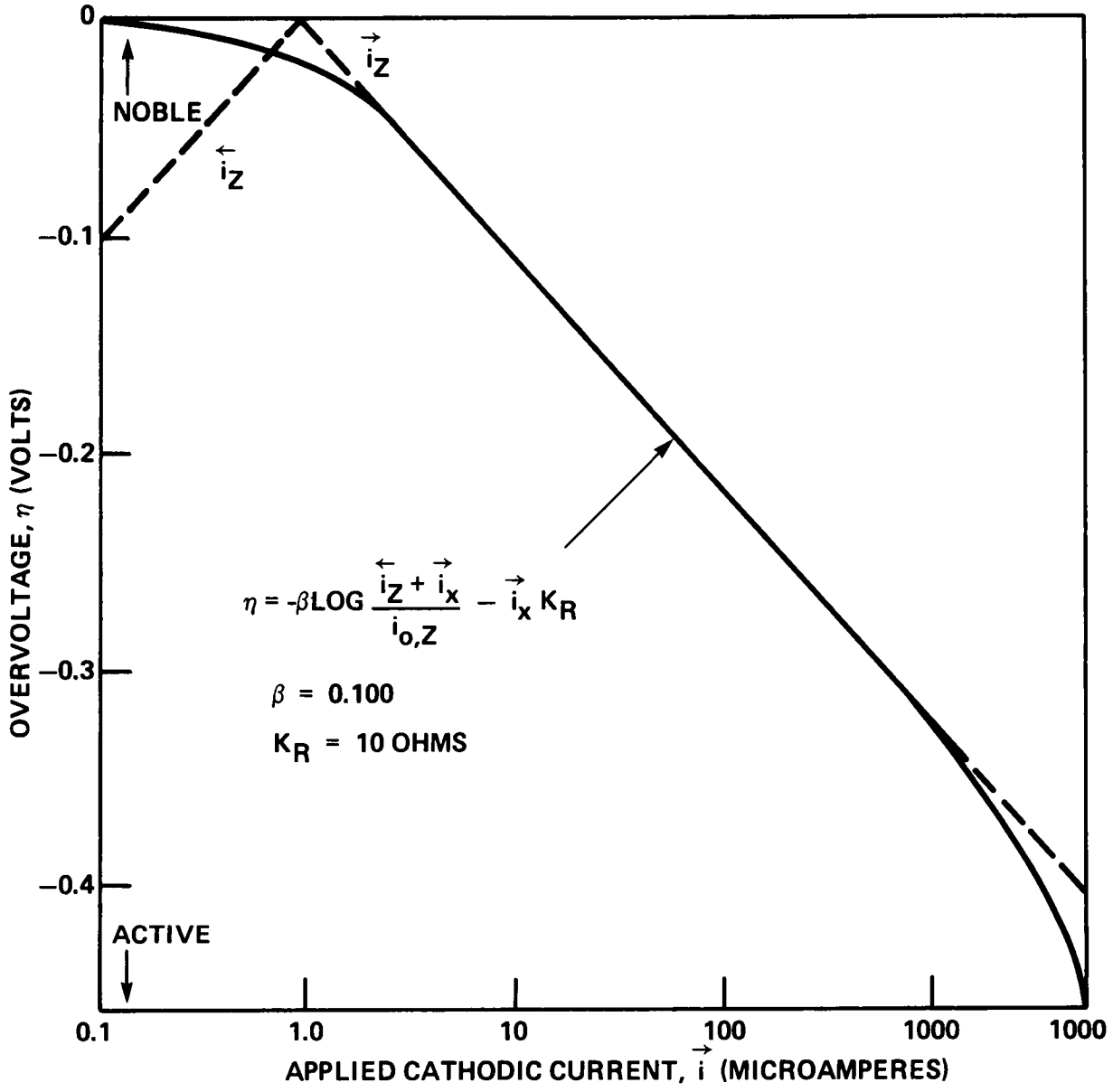


Figure 18. Effect of Resistance Polarization on the Relationship Between Overvoltage and Applied Cathodic Current for a Single Electrode System.[35]

The general shape of a curve including both charge transfer and diffusion polarization is shown in Figure 19. In this particular illustration, i_L was chosen to be 5000 μa. When $\vec{i}_z$ begins to approach 0.1 i_L, the effects of diffusion polarization become significant.

III. PASSIVATION

A process by which a metal exhibits low reactivity to a given environment is passivation. Passivation of an active metal may be induced chemically through reduction of oxidizing inhibitors or electrochemically by anodic polarization with a potentiostat[27]. Regardless of the mechanism, the reduction in corrosion rate of a metal in the passive state is often in the order of 10^4 to 10^6. This reduction in corrosion rate is the result of a typically delicate surface film which is less than 100 angstroms thick.

A metal having active-passive characteristics exhibits an anodic polarization curve of the type illustrated schematically in Figure 20. The curve can be divided into three different regions: active, passive, and transpassive. Initially, the metal reacts in a manner similar to nonpassivating metals. In this active region, as the electrode potential becomes more noble, the metal exhibits typical Tafel behavior with the dissolution rate increasing exponentially. A further increase in potential tends to cause a significant decrease in the electrode dissolution rate which then remains relatively constant over an increasing range of

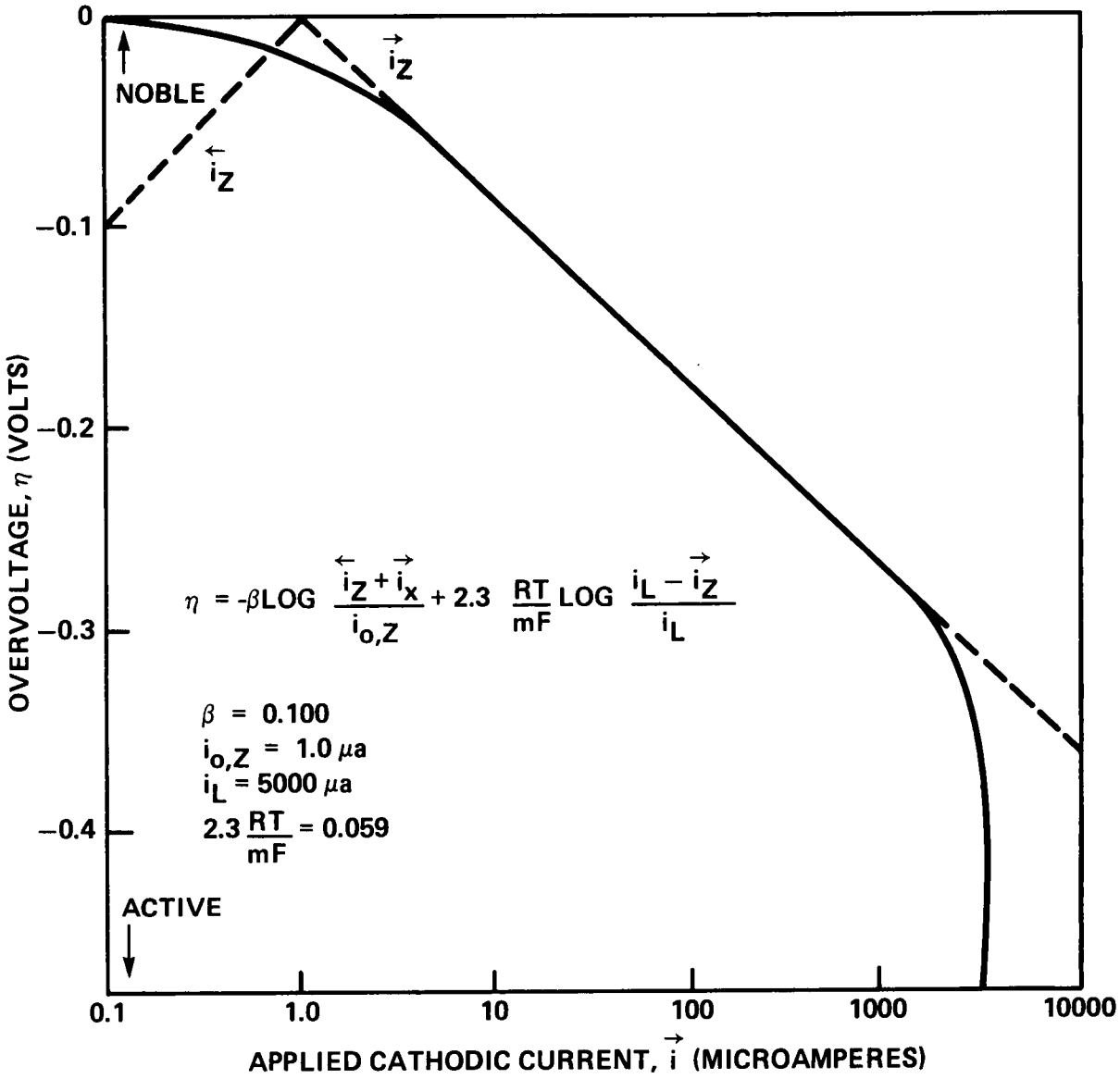


Figure 19. Effect of Diffusion Polarization on the Relationship Between Overvoltage and Applied Cathodic Current for a Single Electrode System.[35]

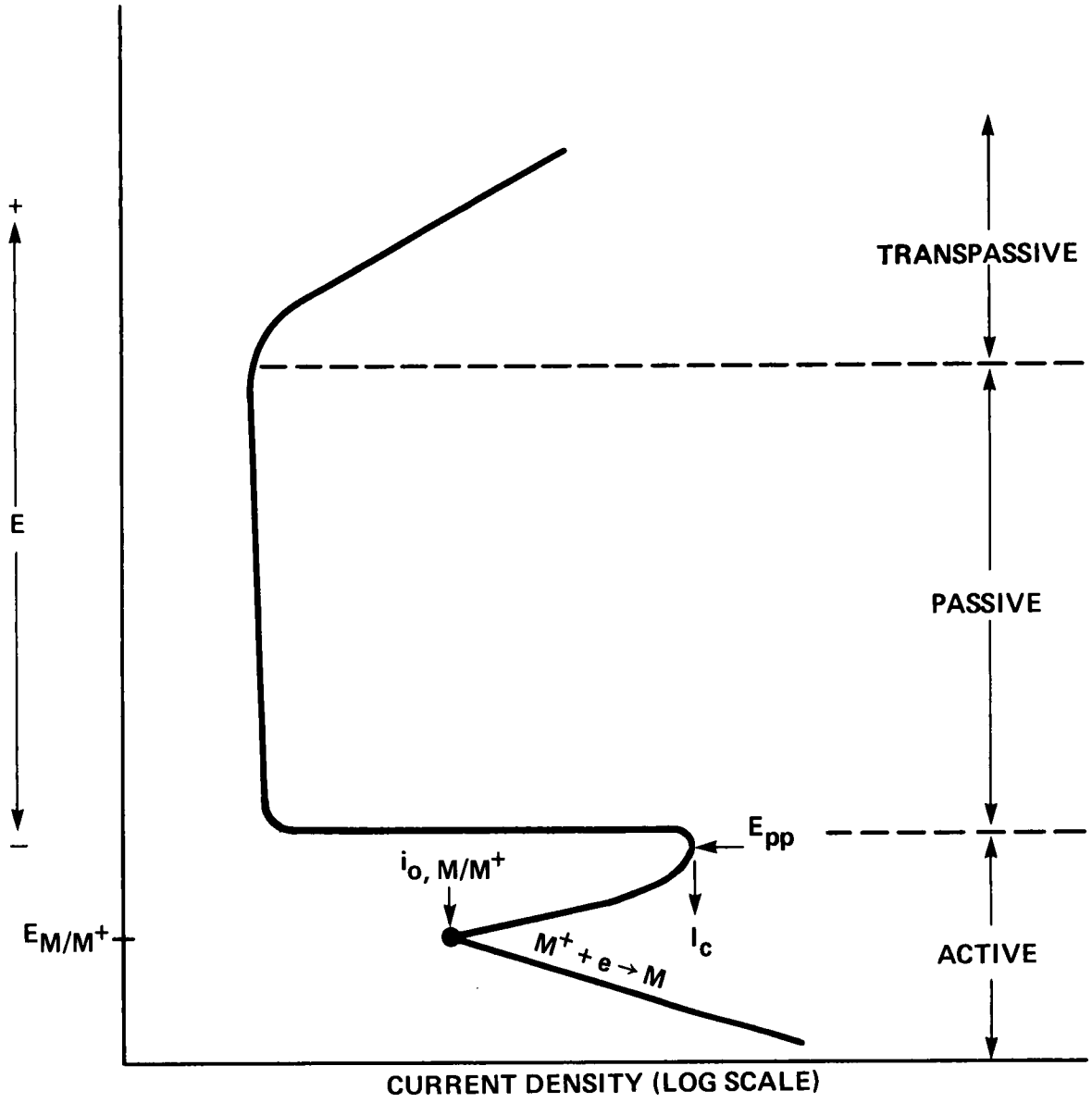


Figure 20. Schematic Anodic Dissolution Behavior of a Metal Exhibiting an Active-Passive Transition.[3]

potential. This is the passive region. At much more noble potentials, the dissolution rate once again begins to increase with increasing potentials, thus marking the transpassive region. The most important parameters describing an active-passive metal are the primary passive potential, E_{pp}, and the critical anodic current density, I_c, corresponding to the current maximum. It is at this point that the protective film formation begins to occur. Only at the very positive potentials does the film begin to break down and give rise to the transpassive region.

If this anodic polarization curve of an active-passive metal is mixed with reduction processes exhibiting charge transfer polarization, three general combinations are formed. Figure 21 illustrates these three conditions which can arise when a cathodic process is superimposed over the oxidation polarization curve. In case 1, the application of mixed potential theory indicates there is only one stable potential at A. It is at point A that the total rate of oxidation equals that of reduction. Three points exist in case 2 where the rate of oxidation is equal to the rate of reduction. However, point C is electrically unstable and cannot exist. Hence, only points B and D are stable. Point B corresponds to an active system of high corrosion rate, while D lies in the passive region and has a correspondingly low corrosion rate. Case 3 has but a single stable potential with it being in the passive region[7]. From the standpoint of

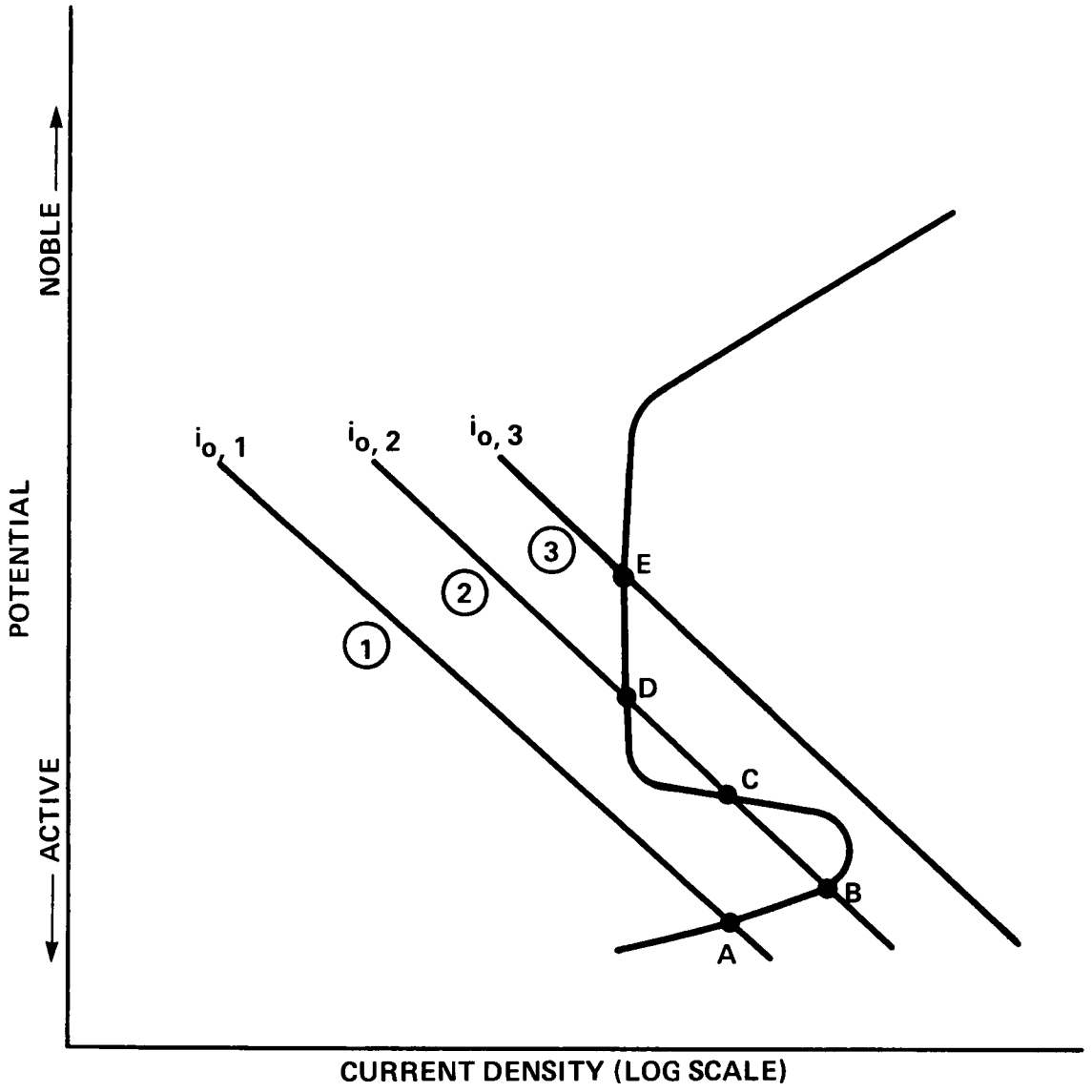


Figure 21. The Corrosion Behavior of Metals Exhibiting Active-Passive Transitions.[7]

corrosion resistance, a metal-corrosion system which will spontaneously passivate similar to case 3 is the most desirable.

For a given reduction curve, the values of the primary passive potential and the critical anodic current density determine if spontaneous passivation of a metal will occur. To illustrate the effect of E_{pp} on passive corrosion behavior, schematic anodic polarization curves for two metals are shown in Figure 22. The reduction process chosen is under charge transfer control and is assumed to influence each anodic system in a similar manner. Curve 1 reflects a metal possessing a relatively noble primary passive potential and, as a result, intersects with the reduction curve in the active region where the corrosion rate is high. A metal having a more active E_{pp}, e.g., curve 2, might intersect within the passive region of the anodic polarization curve and spontaneously passivate. If the same active-passive metals are mixed with a reduction process completely under diffusion control at potentials more noble than E_{pp}, the magnitude of the critical current density dominates resultant corrosion behavior. As shown in Figure 23, curve 1 illustrates a metal that spontaneously passivates at the single stable potential A; curve 2 exhibits both a passive and active stable potential at B and C, respectively. Therefore, a metal under diffusion control can spontaneously passivate if the anodic critical current density is less than the cathodic limiting current density.

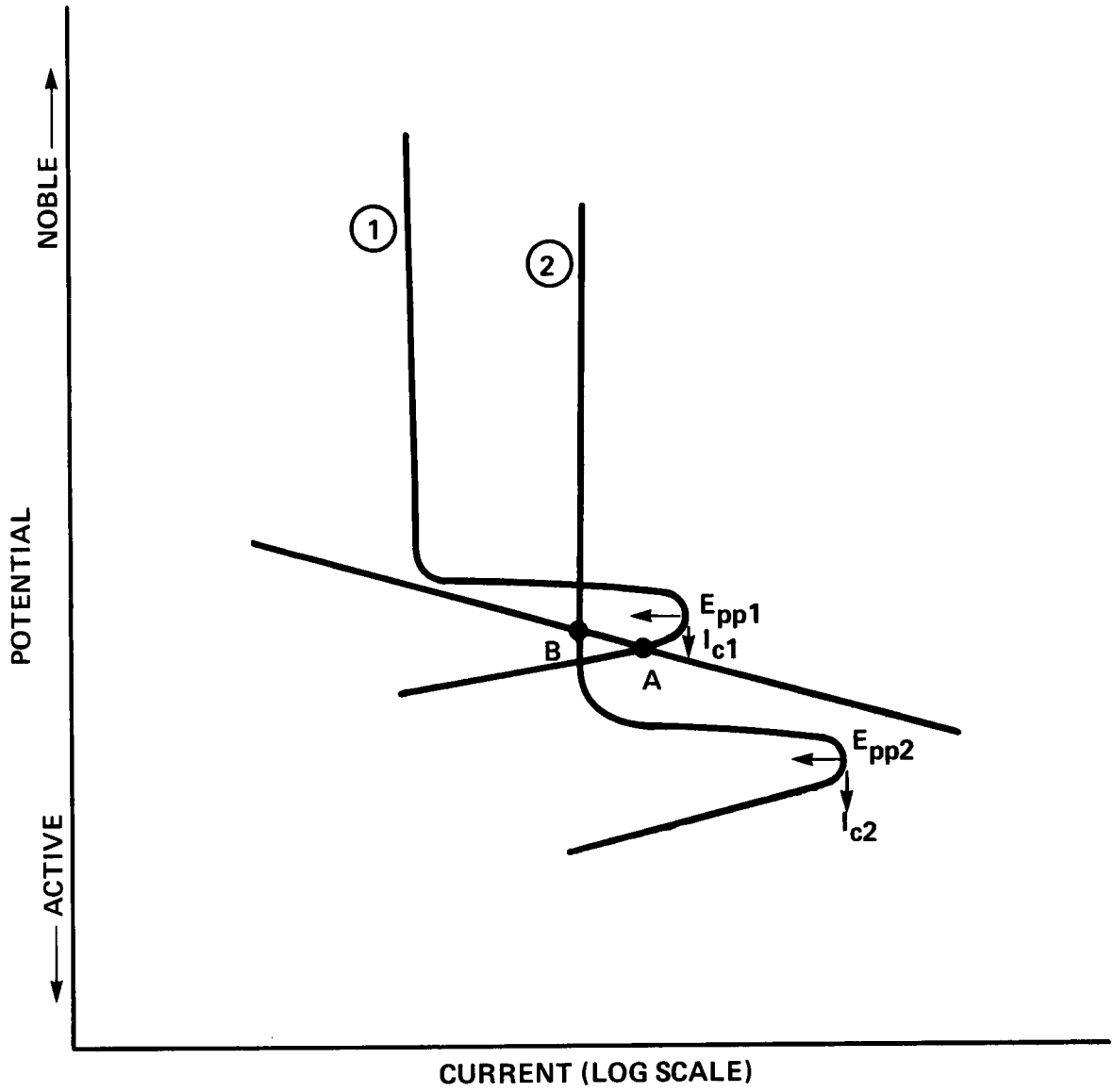


Figure 22. Effect of Primary Passive Potential on Active-Passive System under Charge Transfer Control.[31]

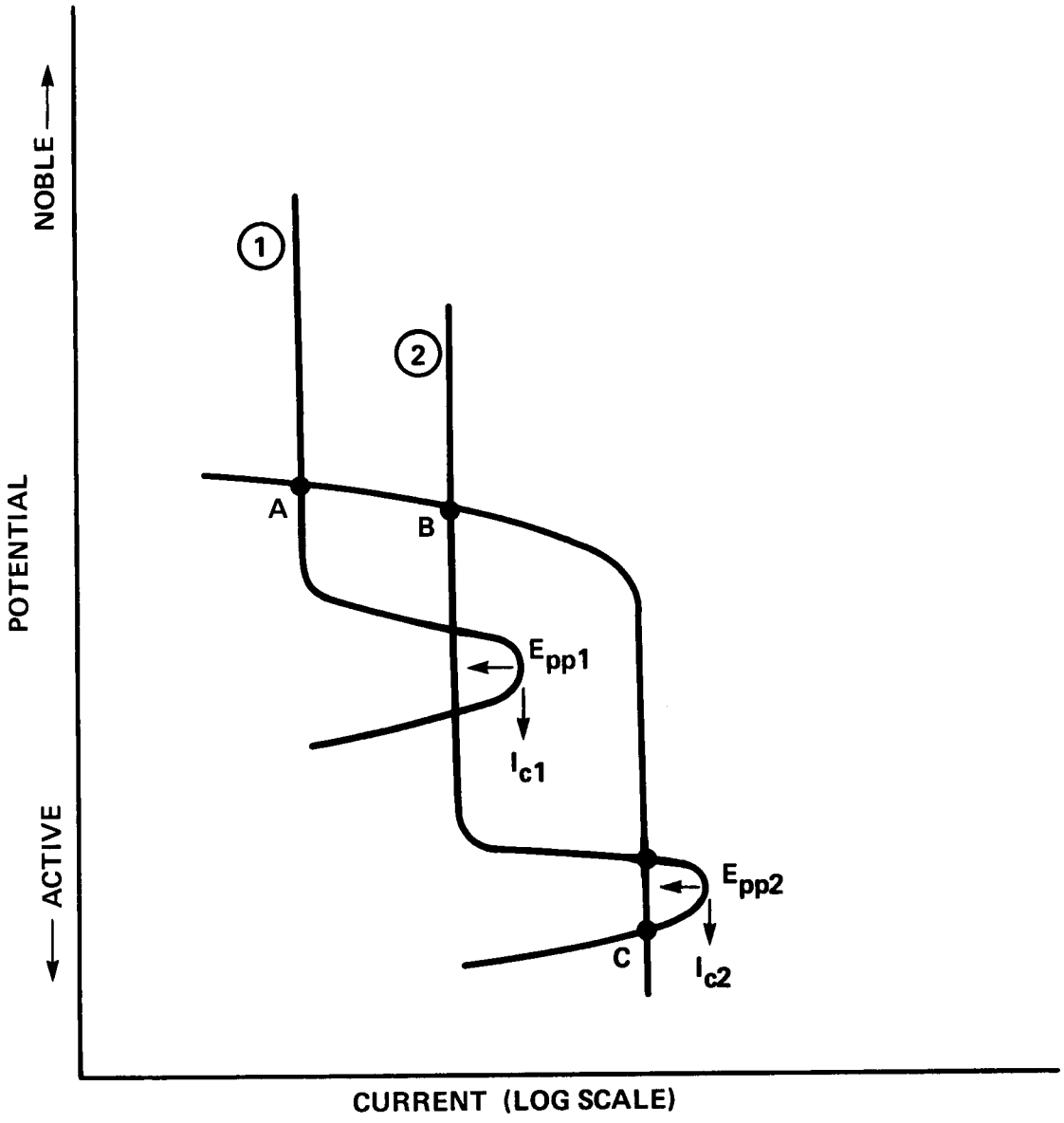


Figure 23. Effect of Critical Anodic Current Density on Active-Passive System under Diffusion Control.[31]

From the above discussion and Figures 22 and 23, two general rules can be stated concerning the ease of passivation. A metal with a very active primary passive potential is typically superior in an environment where the corrosive cathodic reduction process is charge transfer controlled. However, where the corrosive reduction process is diffusion controlled, a metal with a small critical anodic current density will passivate easier[7].

IV. METHODS FOR APPLIED CURRENT-POTENTIAL CURVE DETERMINATION

The study of applied current-potential curves has been achieved mainly with two common experimental methods. The older method is the galvanostatic method in which a constant current is applied and the resultant electrode potential is measured relative to a standard potential. The second method employs potentiostatic techniques to hold the electrode potential constant and to measure the resultant applied current density.

Galvanostatic Method

In the galvanostatic method, a constant current is applied to the electrode and the potential varies. A circuit for achieving this is seen in Figure 24. A direct current source of resistance, r_s, is placed in series with a variable resistance, r_v, and the electrolytic cell having an internal resistance of r_c. The total circuit resistance, R_t, is then

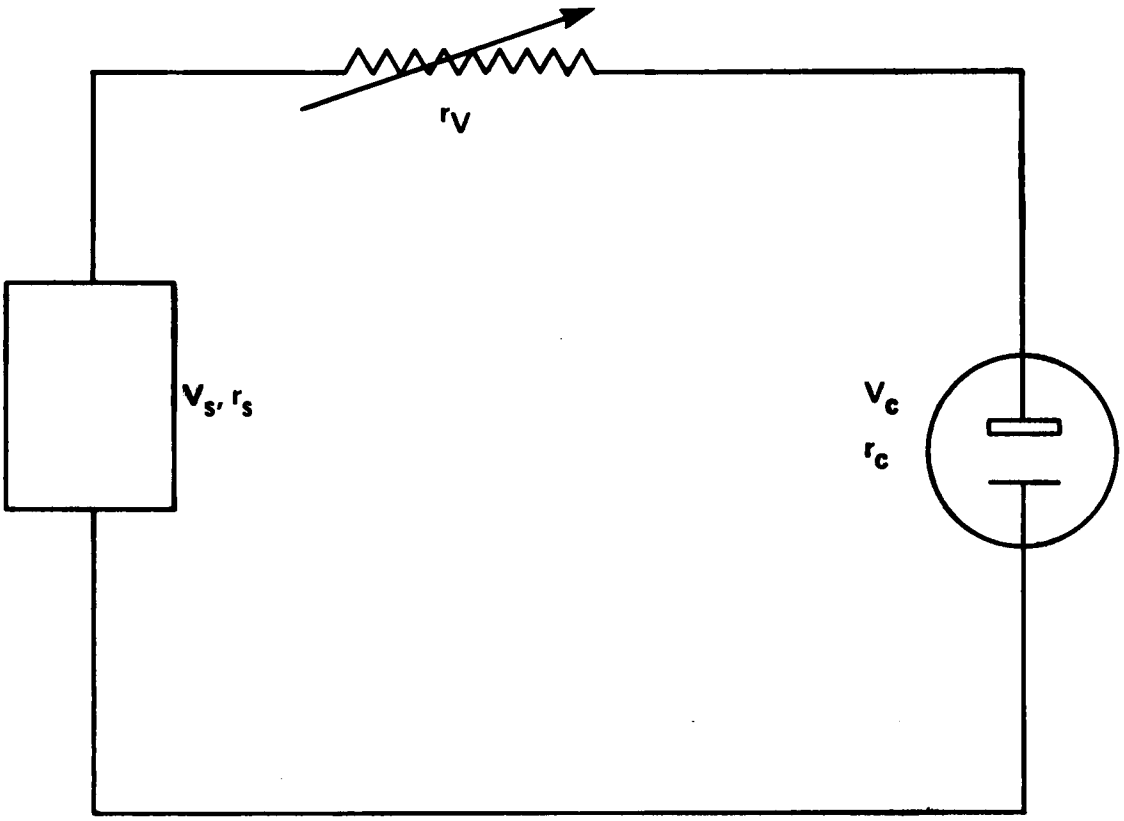


Figure 24. Typical Galvanostatic Circuit Diagram.[2]

$$R_t = r_s + r_v + r_c \ . \tag{17}$$

Application of Ohm's law yields

$$I_{appl} = \frac{V_s - V_c}{R_t} = \frac{V_s - V_c}{r_s + r_v + r_c} \ . \tag{18}$$

If the resistance external to the cell, r_s and r_v, is sufficiently greater than r_c, Equation (18) becomes

$$I_{appl} = \frac{V_s - V_c}{r} \tag{19}$$

from which

$$\frac{\delta V_c}{\delta I_{appl}} = - r \ , \tag{20}$$

where $r = r_s + r_v$. Therefore, as long as r is kept much greater than r_c, the external resistance controls the current and changes in r_c have only negligible effect on the magnitude of I_{appl} [2]. When a circuit of this type is used to obtain an anodic polarization curve of a metal exhibiting active-passive behavior, a discontinuity of the curve develops at currents above I_c as the potential shifts from E_{pp} to a stable position within the transpassive region at a much more noble potential. An example of this condition is seen in Figure 25.

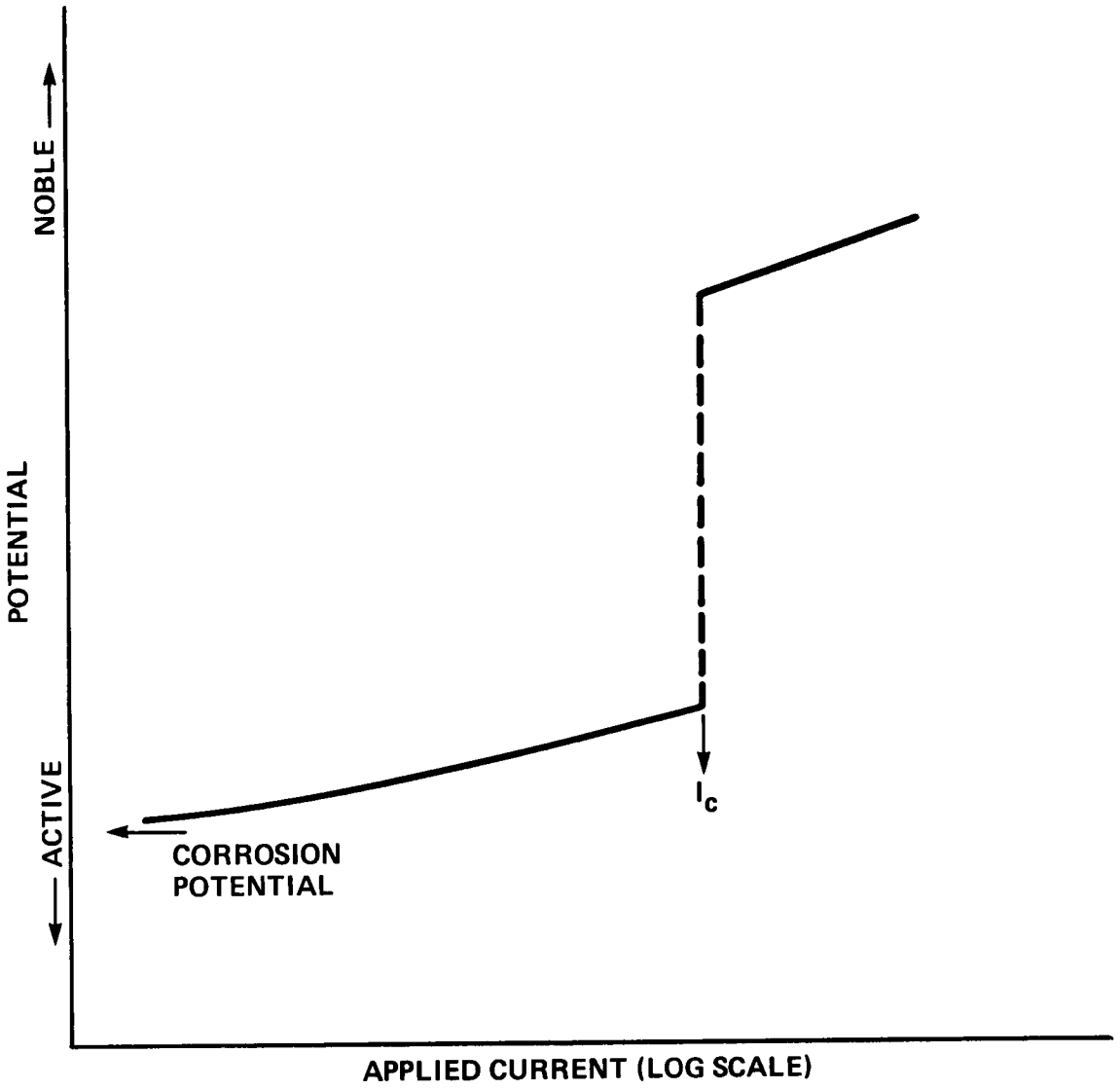


Figure 25. Anodic Polarization Curve Obtained by Varying Current.[8]

Potentiostatic Method

A potentiostat maintains an electrode at a desired potential. The potentiometric circuit shown in Figure 26 can provide a continuously variable potential by employing a voltage divider. The battery potential is E, the resistances of the potential divided are R_1 and R_2, I is the current through the inner loop of the potential divider, i is the output current, and r is the electrolytic cell resistance or any load resistance[8]. If Thevenin's method is applied to this circuit, the equivalent series circuit shown in Figure 27 results. Here,

$$E' = \frac{R_1 + R_2}{ER_1} \tag{21}$$

and

$$r_s = \frac{R_1 R_2}{R_1 + R_2} . \tag{22}$$

E' is the equivalent series potential and r_s is the equivalent series resistance. However, the total resistance of the circuit is given as

$$R_p = r_s + r_i + r_m , \tag{23}$$

where r_i is the ammeter resistance and r_m includes any miscellaneous resistances from wires or contacts in the circuit.

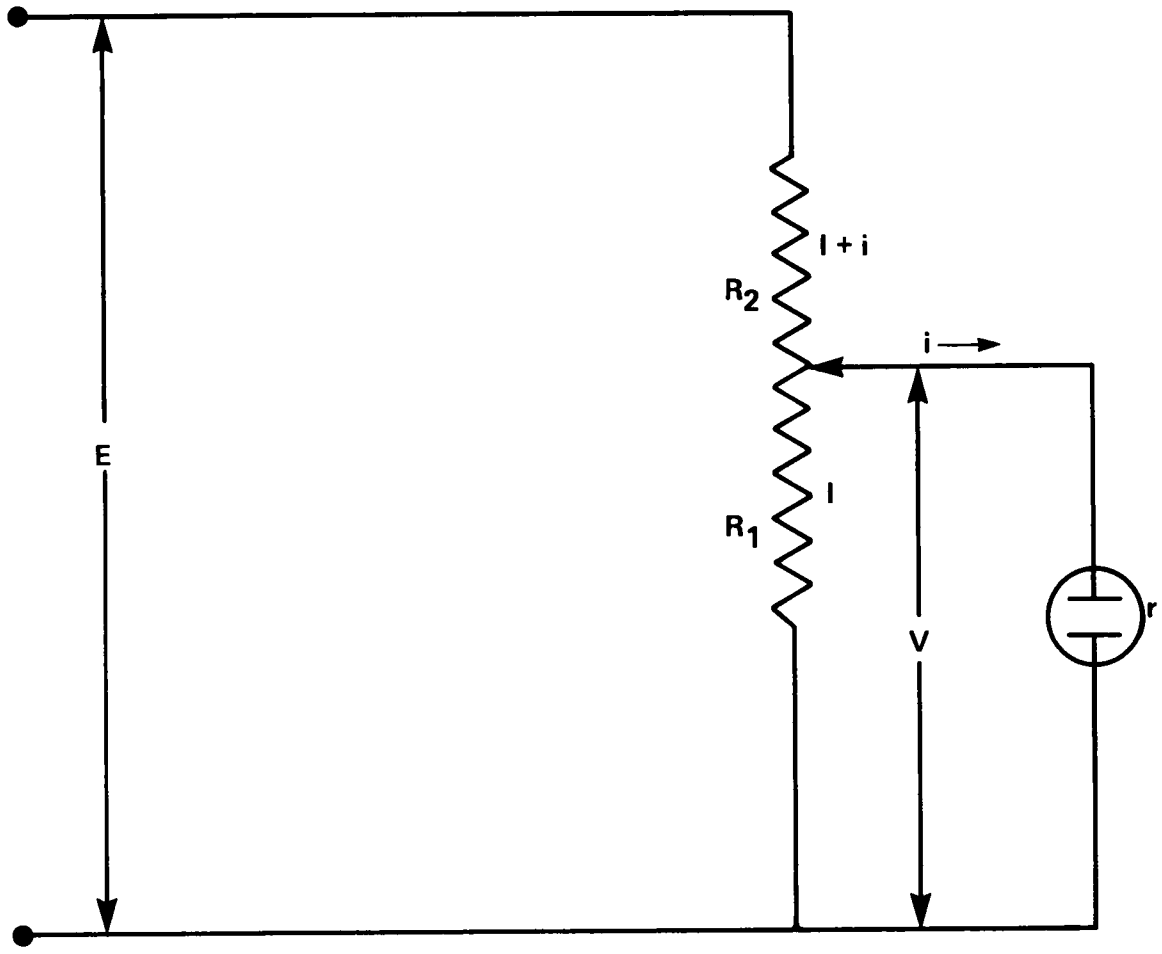


Figure 26. Potentiometric Circuit for Maintaining Desired Potential.[8]

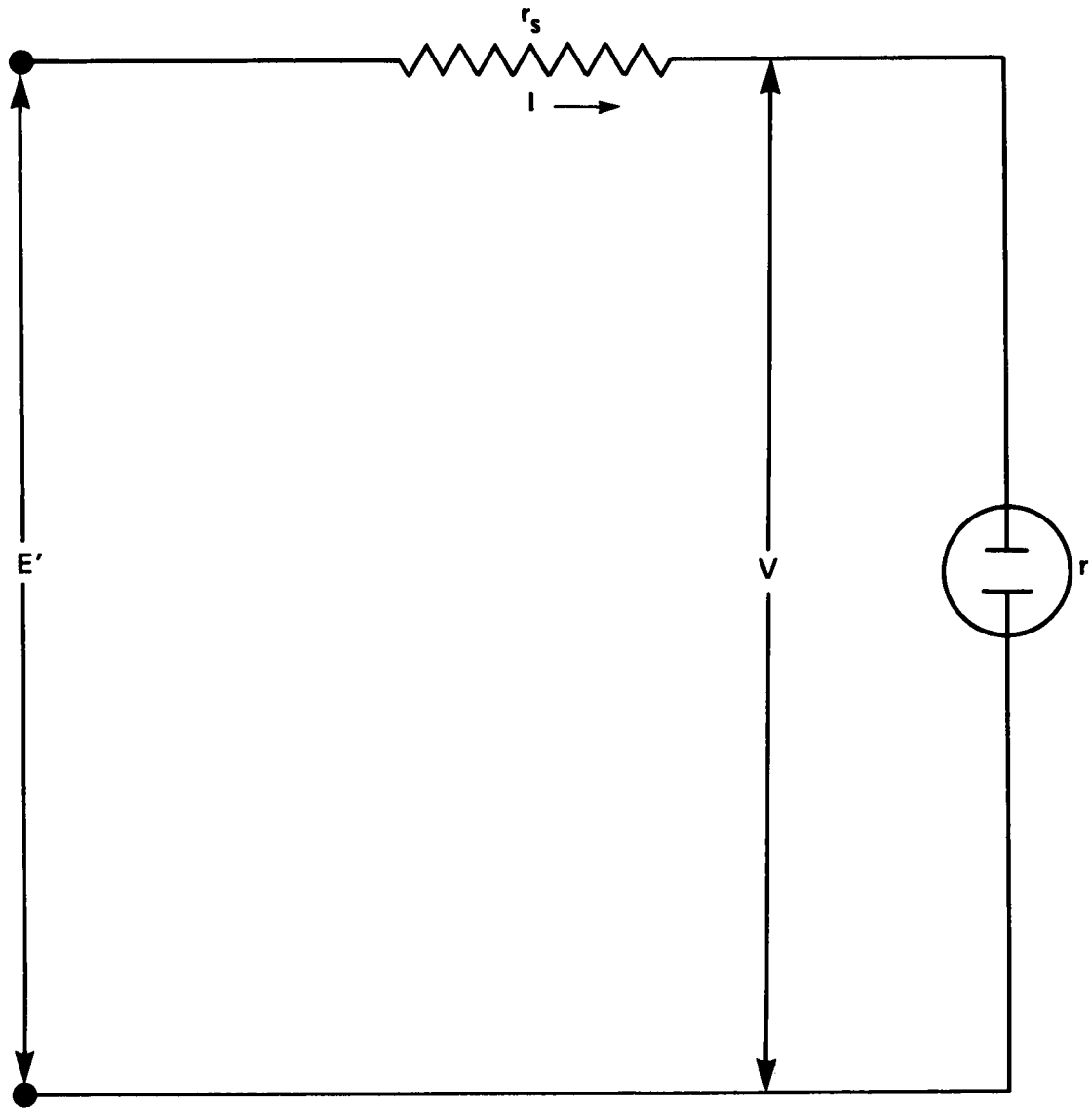


Figure 27. Potentiometric Equivalent Series Circuit.[8]

In addition to these external resistances, the total internal resistance, r, of the cell is comprised of resistances due to anodic and cathodic polarization, plus the resistance of the electrolyte itself. The total internal resistance is

$$r = r_a + r_c + r_e \ . \qquad (24)$$

In most systems, r_a and r_c are not constant but vary with current.

Since the total resistance is the sum of the internal and external resistances, the total resistance, R, of a system cathodically polarized is

$$R = r_s + r_i + r_m + r_c + r_e = R_p + r_c + r_e \ . \qquad (25)$$

The effect of R on the measured anodic polarization curve for a system is illustrated in Figure 28. If R is extremely large, a constant current circuit is obtained. As R decreases, the measured curve more closely approximates the actual curve. The total anodic polarization curve can be obtained only if R is equal to or less than the minimum slope of BC in Figure 28.

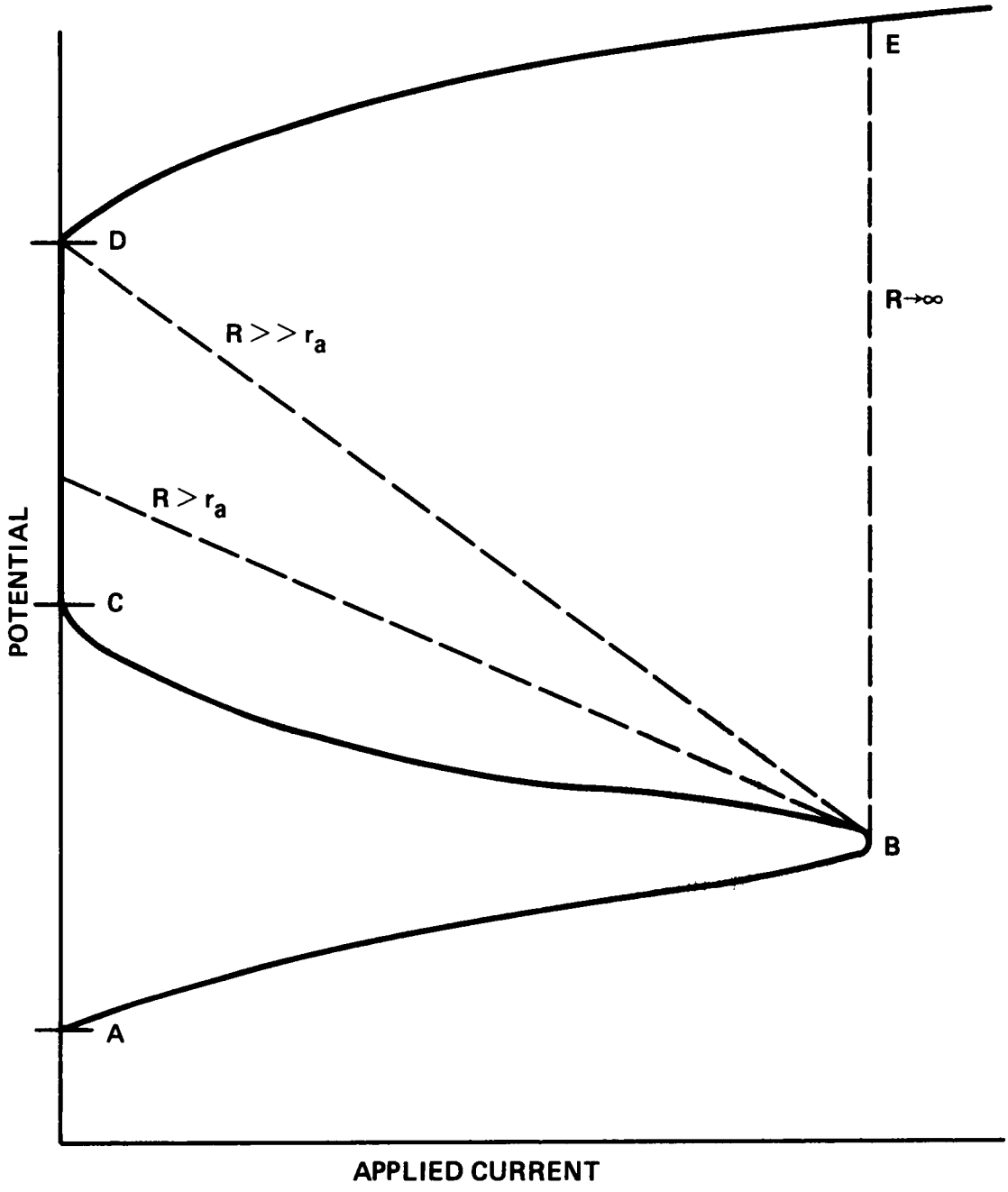


Figure 28. Effect of Total Series Resistance on the Measured Anodic Polarization Curve.[8]

CHAPTER IV

EXPERIMENTAL PROCEDURE

A brief discussion of the experimental procedures and techniques used in this study is presented.

I. ELECTROLYTIC SOLUTIONS

During the course of this investigation, four different acidic solutions were evaluated. A 1.0 N sulfuric acid solution was chosen as the standard solution for purposes of experimental calibration. Because of extensive testing by many investigators[4,9,10,15-17,20], the polarization behavior of most common metals and metallic alloys has been established in sulfuric acid. The test solution was prepared by diluting reagent grade concentrated sulfuric acid with distilled water. Preparation procedures for the other three acidic solutions are described by Streicher[37]. These electrolytes included a reducing acid, i.e., 10% hydrochloric acid solution, and two oxidizing solutions, i.e., 50% sulfuric acid-0.1 M ferric sulfate solution and 10% chromic acid solution.

II. SPECIMEN MATERIALS

The materials used as working electrodes consisted of a 430 stainless steel specimen, a platinized platinum electrode, and three compositions of nickel-chromium-molybdenum alloys. The 430 stainless steel sample was fabricated into

a 0.78-centimeter circular rod, 0.92 centimeter long. One end was drilled and tapped for mounting. This alloy was used in the 1.0 N sulfuric acid solution as a standard[39] to test equipment calibration. The platinized platinum specimen was a small, thin sheet with nominal dimensions of 1 centimeter by 1 centimeter per side. Use of the platinum electrode facilitated characterization of the oxidation-reduction behavior for each test solution. The three nickel-rich alloys of compositions shown in Table III were water-quenched samples prepared for testing as described in an earlier study[24].

III. POLARIZATION TEST CELL

The polarization test cell was a modified version of the standard cell first described by Greene[6]. The 1-liter glass flask contained one large central neck into which the working electrode mounting assembly support (Figure 29) was inserted. Symmetrically positioned around the central neck were four smaller necks necessary for accommodating an auxiliary electrode, a Luggin probe assembly, a purging gas assembly, and a thermometer.

The specimen mounting procedure, shown in Figure 30, was that proposed by Stern and Makrides[36]. This technique yields a crevice-free specimen when properly mounted[11,14]. The auxiliary electrode was formed from cylindrically shaped bright platinum approximately 15 centimeters in length and 5 centimeters tall. Almost encircling

TABLE III

NOMINAL COMPOSITIONS OF THE NICKEL BASE ALLOYS

Alloy	Weight Percent Nickel	Weight Percent Chromium	Weight Percent Molybdenum
1	66	18	16
2	65	25	10
3	60	35	5

Source: G. J. Pitzl. (1971) M. S. Thesis, The University of Tennessee, Knoxville, Tennessee.

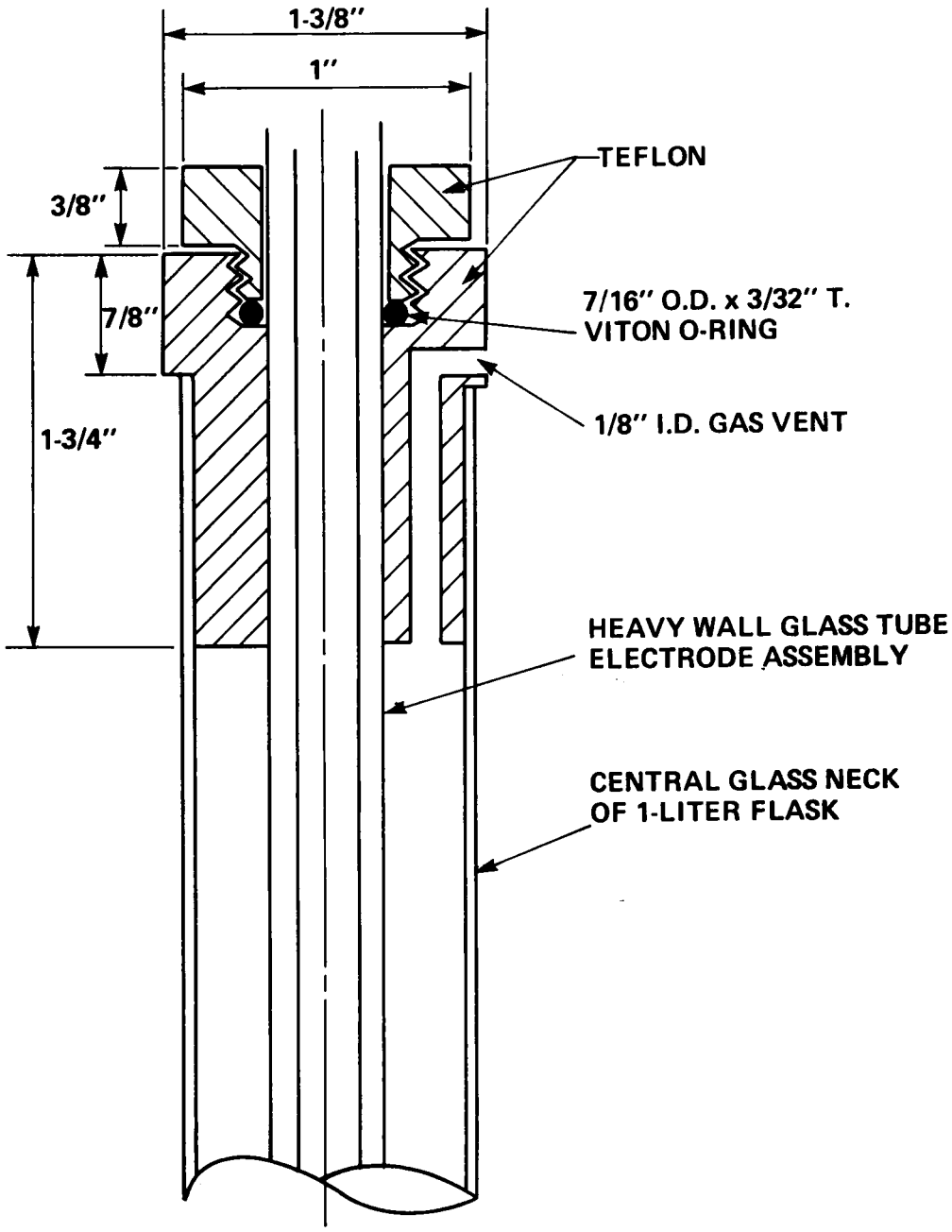


Figure 29. Upper Part of Electrode Assembly System.[24]

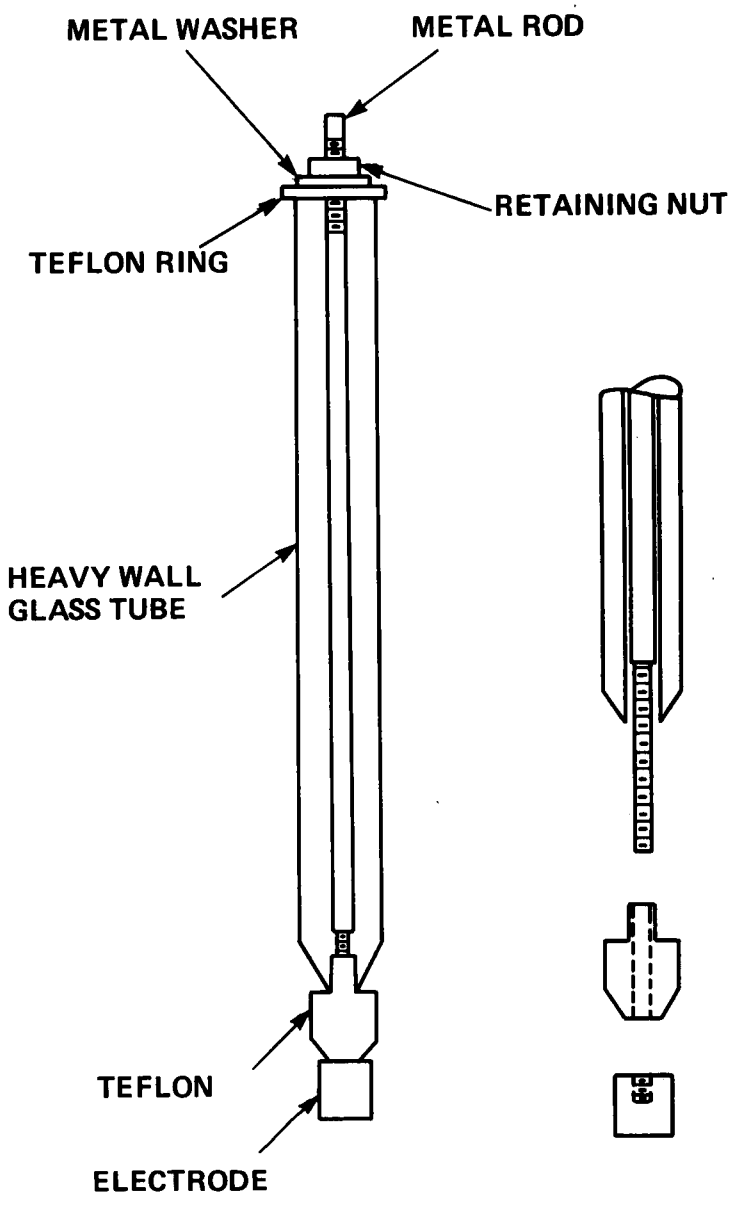


Figure 30. Electrode Assembly.[36]

the working electrode, this large surface area provided a very low polarization resistance and its proximity to the anode maintained a negligible solution resistance.

The Luggin probe acid bridge was similar in design to that suggested by Greene[6]. The acid bridge connected to a two-neck, 500-milliliter glass flask reservoir in which the reference electrode was placed during testing. This arrangement greatly reduced any error due to chloride ion contamination in the vicinity of the specimen. Both the Luggin probe acid bridge and the reservoir were filled with the same electrolyte as in the test cell. The reference electrode was a silver-silver chloride electrode[1,30] prepared in the laboratory utilizing saturated potassium chloride solution. The potential for this electrode was 0.196 volt relative to a standard hydrogen electrode (SHE).

IV. EXPERIMENTAL TECHNIQUE

After cleaning the test cell with acetone and rinsing with distilled water, the glass flask was filled with the test electrolytic solution. If tests were to be performed in a deaerated solution, hydrogen was vigorously bubbled through the cell for at least 1 hour. During the last few minutes of vigorous purging, a freshly prepared anode was immersed into the solution and positioned approximately 2 millimeters from the tip of the Luggin probe. The gas flow would then be reduced so as to maintain a slight positive pressure within the cell without introducing a stirring effect.

The electrodes were then connected to a potentiostat system, similar to systems found in literature[4,12,29], capable of providing potentiodynamic polarization curves automatically. A simplified example of the complete test cell system is shown schematically in Figure 31. The potentiodynamic polarization apparatus used in this study was constructed and modified within the Chemical and Metallurgical Engineering Department from commercially available components. This equipment featured a set point potential range of ± 2 volts set in a feedback circuit to the operational amplifier, and an output current range from ± 0.01 μ amp to ± 1.0 amp. A log converter was used in series with the X-Y recorder because of the extremely broad range of corrosion currents involved in the tests. Twelve scan rates were available, ranging from 4 minutes to 96 hours for a scan through the full 4-volt range. To change polarization directions required manipulation of a manual switch.

Each specimen was cathodically polarized -0.2 volt relative to E_{corr} for 5 minutes prior to the start of a test. The corrosion potential of the anode specimen and the potential of the hydrogen electrode were monitored until "steady-state" values were obtained. Following establishment of "steady state," the polarization scan was conducted until oxygen evolution or hydrogen reduction was noted. All tests were performed at 24 to 26°C.

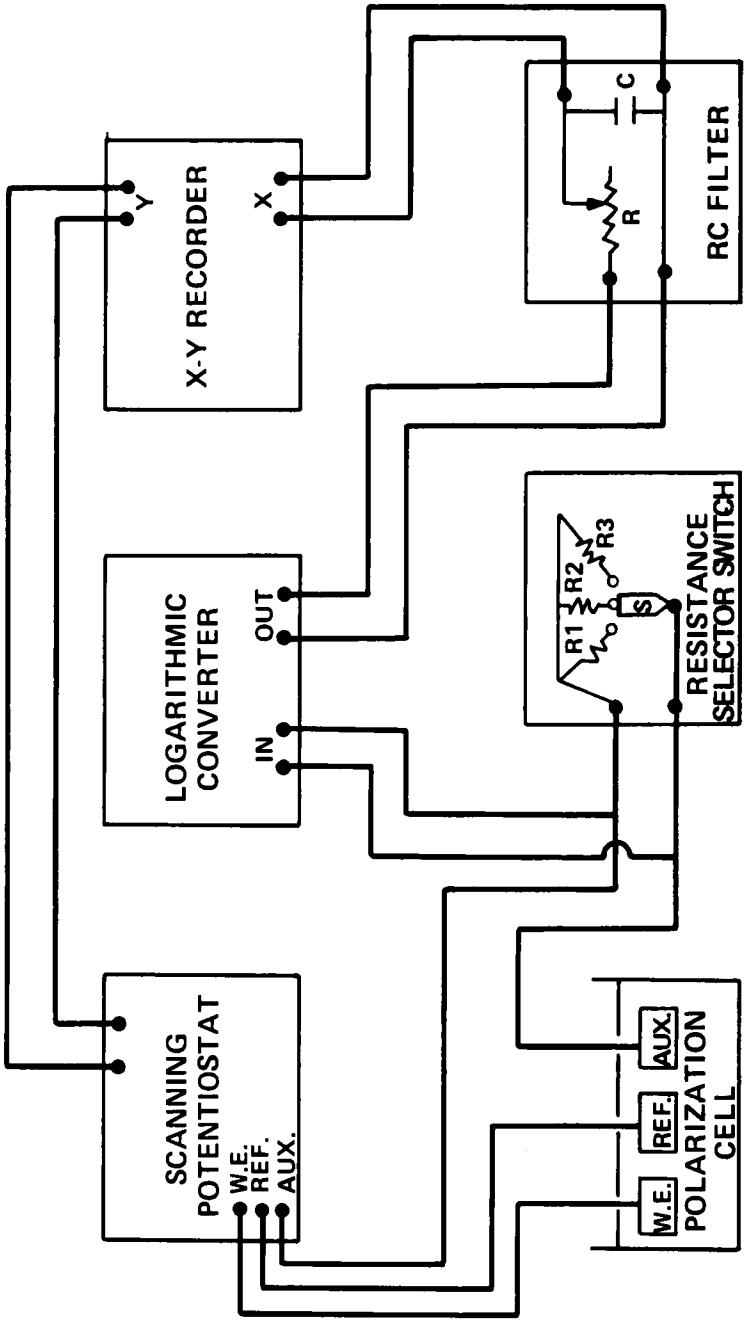


Figure 31. Schematic Circuit for Automatic Potentiodynamic Polarization Apparatus.[4]

CHAPTER V

RESULTS AND DISCUSSION

The following are understood in the presentation and discussion of results: (1) potentials are referred to the standard hydrogen electrode (S.H.E.); (2) current densities were calculated using the geometric area; (3) solution compositions are given in volume percent unless otherwise noted; (4) anodic and cathodic polarization curves were conducted potentiodynamically in the positive and negative directions, respectively, unless otherwise noted; (5) the electrode was polarized or pretreated cathodically prior to each anodic polarization; and (6) all curves were run at a room temperature of 24° to 26°C.

I. EXPERIMENTAL STANDARDIZATION

To properly characterize electrochemically the acid solutions of Streicher's[37,38] investigations, it was essential that confidence in the analytical and electrical systems be demonstrated. The corrosion system selected to evaluate and calibrate the experimental equipment used in the course of this study was $\underline{N}$ H_2SO_4 solution, hydrogen saturated, on a 430 stainless steel electrode. As a result of the extensive testing of this corrosion system by an ASTM Task Group[39], a well-defined polarization curve for $\underline{N}$ H_2SO_4 solution on 430 stainless steel was developed that

is often used as a polarization test standard (see Discussion, pp. 17-24).

For this study, four successive polarization runs (Figure 32) were made on the same 430 stainless steel electrode in $\underline{N}$ H_2SO_4 solution with no cleaning or polishing of the electrode after the first run. Anodic polarization of the electrode was preceded in each run by cathodically polarizing the electrode to overvoltages of about 0.20 V. From the results shown in Table IV, the curve for Run 1 was in good agreement with the standard curve, shown in Figure 10, page 21. Only at fairly noble potentials (above 1.1 V) did substantial deviation begin to occur. For example, the inflection potential, E_I, was 1.24 V for Run 1 but was 1.54 V for the standard curve. However, this study was primarily concerned with the lower potentials typically associated with cathodic processes, the same potentials where the curves demonstrate the best agreement.

The curves for Runs 2 through 4 illustrate the results of initiation and progression of crevice corrosion. The early stages of crevice growth, occurring at the specimen and the Teflon compression gasket interface, were noted by a ten-fold increase of current density in the passive region. Further propagation of crevice growth was indicated in Runs 3 and 4 by additional increases of current density in the curve's passive region. The effect of crevice corrosion, as noted here, was identical to that noted for the standard curve in Figure 13 on page 24 and reported by Jones and Greene[14].

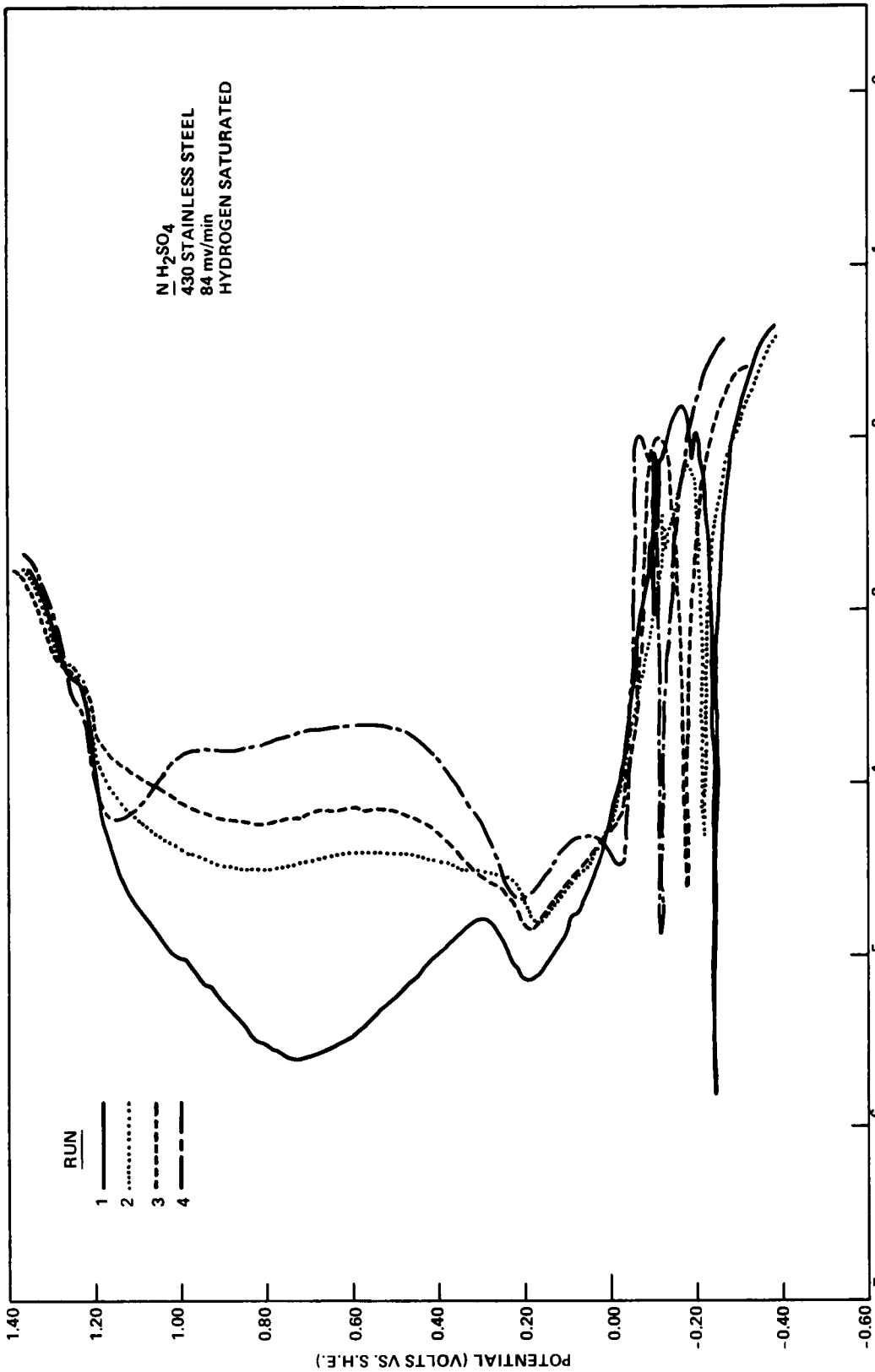


Figure 32. Polarization Curves on 430 S.S. In A Hydrogen Saturated N H_2SO_4 Solution Exhibiting Increasing Crevice Effects.

TABLE IV

ANODIC POLARIZATION PARAMETERS FOR NORMAL SULFURIC ACID ON TYPE 430 STAINLESS STEEL

Run	Polarization Parameters[a]										
	E_{corr}	I_{pc}	E_{pp}	I_{pm}	E_{pm}	I_{sc}	E_{sp}	I_{sm}	E_{sm}	I_{I}	E_{I}
1	- 0.24	1.6×10^{-2}	- 0.16	7.0×10^{-6}	0.18	1.7×10^{-5}	0.29	2.5×10^{-6}	0.73	3.7×10^{-4}	1.24
2	- 0.22	6.0×10^{-3}	- 0.18	1.6×10^{-5}	0.17			3.2×10^{-5}	0.82	5.2×10^{-4}	1.26
3	- 0.18	10^{-2}	- 0.12	1.4×10^{-5}	0.18			5.9×10^{-5}	0.81	4.3×10^{-4}	1.24
4	- 0.12	10^{-2}	- 0.09	2.1×10^{-5}	0.21			1.5×10^{-4}	0.90	3.1×10^{-4}	1.25
Standard[b]	- 0.26	10^{-2}	- 0.18	3.0×10^{-6}	0.14	10^{-5}	0.31	10^{-6}	0.62	1.5×10^{-3}	1.54

[a] I is defined as current density (a/cm^2); E is defined as potential (volts vs S.H.E.).

[b] Standard curve values are approximate as taken from Figure 10.

Thus, the similarity and interpretability noted between this study's polarization curves for 430 stainless steel in $\underline{N}$ H_2SO_4 solution and that of the standard curve demonstrate an adequate level of confidence in the experimental equipment and procedures.

II. 10% HYDROCHLORIC ACID SOLUTION

One of the most frequently investigated electrodes is the hydrogen electrode which has an overall reaction of

$$2H^+ + 2e \rightleftarrows H_2 \ .$$

This reversible electrode typically occurs on an inert metal surface that assumes an indirect role in the reduction of the hydrogen ions and the oxidation of hydrogen gas by providing a site at which the transfer of electrons can take place. It is the nature of the metal surface itself that determines the magnitude of the exchange current density, i_o, where the rate of reduction equals the oxidation rate

$$i_o = \vec{i}_{H^+} = \overleftarrow{i}_{H_2} \qquad (26)$$

with $\vec{i}_{H^+}$ = rate of hydrogen ion reduction and $\overleftarrow{i}_{H_2}$ = rate of hydrogen gas oxidation. The magnitude that a metal surface can affect i_o for this reaction was noted by Fontana and Greene[3], where $i_o \simeq 10^{-2}$ a/cm^2 for platinized Pt, $i_o \simeq 10^{-3}$ a/cm^2 for bright Pt, and $i_o \simeq 10^{-12}$ a/cm^2 for a

Hg surface. The equilibrium potential for this reaction at 25°C is determined from the equation

$$E_{H_2,H^+} = -0.059\ pH - 0.03\ \log\ p_{H_2} \qquad (27)$$

where $E^{o}_{H_2,H^+} = 0.00$ V.

When the hydrogen electrode is polarized anodically by an externally applied current, the oxidation of molecular hydrogen proceeds at a limiting anodic diffusion current density that is dependent upon stirring. At sufficiently large anodic overvoltages (0.7 to 0.9 V), however, a decrease in current density occurs that is independent of stirring. Vetter[41] proposed the theory that a chemisorbed oxide layer forms on the metal surface at which the dissociation and adsorption of molecular hydrogen are slower. Schuldiner[28], on the other hand, formed the conclusion that in acid solutions containing sulfate ions (e.g., H_2SO_4), the decrease in current density resulted from adsorption of sulfate ions onto the metal electrode surface. The latter explanation is more in agreement with Streicher's[37] conclusion that it is the anion of the acid that determines its corrosion behavior, as illustrated in Figure 2, page 8. The interference this layer exhibits toward the hydrogen oxidation reaction begins to dissipate at more positive potentials until the oxidation of water becomes dominant, resulting in increasing current densities.

When the hydrogen electrode is polarized cathodically, the hydrogen reaction is in charge transfer control as hydrogen ions are reduced to hydrogen gas. Dependent upon acid concentration and velocity conditions, diffusion control may become significant at larger current densities. If the solution is maintained at a hydrogen partial pressure of 1 atmosphere, then Equation 27 becomes

$$E_{H^+,H_2} = -0.059 \text{ pH} , \qquad (28)$$

dependent only on pH.

The introduction of oxygen to the acid solution greatly complicates the resultant anodic and cathodic reactions. The reversible oxygen electrode

$$O_2 + 4H^+ + 4e \rightleftarrows 2H_2O,$$

for which E_o = 1.23 V, $i_o \simeq 10^{-9} - 10^{-10}$ a/cm^2 on Pt, and β_a = 0.12 to 0.14 V, is rarely encountered in routine investigative efforts[13] because of the very specific conditions that must exist at the electrode. Instead, Hoare[13] suggests that the equilibrium potential for oxygen on a Pt surface becomes a rest potential of about 1.05 V, involving the O_2/H_2O reaction and the Pt/Pt-O reaction (E_o = 0.88 V)

$$Pt\text{-}O + 2H^+ + 2e \rightleftarrows Pt + H_2O .$$

The electrode's rest potential is influenced by the potential of the cathodic O_2/H_2O reaction

$$E_{H_2O,O_2} = 1.23 + \frac{0.059}{4} \log (p_{O_2})(a_{H^+})^4 \qquad (29)$$

or

$$E_{H_2O,O_2} = 1.23 - 0.059\ pH + 0.015 \log p_{O_2}\ , \qquad (30)$$

which is dependent on solution pH and the partial pressure of oxygen, p_{O_2}. In addition, the rest potential has been shown to be dependent on the degree of coverage of the electrode surface with adsorbed oxygen, which begins adsorbing at about 0.85 V and continues adsorbing until oxygen evolution begins above 1.4 V for an acid solution[13].

This adsorbed oxygen layer can noticeably influence the shape of the anodic polarization curve. Initial runs with a Pt electrode in an oxygen saturated acid solution do not exhibit a linear Tafel region. This has been attributed to an adsorbed oxygen layer continually building up during anodic polarization. Reproducible results were observed on subsequent runs only after a complete adsorbed oxygen layer was formed[41].

Whenever the oxygen electrode is cathodically polarized in acid solutions[41], a stable intermediate product of H_2O_2 is formed by the reaction

$$O_2 + 2H^+ + 2e \rightleftarrows H_2O_2$$

(E_o = 0.682 V) at current densities as large as 10^{-6} a/cm^2. At cathodic current densities above 10^{-5} a/cm^2, the H_2O_2 is reduced to water by the reaction

$$H_2O_2 + 2H^+ + 2e \rightarrow 2H_2O \ ,$$

for which E_o = 1.776 V. Above $\simeq 10^{-3}$ a/cm^2, this reaction enters a limiting current region which is rate controlling until reduction of hydrogen ions begins to take place. It has been shown[41] that for the cathodic reaction of O_2 to H_2O_2 and H_2O on a Pt electrode, four electrons per O_2 molecule are used during the electrochemical conversion at overvoltages more active than about 1.0 V. Thus, the sum of the two partial cathodic reactions is equivalent to the overall reduction reaction, $O_2 + 4H^+ + 4e \rightleftarrows 2H_2O$, of the oxygen electrode in this potential range.

During the present investigation of the 10% HCl solution used by Streicher[37,38] for corrosion behavior determination of Ni-rich alloys, a platinized Pt electrode was selected as the working surface for studying the system's electrochemical reactions in both a hydrogen saturated solution and an aerated solution. The polarization curves for these solutions are shown in Figures 33 and 34, respectively.

The equilibrium potential for the hydrogen saturated (p_{H_2} = 1 atm) 10% HCl solution (pH = -0.3) was $E_{H_2,H^+} = 0.018$ V

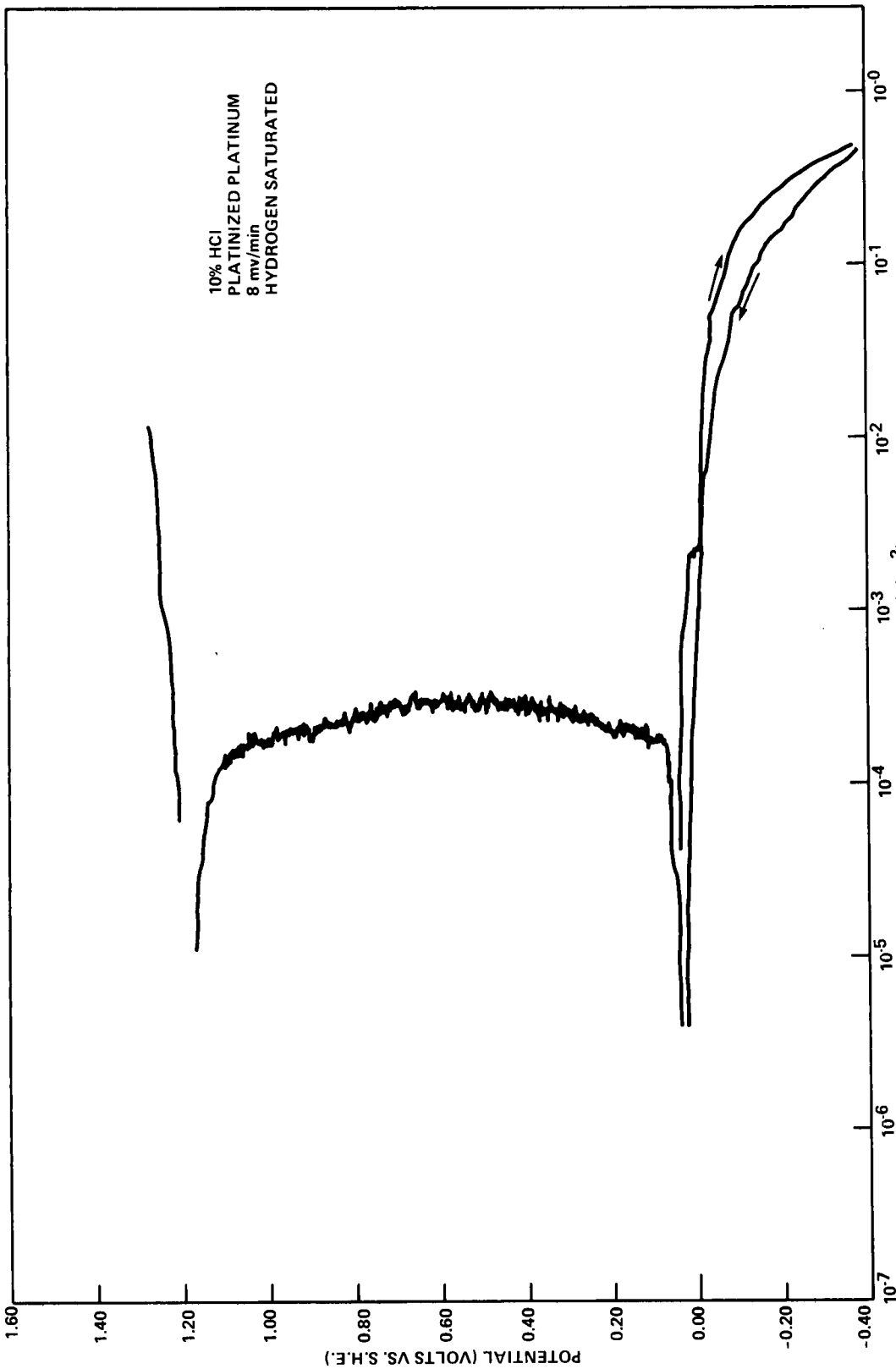


Figure 33. Polarization Curves On Platinum In A Hydrogen Saturated 10% HCl Solution.

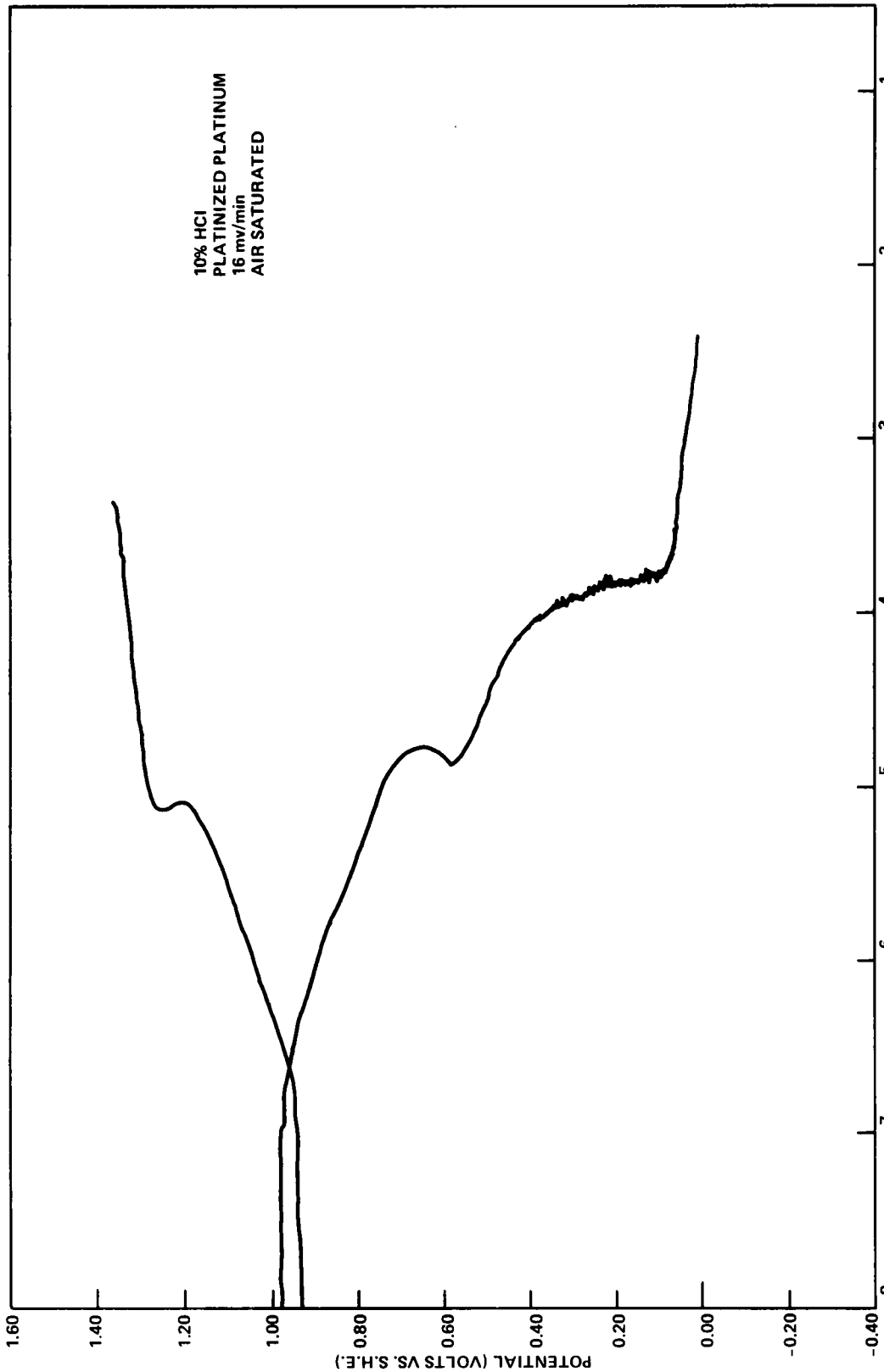


Figure 34. Polarization Curves On Platinum In An Air Saturated 10% HCl Solution.

as calculated from Equation 28. This is in good agreement with the reversible potential exhibited in Figure 33. As was noted in Table II on page 7, the noble potential of 0.56 V recorded by Streicher[37] for boiling 10% HCl indicated the presence of oxygen more than the effect of temperature. The anodic polarization curve in Figure 33 entered a limiting current density region extending from 0.04 to 1.12 V at $i_{L,a} \simeq 3 \times 10^{-4}$ a/cm^2 without exhibiting Tafel behavior. This reaction rate at which molecular hydrogen can be oxidized to hydrogen ions was limited by the finite diffusion rate of the hydrogen gas to the metal surface. From 1.12 to 1.20 V, the current density decreased to values beyond the lower experimental recording limit of $\simeq 10^{-4}$ a/cm^2 established for this curve. Above 1.2 V, initiation of water oxidation begins to take place.

The parameters and shape of the anodic polarization curve shown in Figure 33 are very similar to those of the anodic polarization curve for low velocity H_2SO_4 solution on Pt as reported by Vetter[41]. A value for $i_{L,a}$ somewhat less than 10^{-3} a/cm^2 was recorded up to a potential of $\simeq$ 0.9 V, at which point a decrease of current density occurred that was independent of stirring. This decrease continued to more noble potentials ($\simeq$ 1.5 V) than those noted in Figure 33 for the HCl solution. In the total absence of any sulfate ions, these similarities would tend to support Vetter's[41] contention of a chemisorbed oxide layer resulting in the current decrease above 0.9 V, with any oxygen required

being contained in the hydrogen gas sparge as a trace impurity.

The reduction of hydrogen ions to hydrogen gas in the hydrogen saturated 10% HCl solution is also shown in Figure 33. Preceded by a brief region indicative of Tafel behavior ($\beta_c \simeq -0.02$, estimated), the cathodic polarization curve began to enter a region of limiting current density at about 1 a/cm^2. From literature[41], the reduction reaction should exhibit charge transfer control over a very wide current density range with a Tafel slope of -0.10 to -0.12 V. When hydrogen was reduced by changing to progressively more negative potentials, a faint yellowish tint was noted in the solution beginning at about -0.16 V (0.28 a/cm^2); however, the HCl solution cleared at about the same potential when the potential was moved back in the positive direction. This indicates that an unidentified reduction process was coexisting with the reaction for hydrogen ion reduction.

Figure 34 is the polarization curves for aerated 10% HCl solution on Pt. The experimental value for the equilibrium potential was E_o = 0.97 V with i_o = 2.3 x 10^{-7} a/cm^2, and the Tafel constants were estimated to be β_a = 0.13 V and β_c = -0.16 V. On decreasing the potential, a break occurred in the curve at a current density of 1.6 x 10^{-5} a/cm^2 beginning near 0.7 V. After the break, a brief linear region and then a limiting current density region where $i_{L,c} \simeq 2 \times 10^{-4}$ a/cm^2 were observed; further decrease of potential resulted in a charge transfer control region at

potentials more negative than 0.05 V. The portion of the curve below 0.05 V represented the hydrogen reduction reaction which for a potential $E_{H_2,H^+} = 0.018$ V, had an $i_o \simeq 10^{-3}$ a/cm^2 and an estimated slope of $\beta_c \simeq -0.05$ V. The reduction curve between $E_o = 0.97$ V and the potential 0.1 V closely approximated the overall O_2/H_2O reaction containing the stable peroxide intermediate. The equilibrium potential for the O_2/H_2O_2 reaction that occurred at current densities up to $\simeq 10^{-5}$ a/cm^2 could be determined from the expanded equation

$$E_{O_2,H_2O_2} = 0.682 - 0.059\ pH + 0.03\ \log p_{O_2} - 0.03\ \log a_{H_2O_2} \quad (31)$$

by which the dependence of potential on H_2O_2 concentration can be noted. From this equation, the peroxide activity was calculated to be 2×10^{-10} for E = 0.97 V with pH = -0.3 and $p_{O_2} = 0.2$ atmosphere. This amount of peroxide was probably produced during cathodic pretreatment of the electrode. Although the effect of cathodic pretreatment is often negligible in some systems[10,34], this obviously was not the case for the oxygen electrode. Beyond the break point of 1.6×10^{-5} a/cm^2, the cathodic reaction changed to the reduction of peroxide to water for which the Nernst equation is

$$E_{H_2O_2,H_2O} = 1.776 - 0.059\ pH + 0.03\ \log a_{H_2O_2}. \quad (32)$$

Assuming these two reduction reactions, Equations 31 and 32, interrelate in a normal manner[33], the exchange current density for the H_2O_2/H_2O reaction determined by extrapolating back to the equilibrium potential of 1.776 V would result in exceedingly small current density values.

Anodic polarization of the aerated 10% HCl solution, Figure 34, exhibited H_2O_2 oxidation ($\beta_a = 0.13$) with oxidation of water becoming the dominant anodic reaction at about 1.2 V as the peroxide became depleted.

In Figure 35, the polarization curves for three nickel-rich alloys in hydrogen saturated 10% HCl solution have been superimposed. The three alloys, compositions being given in Table III on page 57, represent essentially a constant amount of nickel with chromium content being varied at the expense of the molybdenum content. In general, each alloy exhibited an active-passive behavior with corrosion potentials close to that of the reversible hydrogen electrode. As indicated by the values given in Table V, there was no significant change in corrosion potential with composition, but the estimated values for i_{corr} ranged from 8×10^{-7} a/cm^2 to 3×10^{-5} a/cm^2. As chromium content was increased, the primary passive potential, E_{pp}, decreased and the potential marking the transition into the transpassive region increased. This resulted in an enlarging of the passive region with increasing chromium content, as was noted by Myers, Beck, and Fontana[20] for nickel-chromium alloys in H_2SO_4 solution. The critical current density, which is indicative of the ease

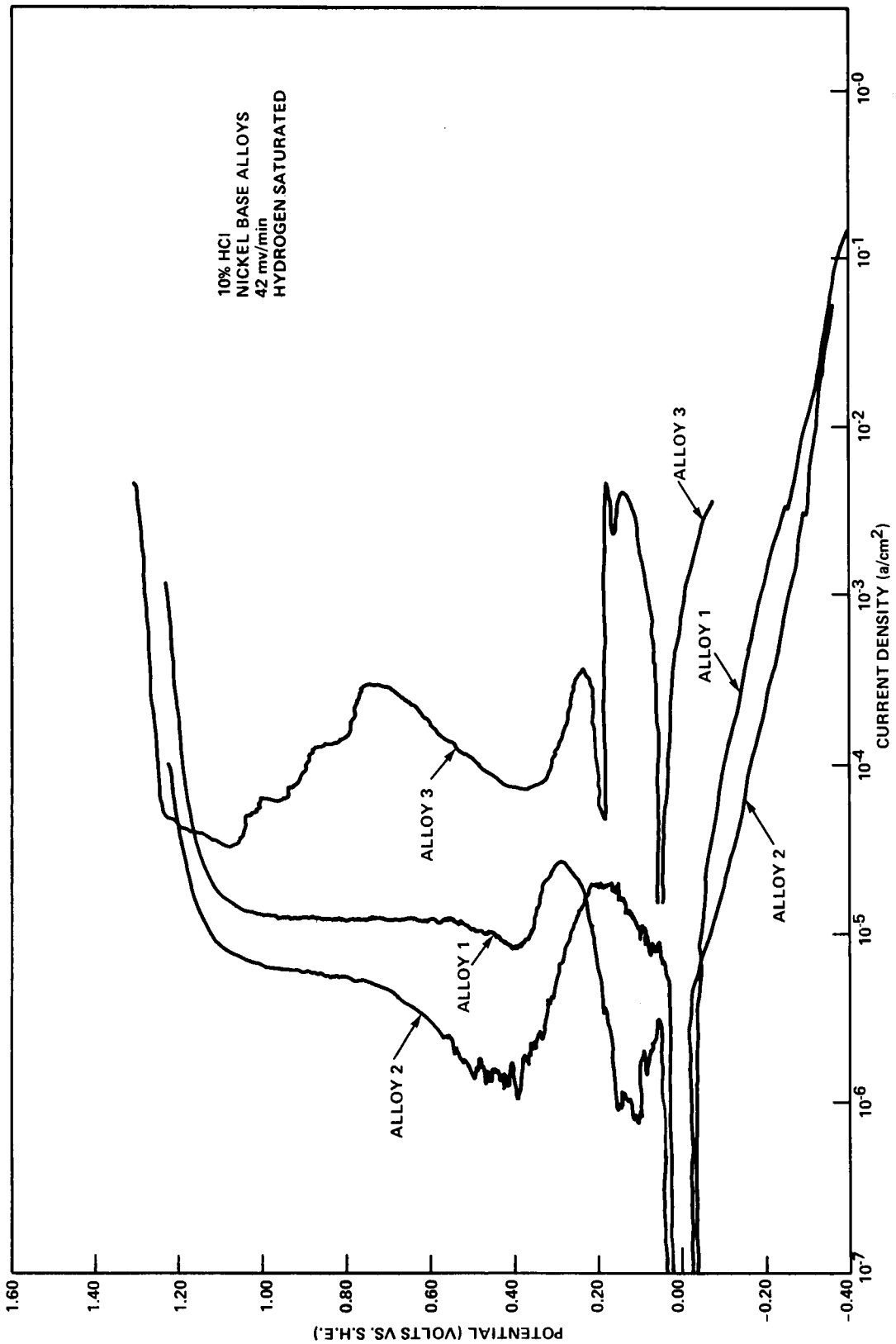


Figure 35. Polarization Curves On Various Nickel Base Alloys In A Hydrogen Saturated 10% HCl Solution.

TABLE V

ANODIC POLARIZATION PARAMETERS FOR 10% HYDROCHLORIC ACID ON NICKEL BASE ALLOYS

	Polarization Parameters[a]			
Alloy	E_{corr}	I_{corr}	E_{pp}	I_{crit}
1	0.00	8×10^{-6}	0.29	2.6×10^{-5}
2	- 0.01	8×10^{-7}	0.18	2.0×10^{-5}
3	0.04	3×10^{-5}	0.14	2.8×10^{-3}

[a]Potential (E) given as volts (vs S.H.E.); current density (I) given as amperes per square centimeter.

of passivation is lowest for Alloys 1 and 2; however, Alloy 2 would be the easiest to passivate because of its lower E_{pp}. Thus, of the three alloys, Alloy 2 would be most resistive to the HCl environment.

In the passive region, the passivating current density, i_p, was observed to change with potential. This dependency, also noted for Hastelloy C in both HCl and H_2SO_4 solutions[9], became more noticeable with increasing chromium content. The passive regions would indicate that spontaneous passivation could be achieved if sufficiently strong oxidizers were used. If weak to moderate oxidizers were present, especially with Alloy 3, it would be essential that an adequate concentration of the oxidizer be maintained to assure passivation.

The reduction of hydrogen ions on the nickel-based alloys exhibited Tafel behavior characteristics to current densities as large as $\simeq 10^{-1}$ a/cm^2 for Alloys 1 and 2. The slopes were -0.11 V and -0.09 V, respectively. The displacement existing between the three individual reduction curves, Figure 35, occurring at any given potential is indicative of the different corrosion current densities of the three nickel base alloys.

III. 50% SULFURIC ACID-0.1 M FERRIC SULFATE SOLUTION

The oxidation-reduction potentiodynamic polarization curves for the 50% H_2SO_4-0.1 M $Fe_2(SO_4)_3$ solution on a Pt electrode are shown in Figures 36 and 37. Figure 36 is for the case of a hydrogen saturated solution, while Figure 37

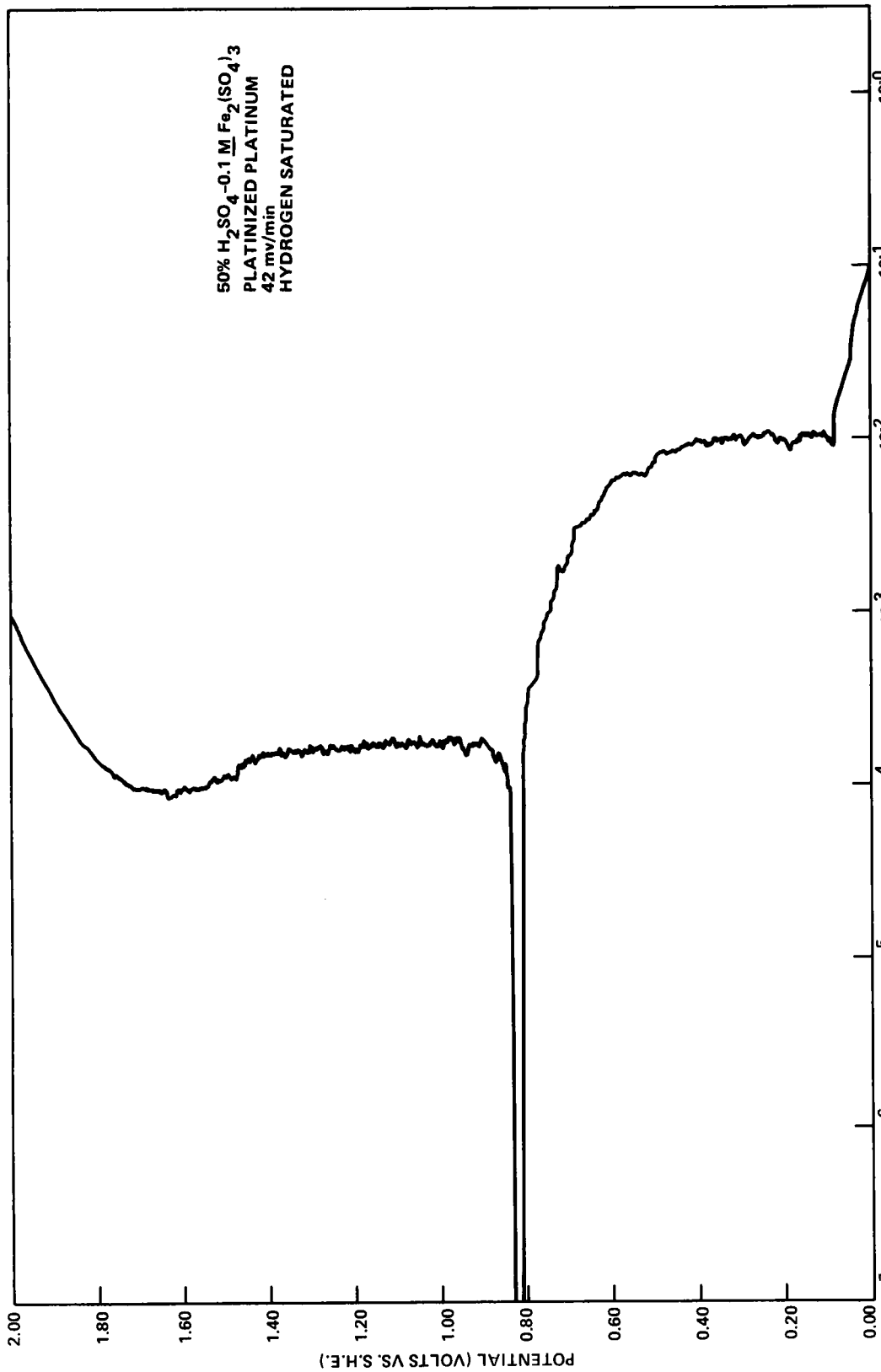


Figure 36. Polarization Curves On Platinum In A Hydrogen Saturated 50% H_2SO_4-0.1 M $Fe_2(SO_4)_3$ Solution.

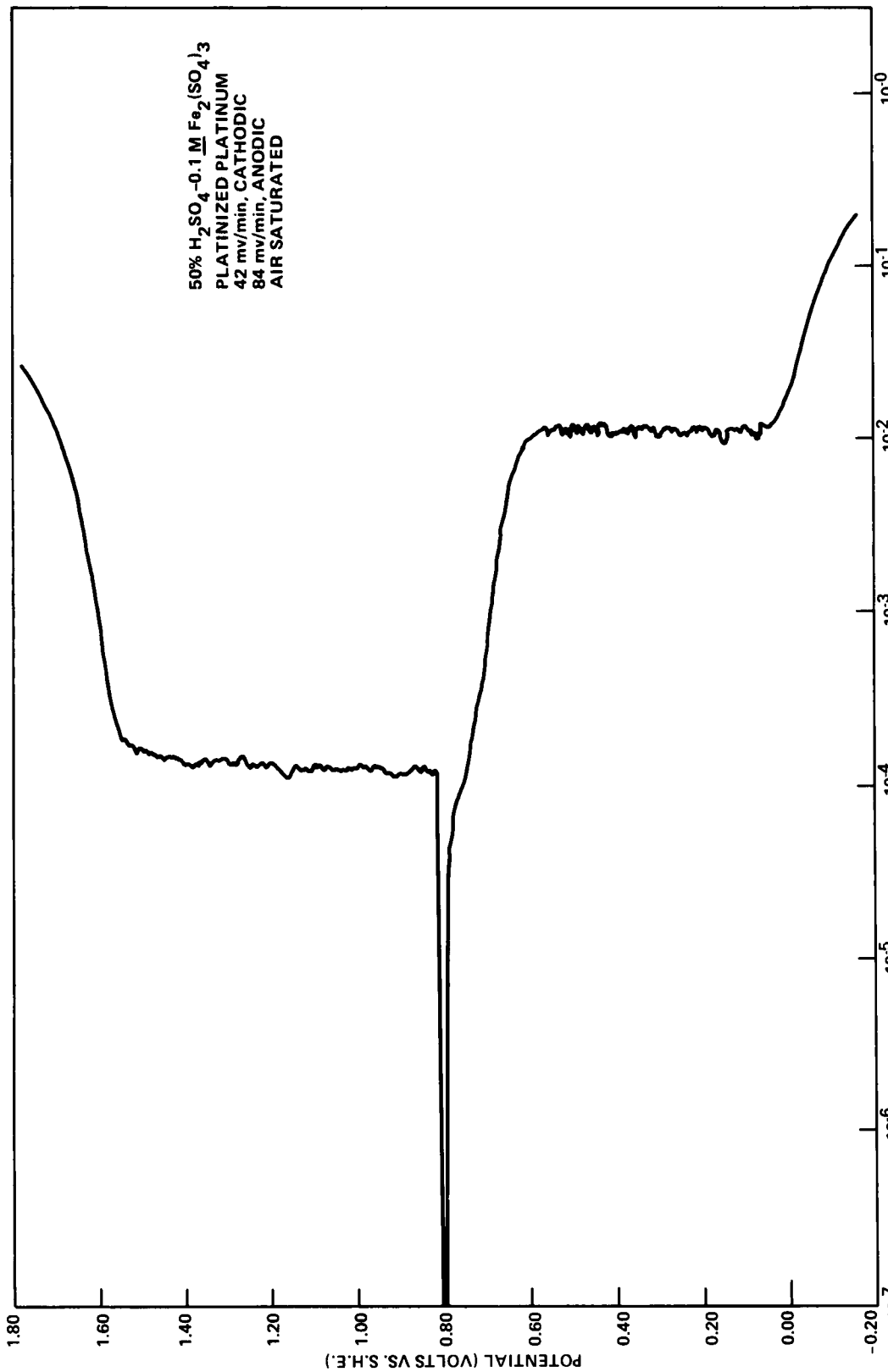


Figure 37. Polarization Curves On Platinum In An Air Saturated 50% H_2SO_4-0.1 M Fe_2 $(SO_4)_3$ Solution.

is that of an air-saturated solution.

The reversible system of principal interest is given by the overall redox reaction

$$Fe^{3+} + e \rightleftarrows Fe^{2+}$$

which has a reversible potential of

$$E_{Fe^{2+},Fe^{3+}} = + 0.771 + 0.059 \log (a_{Fe^{3+}}/a_{Fe^{2+}}) . \quad (33)$$

At the system's equilibrium potential, the rate of ferrous ion oxidation is balanced by the rate of ferric ion reduction

$$i_o = \vec{i}_{Fe^{3+}} = \overleftarrow{i}_{Fe^{2+}} \quad (34)$$

where i_o = exchange current density, $\vec{i}_{Fe^{3+}}$ = current density equivalent of ferric ion reduction rate, and $\overleftarrow{i}_{Fe^{2+}}$ = current density equivalent of ferrous ion oxidation rate. The anodic or cathodic overvoltage as a function of the oxidation rate or the reduction rate for a charge transfer controlled reaction is described ideally by

$$\eta = \beta_a \log \frac{\overleftarrow{i}_{Fe^{2+}}}{i_o} \quad (35)$$

or

$$\eta = - \beta_c \log \frac{\vec{i}_{Fe^{3+}}}{i_o} \tag{36}$$

where β_a and β_c are the oxidation and reduction Tafel slopes, respectively. However, as previously discussed, the experimental representation for a reaction exhibiting charge transfer control is more accurately defined by

$$\eta = \beta_a \log \frac{\overleftarrow{i}_x + \vec{i}_{Fe^{3+}}}{i_o} \tag{37}$$

or

$$\eta = - \beta_c \log \frac{\vec{i}_x + \overleftarrow{i}_{Fe^{2+}}}{i_o} \tag{38}$$

where $\overleftarrow{i}_x$ is the externally applied anodic current density and $\vec{i}_x$ is the externally applied cathodic current density[32].

Measurement of the charge transfer overvoltage is complicated by ion diffusion limitations through the solution and by interaction with other oxidation or reduction reactions. In anodic polarization, deviation from Tafel behavior occurs at small overvoltages due to diffusion polarization and at larger overvoltages by oxygen evolution. In this upper range, the ferrous ion oxidation rate couples with the rate of water oxidation to equal the total applied anodic current at any η. Cathodic polarization is similarly affected by diffusion polarization, but at larger cathodic overvoltages, the interfering reaction is hydrogen reduction.

Experimentally, each of these effects was observed. From Figures 36 and 37, equilibrium potentials were estimated to be 0.80 to 0.82 V with $\beta_c = -0.08$ and $i_o = 10^{-5}$ a/cm^2. From Equation 33, this potential would indicate the activity of Fe^{3+} to be about five times larger than the Fe^{2+} activity. However, the equilibrium potential could not be calculated directly since the Fe^{2+} content was not accurately known. Anodic diffusion polarization occurred at approximately $i_{L,a} = 2 \times 10^{-4}$ a/cm^2 with oxygen evolution beginning above 1.5 V. Reduction of ferric ions was diffusion controlled at a rate of $i_{L,c} = 10^{-2}$ a/cm^2 with hydrogen reduction becoming significant at 0.06 to 0.08 V resulting in increasing current densities as potential became more active.

A similar equilibrium potential value of 0.82 V was reported by Streicher[37] for the Fe^{3+}/Fe^{2+} system on Pt. Further comparison of experimental parameters with Streicher's results could not be made as they were not given. However, on passivated steel, Piotrowski and Lebet[23] found i_o to be 6.6×10^{-7} a/cm^2 with $\beta_c = -0.11$ V for a ferric ion concentration of 0.25 M; Makrides and Stern[19] recorded values of 3.3 to 8.1×10^{-7} a/cm^2, $\beta_c = -0.155$ V, for ferric concentrations in the range 0.014 to 0.066 M. In contrast, Fontana and Greene[13] listed i_o for the $Fe^{3+} + e = Fe^{2+}$ reaction on a Pt electrode as 2×10^{-3} a/cm^2. The value of 10^{-5} a/cm^2, determined from a single cathodic polarization curve measured in an air-saturated solution, could not be more accurately

identified because of insufficient Tafel behavior at low overvoltages.

In the cathodic polarization investigation of this redox system, a limiting diffusion current was found to occur at 10^{-2} a/cm^2 until sufficiently active potentials were attained that hydrogen reduction would become significant. The relative magnitude of $i_{L,c}$ for the reduction of ferric ions was verified experimentally by Piotrowski and Lebet[23] and through calculations for $i_{L,c}$ by Makrides and Stern[19]. The latter team determined that the ferric ion reduction rate was a function of only the ferric ion concentration and flow conditions within the cell. Thus, the cathodic limiting current density is that for ferric ion reduction only and does not include current from the oxygen reduction reaction, which has a limiting current density of 10^{-3} to 10^{-4} a/cm^2 in a stagnant, aerated solution[3,13]. As the ferric ion reduction curve approached potentials of 0.06 to 0.08 V, hydrogen ion reduction became the dominant reaction, with hydrogen gas being evolved. Application of the Nernst equation for the reversible hydrogen electrode[42]

$$E_{H_2,H^+} = -0.059\ pH - 0.03 \log p_{H_2}, \qquad (39)$$

predicts a potential of 0.07 V for the 50% H_2SO_4-0.1 M $Fe_2(SO_4)_3$ solution with a pH = -1.2[20] and p_{H_2} = 1 atmosphere. However, because of the high exchange current density for the hydrogen reaction (10^{-2} a/cm^2 on platinized

Pt and 10^{-3} a/cm^2 on Pt)[3], it is reasonable that the intersection of the ferric ion and the hydrogen reduction curves occurs essentially at the hydrogen reversible potential. At potentials more active than 0.06 V, the reaction rate was determined solely by the rate of hydrogen reduction.

In the anodic potential region, a limiting current density of 1.1 to 1.6 x 10^{-4} a/cm^2 was observed for the oxidation of ferrous ions up to a potential of about 1.4 V. Although this is about two decades less than the cathodic limiting current density, it was to be expected as a result of the significantly greater concentration of ferric ions in the solution. The hydrogen saturated H_2SO_4-$Fe_2(SO_4)_3$ solution, Figure 36, exhibited a decrease of current density in the potential region of 1.4 to 1.8 V which approximated a similar response noted for hydrogen overvoltage on Pt in 1 $\underline{N}$ H_2SO_4. Vetter[41] reasoned that this decrease was caused by the formation of a chemisorbed oxide layer on the metal surface where the dissociation and adsorption of molecular hydrogen could not proceed rapidly enough, leaving only a limiting reaction current density that was independent of stirring. An investigation by Schuldiner[28] of hydrogen oxidation on a passive Pt electrode in 1 $\underline{M}$ H_2SO_4 concluded that the decrease was more apt to result from adsorption of sulfate ions on the metal surface with the limiting current density due to saturation of the surface with sulfate ion. This more closely parallels Streicher's[37] conclusions that the anion of the acid determines its corrosion behavior.

Above 1.8 V, oxygen evolution begins. In this oxygen generating region, the presence of hydrogen has no apparent effect on the rate of oxidation of water[28].

The oxidation of ferrous ions in the aerated H_2SO_4-$Fe_2(SO_4)_3$ solution, shown in Figure 37, also exhibited diffusion polarization at $i_{L,a}$ = 1.1 to 1.6 x 10^{-4} a/cm^2 up to a potential of about 1.5 V. Above 1.5 V, the transition to oxygen oxidation occurred without the preliminary current density decrease noted in the hydrogen saturated solution. The oxygen electrode reaction in aerated (p_{O_2} = 0.2 atm) acid solution of pH = -1.2, given by

$$O_2 + 4H^+ + 4e \rightleftarrows 2H_2O \ ,$$

has an equilibrium potential of E_o = + 1.29 V, calculated from the potential equation

$$E_{H_2O,O_2} = + 1.229 - 0.059\ pH + 0.015 \log p_{O_2} \ . \qquad (40)$$

When the oxidation curve (β = 0.06) for water, which is primarily under charge transfer control, is extrapolated back to the equilibrium potential of oxygen (1.29 V), an exchange current density of $i_o = 10^{-8}$ a/cm^2 is determined. This is one to two decades larger than the exchange current density of 10^{-9} to 10^{-10} a/cm^2 reported by Hoare[13] and West[42] for the standard oxygen electrode on bright Pt. However, the greater exchange current density is probably a result of

the larger geometric surface area of platinized Pt relative to bright Pt.

IV. 10% CHROMIC ACID SOLUTION

Of the various solutions investigated by Streicher[37,38] for determining the corrosion behavior of nickel base alloys, the most oxidizing solution was 10% chromic acid with a standard electrode potential of 1.33 V. Prepared from crystalline chromium trioxide, CrO_3, the chromic acid results in an overall electrode reaction of

$$Cr_2O_7^{2-} + 14H^+ + 6e \rightleftarrows 2Cr^{3+} + 7H_2O \ .$$

This follows from the reactions

$$CrO_3 + H_2O \rightarrow H_2CrO_4 \rightarrow 2H^+ + CrO_4^{2-}$$

and

$$2H^+ + 2CrO_4^{2-} \rightarrow Cr_2O_7^{2-} + H_2O \ ,$$

for which the equilibrium expression of the chromate to dichromate reaction is given by[25]

$$\log \frac{(CrO_4^{2-})}{(Cr_2O_7^{2-})} = -14.59 + 2\ pH \ . \qquad (41)$$

At a pH = 0, this reaction would go to completion with an equilibrium constant of 2.6×10^{-15}, as calculated from Equation 41. The equilibrium potential for this system can be calculated from the equation

$$E_{Cr^{3+},Cr_2O_7^{2-}} = 1.33 + \frac{0.059}{6} \log \frac{(a_{Cr_2O_7^{2-}})(a_{H^+})^{14}}{(a_{Cr^{3+}})^2} \quad (42)$$

or, in the expanded form,

$$E_{Cr^{3+},Cr_2O_7^{2-}} = 1.33 - 0.14\ pH + 0.01 \log \frac{a_{Cr_2O_7^{2-}}}{(a_{Cr^{3+}})^2}. \quad (43)$$

The chromic acid solution prepared for this investigation had an analytically determined pH = 0 and an open circuit potential of E_o = 1.17 V, which was somewhat lower than the 1.26 V reported by Streicher[37]. From Equation 43 above, the activity log term of dichromate ions to chromic ions would have been 10^{-16} for this system at equilibrium, with $a_{Cr^{3+}} = (10^8)(a_{Cr_2O_7^{2-}})$. This would appear to be consistent with results taken from potential - pH equilibrium diagrams[25,26] for areas of relative domain.

When the hydrogen saturated 10% chromic acid solution (Figure 38) was potentiodynamically polarized on Pt, both the anodic and the cathodic curves exhibited limiting current densities indicative of diffusion control. Anodically, the expected reaction was oxidation of chromic ions, Cr^{3+}, to dichromate ions, $Cr_2O_7^{2-}$. The observed limiting current density of $i_{L,a} = 3.5 \times 10^{-6}$ a/cm^2 would suggest

that the oxidation of Cr^{3+} would probably tend to go into a region of diffusion polarization except for the current demand for decomposition of water with evolution of oxygen which dominates at potentials above 1.5 V. The curve for water oxidation had a slope of β_a = 0.13 V which, when extrapolated back to E_o^o = 1.23 V (pH = 0 and p_{O_2} = 1 atm with O_2 evolution), yielded an estimated exchange current density of 3 x 10^{-8} a/cm^2 for the oxygen electrode. This is slightly higher than the values of 10^{-9} to 10^{-10} a/cm^2 reported in literature[13,42].

Cathodically, the deaerated chromic acid solution entered a region of limiting current density at about $i_{L,c}$ = 3 x 10^{-5} a/cm^2, as shown in Figure 38. Extending from the equilibrium potential of 1.17 V to a potential of -0.03 V, the diffusion controlled region had numerous breaks in the curve, suggesting the possibility that several different reduction steps of different reaction rates were occurring. Below approximately -0.04 V, the reduction of hydrogen ions was observed. This portion of the curve had an estimated slope of β_c = -0.05 V which yielded an i_o = 8 x 10^{-6} a/cm^2 for the hydrogen reaction. The reduction of dichromate ions through the oxidation of hydrogen did not appear to be a factor. When hydrogen gas was bubbled through the chromic acid, the electrode potential would be expected to move to a more active potential if the $Cr_2O_7^{2-}$ were being depleted by the oxidation of hydrogen. Although this did not occur in a reasonable amount of time, it might have been

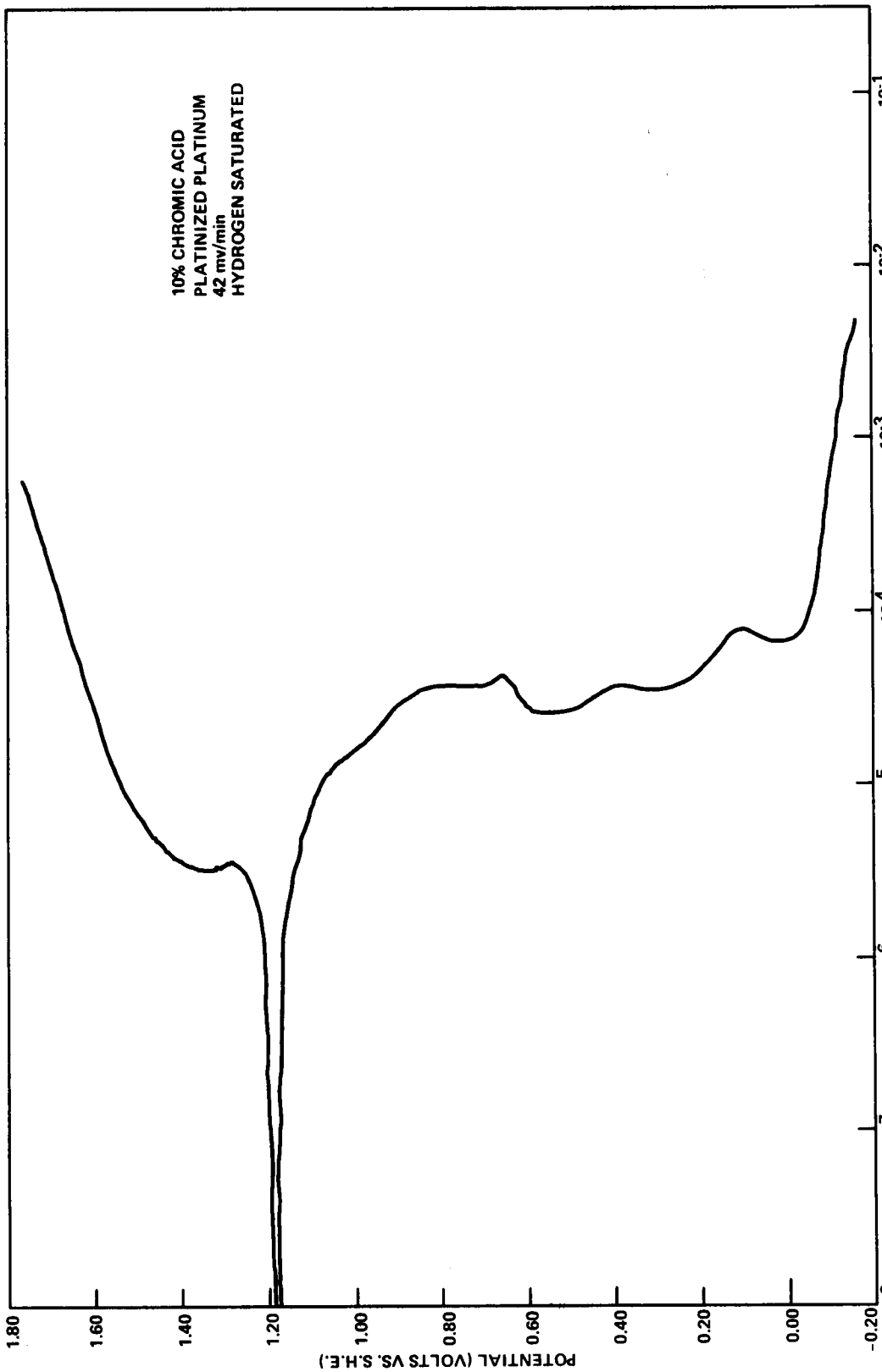


Figure 38. Polarization Curves On Platinum In A Hydrogen Saturated 10% Chromic Acid Solution.

dependent on the contact time for H_2 on Pt which would have been limited due to the very small surface area of Pt relative to liquid volume. This curve demonstrates general agreement with that reported by Pitzl[24] for an unstirred $\underline{N}$ H_2SO_4 solution containing potassium dichromate on Pt.

Aerating the chromic acid solution had negligible effect on the shape of the polarization curves, as shown in Figure 39. Because the chromic acid is such a powerful oxidant at this concentration, the presence of air should have no effect on the results, as was the case for Nagayama and Okamoto[22].

When the nickel base Alloy 2 was potentiodynamically polarized in the 10% chromic acid solution, there was again no significant distinction between the curve for hydrogen saturated solution and that for aerated solution (Figures 40 and 41, respectively). In the hydrogen saturated solution, the corrosion potential was 0.98 V with $i_{L,a} = 6 \times 10^{-6}$ a/cm^2 up to a potential of 1.20 V at which point a transpassive region of increasing current density was entered. The cathodic limiting current density occurred rather abruptly at $i_{L,c} = 3 \times 10^{-5}$ a/cm^2, with the current increasing below -0.1 V due to hydrogen ion reduction. The aerated solution, Figure 41, produced a slightly more active corrosion potential of 0.90 V and a lower $i_{L,a}$ value of 1.5×10^{-6} a/cm^2. The cathodic curve exhibited a much slower approach into the region of limiting current density than that shown for the hydrogen-saturated solution; however, $i_{L,c}$ was about identical

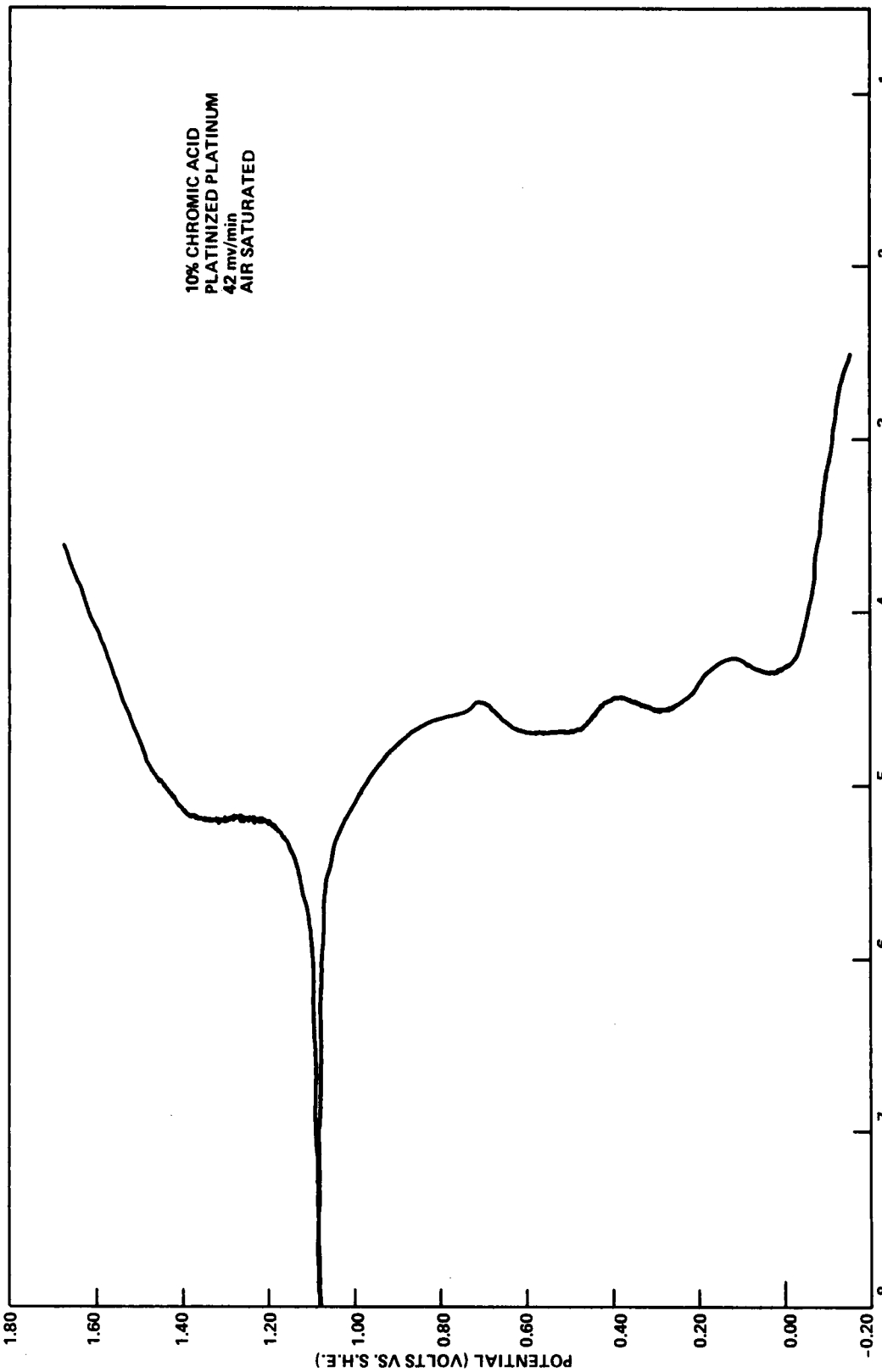


Figure 39. Polarization Curves On Platinum In An Air Saturated 10% Chromic Acid Solution.

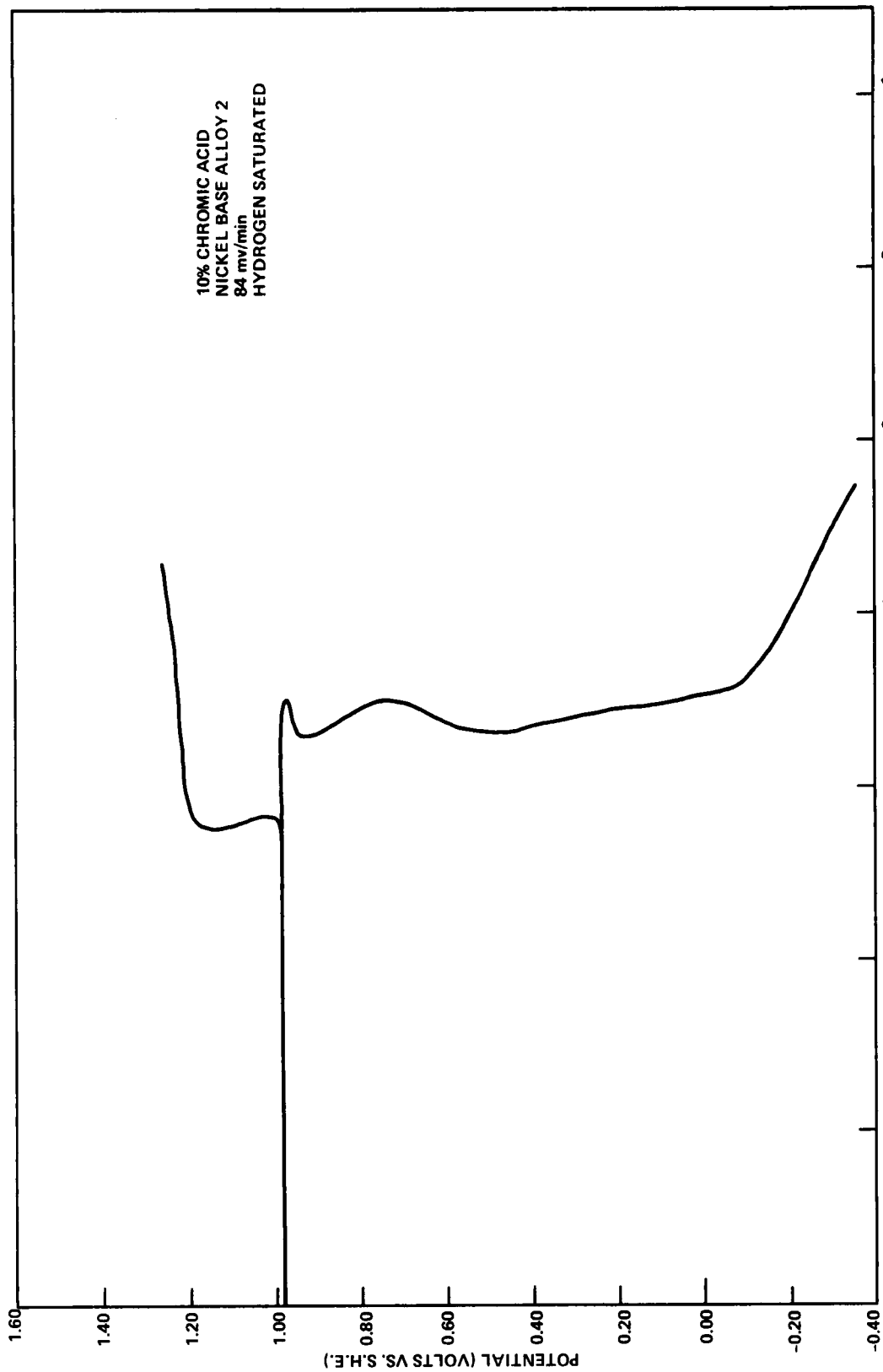


Figure 40. Polarization Curves On Nickel Base Alloy 2 In A Hydrogen Saturated 10% Chromic Acid Solution.

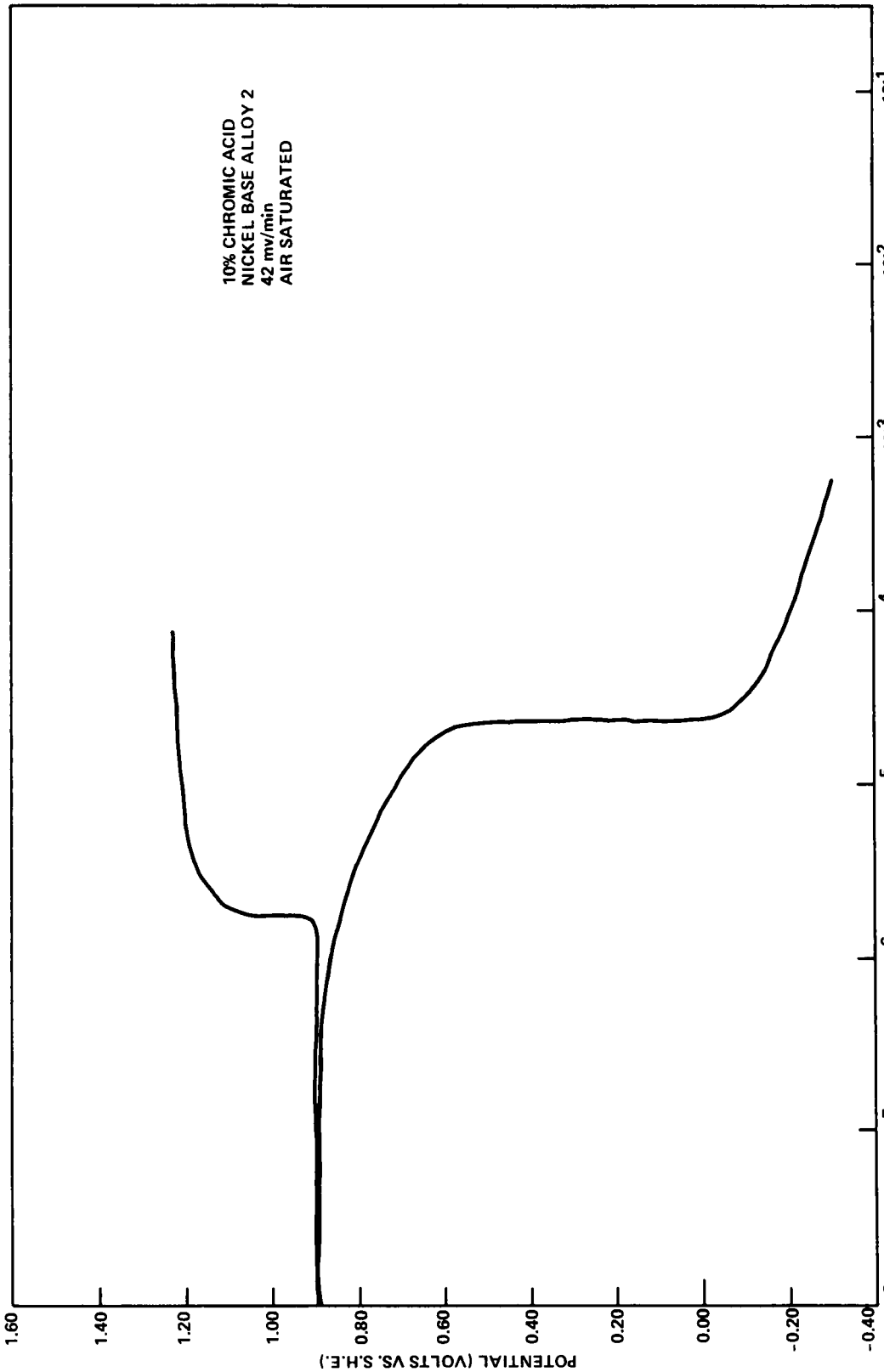


Figure 41. Polarization Curves on Nickel Base Alloy 2 In An Air Saturated 10% Chromic Acid Solution.

to that shown in Figure 40. The nickel-rich Alloy 2 electrode performed in a manner very similar to that for chromic acid on Pt, with the exception of the more active corrosion potentials. However, this is in directional agreement with the corrosion potential of 1.08 V reported by Streicher[38] for boiling 10% CrO_3 solution on Hastelloy C.

CHAPTER VI

CONCLUSIONS AND RECOMMENDATIONS

I. CONCLUSIONS

The following conclusions summarize the results of this investigation. All potentials are referred to the standard hydrogen electrode (S.H.E.).

1. The equilibrium potentials for hydrogen saturated solutions of both sulfuric acid-ferric sulfate and chromic acid on platinized Pt showed close agreement with values reported by Streicher[37] for these solutions; however, no comparison could be made for hydrochloric acid solution because of the interference from oxygen noted by Streicher.

2. Except for the values of E_{corr}, Streicher[37] did not characterize the three solutions electrochemically; thus, no significant correlations could be made between his work and the results of this investigation.

3. The cathodic i_L is larger than the anodic i_L in each of the three solutions due to the greater concentration of reducible species.

4. The oxidation of hydrogen in hydrogen saturated 10% HCl on Pt exhibits diffusion control at $i_{L,a} = 3 \times 10^{-4}$ a/cm^2 from 0.04 V to 1.12 V; from 1.12 V to 1.20 V, a decrease in current density occurs that is independent of stirring. These results are consistent with curves found in literature[41].

5. The oxygen electrode, as noted for aerated 10% HCl on Pt, is indeed complicated and is difficult to reproduce both anodically because of a continuous oxide film formation on the electrode surface and cathodically because of peroxide formation during the reduction of oxygen. Increasing formation of the stable intermediate peroxide during the overall reduction of 0_2 to H_20 causes the rest potential for the electrode to become progressively more negative.

6. Anodic polarization of nickel base Alloys 1, 2, and 3 in hydrogen saturated 10% HCl exhibited active-passive behavior with E_{corr} close to the reversible hydrogen electrode. Increasing chromium content tends to decrease E_{pp}, extending the passive region. Alloys 1 and 2, where $i_{crit} \simeq 2 \times 10^{-5}$ a/cm^2, will tend to spontaneously passivate more readily than Alloy 3, where $i_{crit} = 3 \times 10^{-3}$ a/cm^2.

7. Although the actual Fe^{2+} concentration in the 50% H_2SO_4-0.1 $\underline{M}$ $Fe_2(SO_4)_3$ solution was not known, the Fe^{2+} activity was experimentally determined to be five times smaller than the activity of Fe^{3+} when $E_o = 0.82$ V.

8. A limiting current density of $i_{L,c} = 10^{-2}$ a/cm^2 was observed between $E_o = 0.82$ V and E = 0.08 V for the reduction of ferric ions; this is about a humdred times larger than the limiting current density for the reduction of either oxygen or chromic acid, where $i_{L,c} \simeq 10^{-4}$ a/cm^2. Based on the i_{crit} and E_{pp} values (Table V, page 79) found for the three nickel base alloys in hydrogen saturated 10% HCl, the large redox potential and $i_{L,c}$ values for Fe^{3+}

reduction are sufficient to spontaneously passivate each of the three alloys.

9. The 10% chromic acid solution, with E_o = 1.17 V, is more oxidizing than 10% HCl or 50% H_2SO_4-0.1 $\underline{M}$ $Fe_2(SO_4)_3$; it is such a powerful oxidant at this concentration that the presence of oxygen has no effect on the results.

10. The reduction of chromic acid was observed to be diffusion controlled at $i_{L,c} = 3 \times 10^{-5}$ a/cm^2 down to potentials of about E = -0.03 V; thus, chromic acid will spontaneously passivate only the nickel base Alloys 1 and 2 which have an i_{crit} less than $i_{L,c}$.

II. RECOMMENDATIONS

The following recommendations are proposed:

1. An inert electrode material possessing lower exchange current density values than Pt should be used to improve study of Tafel regions.

2. A more detailed investigation of the oxygen electrode with peroxide formation should be made on both Pt and various nickel base alloys.

3. Polarization curves for the three acid solutions should be conducted on various Ni-Cr-Mo alloys selected from several different regions of the composition-phase diagram for this ternary system, allowing a correlation of alloy composition to the electrochemical parameters for both the alloys and the solutions.

4. Investigation of the three acid solutions should be made at elevated temperatures that would parallel more closely with Streicher's work.

LIST OF REFERENCES

LIST OF REFERENCES

1. Compton, K. G., "The Use of Reference Electrodes in Corrosion Studies," *Materials Research and Standards, 10*, 13 (1970).

2. Crowe, C. R., *A Study of the Electrochemical Behavior of Ternary Nickel-Chromium-Molybdenum Alloys Using Potentiostatic Polarization Methods*, M. S. Thesis, The University of Tennessee, Knoxville, Tennessee (1968).

3. Fontana, M. G., and Greene, N. D., *Corrosion Engineering*, McGraw-Hill Book Company, New York (1967).

4. France, W. D., and Lietz, R. W., "Improved Data Recording for Automatic Potentiodynamic Polarization Measurements," *Corrosion, 24*, 298-301 (1968).

5. Greene, N. D., "Effect of Oxygen on the Active-Passive Behavior of Stainless Steel," *J. Electrochem. Soc., 107*, 457-458 (1960).

6. Greene, N. D., *Experimental Electrode Kinetics*, Rensselaer Polytechnic Institute, Troy, New York (1965).

7. Greene, N. D., "Predicting Behavior of Corrosion Resistant Alloys by Potentiostatic Polarization Methods," *Corrosion, 18*, 136t-142t (1962).

8. Greene, N. D., "The Classical Potentiostat: Its Application to the Study of Passivity," *Corrosion, 15*, 369t-372t (1959).

9. Greene, N. D., "The Passivity of Nickel and Nickel-Based Alloys," *First International Congress on Metallic Corrosion*, 113-117, Butterworths, London (1962).

10. Greene, N. D., and Leonard, R. B., "Comparison of Potentiostatic Anodic Polarization Methods," *Electrochimica Acta, 9*, 45-54 (1964).

11. Greene, N. D., France, W. D., and Wilde, B. E., "Electrode Mounting for Potentiostatic Anodic Polarization Studies," *Corrosion, 21*, 275-276 (1965).

12. Henry, W. D., and Wilde, B. E., "An Automatic Polarization Apparatus for Electrochemical Corrosion Studies," *Corrosion, 25*, 515-519 (1969).

13. Hoare, J. P., *The Electrochemistry of Oxygen*, John Wiley & Sons, Inc., New York (1968).

14. Jones, D. A., and Greene, N. D., "Electrochemical Detection of Localized Corrosion," *Corrosion, 25*, 367-370 (1969).

15. Leonard, R. B., "The Electrochemical Behavior of Some Nickel Base and Cobalt Base Alloys," *Corrosion, 24*, 301-307 (1968).

16. Littlewood, R., "The Effect of Variations in Technique on Polarization Curves Obtained with a Potentiostat," *Corrosion Science, 3*, 99-105 (1963).

17. Makrides, A. C., "Dissolution of Iron in Sulfuric Acid and Ferric Sulfate Solutions," *J. Electrochem. Soc., 107*, 869-877 (1960).

18. Makrides, A. C., "Some Electrochemical Methods in Corrosion Research," *Corrosion, 18*, 338t-348t (1962).

19. Makrides, A. C., and Stern, M., "Inhibition of Metal Dissolution by Ferric Sulfate," *J. Electrochem. Soc., 107*, 877-883 (1960).

20. Myers, J. R., Beck, F. H., and Fontana, M. G., "Anodic Polarization Behavior of Nickel-Chromium Alloys in Sulfuric Acid Solutions," *Corrosion, 21*, 277-287 (1965).

21. "N.A.C.E. Glossary of Corrosion Terms," *Corrosion, 20*, 267t-268t (1964).

22. Nagayama, M., and Okamoto, G., "The Anodic Behavior of Passive Iron in Chromic Acid-Chromate Solutions," *Corrosion Science, 2*,203-210 (1962).

23. Piotrowski, A., and Lebet, R., "The Electrochemical Parameters of Stainless Steel Passivation by Some Reversible Redox-Systems," *Corrosion Science, 7*, 231-237 (1967).

24. Pitzl, G. J., *The Electrochemical Behavior of Ni-Cr-Mo Alloys Using Potentiodynamic Techniques*, M. S. Thesis, The University of Tennessee, Knoxville, Tennessee (1971).

25. Pourbaix, M. J. N., *Atlas of Electrochemical Equilibria in Aqueous Solutions*, Pergamon Press, New York (1966).

26. Pourbaix, M. J. N., *Lectures on Electrochemical Corrosion*, Plenum Press, New York-London (1973).

27. Reinoehl, J. E., and Beck, F. H., "Passivity and Anodic Protection," *Corrosion, 25*, 223-241 (1969).

28. Schuldiner, S., "Oxidation of Hydrogen on a Passive Platinum Electrode," *J. Electrochem. Soc., 115*, 362-364 (1968).

29. Shaw, D., and Edwards, A. M., "A Transistorized Potentiostat System for Corrosion Studies," *Corrosion Science, 5*, 413-424 (1965).

30. Stansbury, E. E., *A Set of Supplementary Notes to Corrosion*, The University of Tennessee, Knoxville, Tennessee (1969).

31. Steigerwald, R. F., "Electrochemistry of Corrosion," *Corrosion, 24*, 1-10 (1968).

32. Stern, M., "Electrochemical Polarization II. Ferrous-Ferric Electrode Kinetics on Stainless Steel," *J. Electrochem. Soc., 104*, 559-563 (1957).

33. Stern, M., "Electrochemical Polarization III. Further Aspects of the Shape of Polarization Curves," *J. Electrochem. Soc., 104*, 645-650 (1957).

34. Stern, M., "The Electrochemical Behavior, Including Hydrogen Overvoltage, of Iron in Acid Environments," *J. Electrochem. Soc., 102*, 609-616 (1955).

35. Stern, M., and Geary, A. L., "Electrochemical Polarization I. A Theoretical Analysis of the Shape of Polarization Curves," *J. Electrochem. Soc., 104*, 56-63 (1957).

36. Stern, M., and Makrides, A. C., "Electrode Assembly for Electrochemical Measurements," *J. Electrochem. Soc., 107*, 782 (1960).

37. Streicher, M. A., "Relationship of Heat Treatment and Microstructure to Corrosion Resistance in Wrought Ni-Cr-Mo Alloys," *Corrosion, 19*, 272t-284t (1963).

38. Streicher, M. A., "Effect of Composition and Structure on Crevice, Intergranular, and Stress Corrosion of Some Wrought Ni-Cr-Mo Alloys," *Corrosion, 32*, 79-93 (1976).

39. *The Reproducibility of Potentiostatic and Potentiodynamic Anodic Polarization Measurements*, ASTM G-1/XI Interlaboratory Testing Program, June 29, 1967.

40. Uhlig, H. H., *Corrosion Handbook*, John Wiley & Sons, Inc., New York (1948).

41. Vetter, K. J., *Electrochemical Kinetics*, Academic Press, New York (1967).

42. West, J. M., *Electrodeposition and Corrosion Processes*, D. Van Nostrand Company, Ltd., London (1965).

VITA

Von Carlos Huffstetler was born in Maryville, Tennessee, on October 5, 1948. He graduated from West High School in Knoxville, Tennessee, in June 1966. That same month, he entered The University of Tennessee at Knoxville where, in June 1971, he received a Bachelor of Science Degree in Chemical Engineering. Participating in The University of Tennessee Engineering Scholastic Cooperative Work Program, he worked seven quarters with Rohm and Haas Company, Knoxville, Tennessee, before graduation.

In September 1971, he entered The University of Tennessee graduate program with a Graduate Teaching Assistantship in the Chemical and Metallurgical Engineering Department. Two years later, he began employment with the Foods Division of Procter and Gamble Manufacturing Company at Jackson, Tennessee. In June 1976, he joined Union Carbide Corporation in the Materials and Systems Development Department, Gaseous Diffusion Development Division, Oak Ridge Gaseous Diffusion Plant, where he is presently employed. Resuming his graduate study, he received a Master of Science Degree in Chemical Engineering in December 1977.

He is married to the former Mary Ann Graham of Nashville, who received a Bachelor of Science Degree in History from The University of Tennessee in 1976 and who is presently pursuing a Master of Science Degree in Library Science.